This is a preprint, the final version is subject to change, of the American Mineralogist (MSA)
Cite as Authors (Year) Title. American Mineralogist, in press.
DOI: https://doi.org/10.2138/am-2019-6594

1 **Revision 1, Correction 08/01/2019**

2

3 **Invited Centennial Review**

4

5 # High-Pressure Minerals

6 Oliver Tschauner

7 **ORCID:** 0000-0003-3364-8906

8

9 University of Nevada, Las Vegas, Geoscience, 4505 Maryland Parkway, Las Vegas,

10 Nevada 89154-4010, U.S.A.

11 This article is dedicated to occurrence, relevance, and structure of minerals whose formation
12 involves high pressure. This includes minerals that occur in the interior of the Earth as well as
13 minerals that are found in shock-metamorphized meteorites and terrestrial impactites. I discuss
14 the chemical and physical reasons which render the definition of high-pressure minerals
15 meaningful, in distinction from minerals that occur under surface-near conditions on Earth or at
16 high temperatures in space or on Earth. Pressure-induced structural transformation in rock-
17 forming minerals define the basic divisions of Earth's mantle in the upper mantle, transition
18 zone, and lower mantle. Moreover, solubility of minor chemical components in these minerals
19 and the occurrence of accessory phases are influential in mixing and segregating chemical

elements in Earth as an evolving planet. Brief descriptions of the currently known high-pressure minerals are presented. Over the past ten years more high-pressure minerals have been discovered than during the previous fifty years, based on the list of minerals accepted by the IMA. The previously unexpected richness in distinct high-pressure mineral species allows for assessment of differentiation processes in the deep Earth.

Introduction

1.General aspects of compression of matter over large pressure ranges

The pressure in Earth ranges from atmospheric to 136 GPa at the core-mantle boundary, and further, to 360 GPa in the center of the Earth (Dziewonski and Anderson 1981). These gravitationally generated pressures are not high on a general scale of planetary or stellar objects, where gravitational energy balances or overcomes the electronic binding energy in atomic matter such as in the interior of giant planets or where it vastly exceeds it such as in the interior of Sun-like stars or beyond (Hund 1936, Landau and Lifshitz 1985). Thus, even in the deepest parts of Earth matter is well within the range of chemical bonding between discrete atoms rather than that of dense or degenerate plasma. However, in Earth the pressures are high enough to modify the chemical behavior of elements and thereby the compounds that they form and the crystalline or liquid structures that these compounds assume. Roughly, the difference of 100 GPa between Earth's surface and the bottom of the lower mantle corresponds to an increase in energy of ~ 1eV/e^-. This approximate value may be obtained from relating the

42 average contraction of the volume of a valence electron in rock-forming minerals over a
43 pressure-intervall of 100 GPa to energy through the Mie-Grüneisen equation (Bukowinski 1994).
44 This increase in energy is equivalent to a temperature of the order 10000K. However, the
45 temperature at the inner core-outer core boundary is less than 6000 K (Boehler 1993, Shen et al.
46 1998, Anzelini et al. 2013, Zhang et al. 2016) and less than 3000 K in the mantle (Brown and
47 Shankland 1981, Korenaga 2008). Hence, in Earth's deep mantle the effect of pressure on the
48 properties of matter dominates over the effect of temperature. The general effect of pressure
49 on chemical bonding is a consequence of the nature of electrons as fermions: The Pauli
50 exclusion principle restricts the occupancy of an electronic state to two electrons with up- and
51 down spin. In consequence, increasing pressure induces an increase in electron kinetic energy
52 with a power 2/3 whereas their binding potential energy increases with power 1/3 (Landau and
53 Lifshitz 1985). Hence, at sufficiently high pressure the kinetic energy causes electrons to be
54 released from their bond states resulting in a electron fermion plasma that is spatially confined
55 by the Coulomb attraction through the nuclei (Hund 1936, Landau and Lifshitz 1985). These
56 processes occur at pressures beyond the pressure range within Earth. However, the
57 approximate scale of the pressure-induced increase in electron energy in Earth has observable
58 effects on the chemical behavior of elements because it is of a magnitude comparable to energy
59 differences between valence electronic states in solids which are of the order 1eV. This
60 distinguishes Earth from smaller planets like Mercury and Mars. The increase of kinetic energy
61 of the electrons is observable as shifting and broadening of their energy states. Within this
62 context the local density of the different orbital states is relevant: d- and f- electrons exhibit
63 pressure-induced shifting and broadening at lower pressures than s- and p-electrons (Duthrie
64 and Pettifor 1977, Nellis et al.1988, Holzapfel 1995). Eventually, these states overlap with other
65 electronic states and thereby reconfiguration of bonding and antibonding states with

subsequent structural transitions may occur. Particularly relevant for Earth is the occupation of Si 3d states which are empty and markedly above valence level at reference conditions but partially hybridize with the 3s and p states under pressures of the deeper Earth mantle where Si assumes a six-fold coordination by O anions (Li et al. 1993, Wu et al. 2012, Du and Tse 2017). The change in coordination corresponds into a rearrangement of valence orbital states from sp^3 toward a 3p-dominated state hybridized with 3s and 3d states (Li et al. 1993, Wu et al. 2012, Du and Tse 2017). Similarly, 4d states become involved in bonding for Ca at pressures corresponding to the mid mantle (Oganov et al. 2010) and one can expect Ca to exhibit overall a chemical behavior similar to Sc at reference conditions.

Other noticeable results of pressure induced changes in electronic states are isolator-metal transitions and high spin-low spin transitions. These electronic transitions affect the redox potential of elements with occupied d-states, notably Fe (for a review, see Sturhahn et al. 2005 and Lin et al. 2013), and thereby induce depth-dependent changes in the relative stability of Fe and other transition metal elements in their various oxidation states (Frost et al. 2004, Frost and McCammon 2008, Rohrbach and Schmidt 2011) and the partitioning of elements between oxidized and reduced states in coexisting phases over an extended pressure range (Li and Agee 1996, Tschauner et al 1998, Righter and Campbell 2009).

Since the increase in kinetic energy is overall more noticeable for outer shell electrons and for shells with high occupancy (f- over d- over p- over s-shells (Duthrie and Pettifor 1977)) quite often trends of compression-induced structural changes in elements and compounds mimic structures and properties of their higher Z equivalents in the same row or adjacent right row in the period table at lower pressure: For instance, the stable form of carbon at standard conditions is graphite. Diamond, the fully sp^3-bonded three dimensional network structure of

carbon becomes stable above 1.94 GPa at 0 K (Kennedy and Kennedy 1976). The stable phases of Si and Ge under standard conditions are isotypic to diamond. Both elements undergo a variety of transitions with increasing pressure and ultimately assume the α-Sn structure above 10 GPa (Jamieson 1963). Sn itself is dimorphic at reference conditions with the metastable diamond-like β-Sn structure and the metallic α-Sn structure, which remains stable up to 20 GPa where α-Sn transforms into a fcc-structure (Olijnik and Holzapfel 1984). Pb assumes this fcc structure at ambient pressure already and transforms to a hexagonal, dense-packed phase above 10 GPa (Takahashi et al. 1969).

We see that the sequence of pressure-induced transformations is reproduced by the change of structure with increasing Z within the group V elements. Moreover, better screening of outer shell electrons from the nuclei causes a general change in physical properties from insulating to semiconducting to metallic (C to Si to Ge to Sn to Pb). This change is reproduced by the pressure-driven increase in electron kinetic over binding energy and pressure causes isolator-metal transitions for many elements and compounds. The correlation between Z and the pressures of phase transitions can be well observed for a group of similar elements cuh as rare earths (Holzapfel 1995). We note that this trend does not accommodate particular intermediate structures, hence, it does not define a law of pressure-induced transitions but a pattern. In this, somewhat vague, sense it also applies for compounds. The role of cations and anions in polyatomic structures is not simply additive. Moreover, the geometric density of packing is an insufficient parameter in assessing pressure-induced structural transformations: The fcc lattice is geometrically denser than the bcc lattice, but the alkali halides undergo pressure-induced transitions from the former to the latter, because , within a simple ionic bonding concept, the anion is generally more compressible than the cation or, more generally, the electron-density distribution around the cation- and anion nuclei determines which structure is assumed at a

given pressure, while compression affects anions and cations differently. In fact, upon pressure-induced phase transformations cation-anion distances generally increase with increasing pressure but molar volume decreases because the coordination of cation and anion increase (Shannon and Prewitt 1968, Prewitt and Downs 1998).

High pressure modifies the chemical behaviour of elements within the pressure range of Earth but it does not evoke entirely new structure types. Rather, under compression compounds and elements assume structures which their higher-Z analogues assume at low or ambient pressure. This observation holds at least to about 100-200 GPa where indeed distinct types of structures occur which lack any equivalent at ambient conditions, such as the cubic-gauche phase of N (Eremets et al. 2004), or transparent sodium whose structure is controlled by a large electron density in antibonding orbitals which act equivalently to a small interstitial ion (Wang et al. 2006).

It is understood that these trends of 'chemical pressure' are not meant to substitute for more minute ab initio calculations of electronic band structure or orbital configurations but to illustrate some general features of the effect of pressure on crystal structures. However, it is this generality that is required for defining high-pressure minerals.

1.2 Earth materials and high pressure

The examination of pressure-induced changes in chemical and physical properties has prevailed over more than a century and continues to be an important domain in condensed matter chemistry and –physics (Mao et al. 2018). Already P.C. Bridgman (1924), the doyen of high-pressure research, examined the effects of pressures in the GPa-range on minerals, and V.M.

Goldschmidt (1937) inferred the geochemical effects of pressure in the Earth's interior. The study of pressure-induced phenomena in geologically relevant materials comes with the additional technical challenge of the corresponding increase in temperature with pressure along a geothermal gradient. Over the second half of the 20th century experimental research of minerals and rocks at high pressures has progressed from a 10th of a GPa to hundreds of GPa along with a steady improvement of experimental and analytical techniques (Ahrens 1988, Eremets 1996, Hemley and Mao, 1998, Mao et al. 2017). The discovery of natural occurrences of high-pressure phases has usually followed the trace of experimental synthesis. More recently, genuine high-pressure minerals were discovered that have not yet been synthesized. Furthermore, the complexity of natural minerals which almost always contain minor- and trace-components outlines a petrologically relevant space of chemical parameters that experiments can fill for the benefit of understanding the geochemistry of the deep Earth: For instance, the observation of a high Si-content in recently discovered liuite ($FeTiO_3$-perovskite, Ma and Tschauner 2018) points toward a previously unknown high compatibility of Ti in Fe-rich bridgmanite. Some shock-metamorphic minerals are dominated by endmembers that evade static synthesis and allow for assessment of mixing relations that were previously poorly constrained or inaccessible such as in the akimotoite-hemleyite system (Bindi et al. 2017, Tschauner et al. 2018) or the Ca-Eskola component in tissintite (Ma et al. 2016). These findings have to be placed into the petrologic context of mantle melt extraction and metasomatism. The previously unexpected richness in distinct high-pressure mineral species allows for assessment of differentiation processes in the deep Earth.

The new developments in the study of minerals that form at high pressure ask for a more specific conceptual assessment. What defines a high-pressure mineral, if there is no particular pressure-range and are no particular high-pressure structures? A previous review of high

pressure minerals (Prewitt and Downs 1998) predates the discovery of about two thirds of the high-pressure minerals that are currently known. Other previous reviews of minerals that form at high pressures have focused on a specific type of formation such as shock-metamorphism (Langenhorst and Deutsch 2012), meteorites (Rubin and Ma 2017, Tomioka and Miyahara 2017) or inclusions in diamonds (Kaminsky 2012). Here we provide an overview about high-pressure minerals themselves. We also attempt to provide a definition for these minerals, which places them in the context of geochemical, geophysical, and planetary phenomena and their investigation. Since the formation of high-pressure minerals marks fundamental divisions in the interior of the Earth it is important to find a general definition of this group of minerals, if possible.

2. Definition of high-pressure minerals

A distinction between high-pressure and other minerals has to be based on the chemical and structural features which are bound to and are characteristic of high pressures of formation. Moreover, a definition of high-pressure minerals has to be sufficiently general to encompass the range of compounds and structures that have been observed in nature.

Minerals in general are naturally occurring, crystalline phases with well-defined composition and structure, which have formed without human intention (Nickel and Grice 1998). A first, general definition of high-pressure minerals may encompass any mineral whose stability field does not overlap with ambient pressure. This definition appears as clear as it is simple, but, in fact, it is prone to create more confusion than clarification: For instance, the research of so called ultrahigh pressure metamorphic rocks that occur in continental roots is centered on minerals which form and break down at pressures that are minor fractions of the stability field of

minerals like forsterite or periclase. However, neither forsterite nor periclase are high-pressure minerals because their stability field extends to ambient pressure. Thus, the absolute scale of pressure does not provide a good criterion for high-pressure minerals. This fundamental point was already mentioned above and is illustrated in Figure 1 which shows the relation of the density increase in percent upon pressure-induced phase transitions of minerals as function of their density as reference conditions. One notices that the gain in density decreases the higher the initial density is. The plot can also read as illustration of the trend of pressure-induced transformations towards phases equivalent to ambient pressure phases of elements with higher Z.

Most of the, in many respects quite interesting and important, minerals in ultra-high pressure metamorphic rocks are stabilized by volume reductions due to sterical rearrangements of tetrahedral silicate or alumosilicate-networks without any fundamental change of chemical bonding of the silicate. Primarily sterical pressure-induced structural changes should be conceptually separated from structural changes that originate in pressure-induced changes in bonding. Therefore, within the regime of minerals whose stability range does not overlap with ambient pressure we distinguish a) incipient high-pressure minerals and b) high-pressure minerals proper.

Incipient high-pressure minerals are phases which form by sterical reconfigurations of structural patterns but without fundamental changes in bonding. Examples are coesite, ellenbergerite, jadeite, ice-VII. In contrast, we define high-pressure minerals as minerals whose structure is established through a marked change in chemical bonding of its constituent elements. Usually this change in bonding is correlated with a change in coordination of ions. Examples are

stishovite, akimotoite, and bridgmanite. The stability fields of both, incipient- and proper high-pressure minerals do not extend to ambient pressure.

This basic distinction raises the question how to define a fundamental change in chemical bonding for a vast class of compounds and structure-types. Ab initio methods of calculating electronic band structure cannot provide a general criterion because they only address, though often rather accurately, specific states in specific structures. For a constrained set of elements and structures this may work well: For instance the change in c/a ratio of hexagonal dense packed transition metals as function of Z and of pressure can be best addressed by such calculations (see for instance Duthrie and Pettifor 1977, Holzapfel 1995). However, it cannot serve as criterion for phases as different in structure and bonding character as stishovite, hexaferrum, or bridgmanite.

In need of a criterion for many different structures and compositions we have to abstract from direction-dependent electronic properties. This throws us back onto the concept of effective ionic radii (Goldschmidt 1934, Pauling 1960, Shannon 1976). However, we also have to avoid the issues of applying a quasi-classical bond model to structures where direction-dependent distributions of states are evidently important.

Therefore, we use the ionic radii concept only in the negative by defining a high-pressure mineral as a phase which assumes a structure-type at elevated pressure although it's ambient pressure effective ionic radii place it far outside the tolerance fields for this structure. Incipient high-pressure phases remain within or in proximity of these tolerance fields. Despite the rather generic approximation of bonding the effective ionic radii allow us to define fields of structure-types for given stoichiometries (Goldschmidt 1934). These fields of structure types (hereafter: 'structure fields') are defined by ranges and ratios or radii and have been used successfully in

material science and chemistry (e.g. Roth 1957, Kugimiya and Steinfink 1968, Manjon et al. 2007). Here we use these radii relations to identify structures whose formation is not compatible with ambient pressure solid state chemistry but we leave aside the specifics of this change in bonding as it will be very different for metals like iron and for compounds like silica: For instance, bridgmanite is $MgSiO_3$ in a perovskite-type structure with an effective A- and B cation- radii of 0.8 and 0.4 while ABO_3 –perovskites have radii of A and B above 0.95 and 0.8, respectively (Fig. 9). Hence, bridgmanite is a high-pressure mineral according to our definition.

It needs to be stressed that any such definition is in reference to 1 bar pressure and generally the radii of ions in their coordinations within stable phases at that reference pressure should be used. An attempt to assess more narrowly effective radii of high-pressure phases is equivalent to an attempt to define high-pressure bonding. This is not our goal here. We only try to define a qualitative measure for distinguishing high-pressure from incipient high- and from low-pressure minerals.

The gradual pressure-induced shift of compounds across such structure fields has been explored in systematic fashion for instance for ABO_4 compounds (Manjon et al. 2007). A possibly ambiguity arises from a too narrow definition of structure-types. We avoid this issue by considering structures as distinct only if they involve topologically different bond vectors in the same sense as outlined by Nickel and Grice (1998). In this sense zircon- and scheelite-type phases are not considered as distinct but rather mark a transition from an ambient to an incipient high-pressure mineral or a transition between incipient or between high-pressure phases, respectively. Also, dense solid molecular phases, for instance of N_2, H_2O, CO_2 are generally incipient high-pressure phases according to our scheme, whereas the covalently

bounded phase CO_2-V, polymeric N, or ionic ice-X are high-pressure phases proper (but have not been found as minerals).

We note that the concept of effective radii is not very applicable for metallic, molecular, and persistently covalently bonded structures. As we stated above, we consider transitions between different arrangements of molecular species such as CO_2 as incipient high-pressure phases. For strictly covalently bonded and for metallic systems we return to the general observation of 'chemical pressure' that we outlined in the introduction. For instance, iron and taenite (α-and γ-iron) are the ambient and high-temperature mineral polymorphs of Fe, whereas hexaferrum (ε-Fe) is a high-pressure mineral because its structure is isotypic to that of the next lower row of group 8b elements in the periodic table. Equivalently, diamond, isotypic with silicon, is a high-pressure mineral polymorph of carbon etc. This additional criterion also removes occasional ambiguity of radii-relations for structure fields of some compounds such as for rutile- and pyrite-type AB_2 compounds (see section 3.5)

Thus, our definition is:

A high-pressure mineral is a naturally occurring crystalline phase whose stability field does not extend to ambient pressure and whose structure reflects a marked change in chemical bond character compared to ambient pressure. This change in bond character is quantified by

a. a structure that is clearly not consistent with the ambient pressure effective ionic radii of this compound.

For metals, molecular compounds, and other compounds which do not fit well into the ionic radii concept, we define a high-pressure mineral as

b. a phase that assumes a structure isotypic or closely structurally related to the stable structure of phases with higher-Z elements of the same rows in the periodic table: such as Diamond-silicon-germanium, CO_2-V – cristobalite etc.

Both criteria overlap, for instance stishovite is a high-pressure mineral according to the first as well as second criterium being isotypic to β-GeO_2, to cassiterite (SnO_2), plattnerite (β-PbO_2), and rutile.

With respect to Earth the distinction between ambient-, incipient high-, and high-pressure minerals is meaningful because it delineates the major zones in the Earth's mantle: Crust, upper mantle, transition zone, lower mantle, and core (Fig. 2). It also removes the confounded use of the term 'high-pressure' for natural environments of vastly different pressure ranges. Consequently, we list minerals according to their structures which in their turn indicate the relevant pressure induced changes in chemical bonding. For instance, bridgmanite is listed as perovskite-type oxide rather than as inosilicate along with enstatite.

Reference is always the state of matter at thermodynamic reference conditions. Hence, a mineral like periclase, whose stability range extends from ambient pressure to beyond the pressures in the Earth's core ranks as an ambient-pressure mineral. Such minerals are discussed here only in context with high-pressure minerals. Emphasis is on high-pressure minerals. Placing these minerals into context requires occasional discussion of incipient high-pressure minerals and experimentally synthesized high-pressure phases that are related to high-pressure minerals or are currently not approved as minerals.

292

293 **3.1 Elements and alloys**

294 **General aspects of elements and alloys under high pressure**

295 Already in the introduction we have outlined the basic trends of pressure-induced changes
296 in chemical properties of the elements and the accompanying sequences of structural
297 transformations. Elements which occur in the native state in nature do not always form
298 condensed phases, for example the noble gases. Others occur as condensed elemental
299 phases but do not undergo structural transitions within the pressure range of the Earth's
300 interior such as gold and the platinum group elements (PGEs). We only discuss elemental
301 materials which have been found as high-pressure minerals. The recently discovered natural
302 δ-N_2 is discussed along with other molecular phases and minerals further below (section 3.4).

303

304 **Diamond**

305 The stable phase of carbon at standard conditions is graphite. Following a positive Clapyeron
306 slope graphite transforms into diamond above 1.94 GPa at 0 K (Kennedy and Kennedy 1976).
307 Diamond is the high-pressure phase of carbon: Although the ionic radius concept applies
308 neither to graphite nor to diamond, we apply the 2nd criterion of a high-pressure phase,
309 isotypism with higher-Z elements of the same group in the periodic table: Si, Ge, α-Sn, which
310 all assume the diamond-structure. This criterion is also consistent with the actual drastic
311 changes in chemical bonding from an sp^2-bonded carbon sheets with interlayer p-bonding to
312 a three-dimensional sp^3-bonded covalent network structure (Pauling 1960).

Fullerite (Buseck et al. 1992) is a low-pressure/high-temperature polymorph of C that occurs in a variery of natural environments on Earth and in space (Buseck 2002). Compression induces polymerization of fullerite (Sundqvist 1999). Dynamic compression can induce the transformation from graphite to polymerized C_{60} (Luo et al. 2005). The peak shock-pressures in many carbonaceous chondrites are well in the range of these polymerization conditions (Scott et al. 1992). Hence, polymerized C_{60} is expected to occur in nature.These polymers are to be considered as incipient high-pressure phases. They assume higher density through partial formation of new bounds rather than a complete change in bonding character such as it is the case for the transition from graphite to diamond. We note that none of these crystalline C_{60}-polymers have been clearly identified in nature and consequently established as minerals. Chaoite, a structurally insufficiently characterized carbon-phase from the Ries-impact crater (ElGoresy and Donnay 1968) has a unit cell of $8.948 \times 8.948 \times 14.078$ Å^3 and may be such a partially polymerized fullerene-polymorph. El Goresy et al. (2003) reported another carbon-phase of unknown structure from the Popigai impact crater which also exhibits a very large unit cell.

Lonsdaleite, the 2H polytype of diamond (which represents the 3C-polytype of the Si-structure) had been reported but the presumed type material was recently shown to be diamond (3C) with large density of stacking faults (Nemeth et al. 2014).

A number of metastable carbon phases with varying degrees of sp^2- and sp^3-bonding have been predicted by computational methods (Oganov et al. 2013) or synthesized (Mao et al. 2003) but not yet been clearly identified in nature. Computational studies predict that diamond transforms into the 'BC8-structure' at pressures far beyond those of the Earth's interior but possibly metastable at ambient conditions (Mailhoit and McMahan 1991).

Despite its importance in the deep carbon cycle of Earth, ice planets, and stellar nebulae, discussion on diamond can be cut short here because it has been extensively discussed in a number of recent review papers (Shirey et al. 2013, Stachel and Luth 2015). The potential of diamond to retain mineral inclusions with high residual pressures and the reconstruction of the depth of entrapment of these inclusions has guided the discovery of high-pressure minerals and -phases and we discuss this aspect of diamond research along with the high-pressure mineral inclusions that were discovered that way.

Hexaferrum

Iron assumes three distinct structures in nature: α-, γ-, and ε-Fe, which are the bcc, the fcc- and the hcp-structures, respectively. Pure γ-Fe is stable only at temperatures above 800 K (at the triple point) and ε-Fe forms at 300 K above 13 GPa following a steep, negative Clapeyron slope of transition from α-Fe, and a gently positive Clapeyron slope of the transition from the γ-Fe phase above 800 K (Boehler 1986). It appears to be largely ignored that ε-Fe is actually an approved mineral with the name hexaferrum (Mochalov et al. 1998) Since minerals are defined by structure and dominant endmember, 'iron' as a mineral is α-Fe and γ-Fe is taenite, despite the fact that the latter often contains appreciable amount of Ni (and is stabilized at 300 K through Ni): In taenite and its Ni-rich variety kamacite, Ni does not assume sites different from Fe. Both, iron and taenite have been found as inclusions in diamond (Kaminsky and Wirth 2011, Mikhail et al. 2014, Smith et al 2018). In some cases, these inclusions have high remnant pressures of 1- 7 GPa which imply their entrapment in diamond in the transition zone, Tschauner et al 2018b) but they represent the low-pressure and the high-temperature phases of iron.

Since iron is a metallic, elemental phase, the ionic radius-concept cannot be applied and we use our 2nd criterion to assess which of the natural iron-phases is a high-pressure mineral, if any: the hcp-structure is assumed by the group VIIIb elements of the rows 5 and 6 (Pd-Os, Rh-Ir), thus, hexaferrum is a high-pressure mineral according to our criterion as well as by common notion. Type hexaferrum is stabilized by 35 at % Ir, Os, and Ru (Mochalov et al. 1998) and has not formed at high pressure. Hexaferrum is commonly assumed to be the dominant phase in the Earth's inner core (Mao et al. 1990), although the presence of minor chemical components may change the structure (Lin et al. 2002, Dubrovinski et al. 2007, Tateno et al. 2010). Its melting curve fixes the temperature of the inner core-outer core boundary, one of the few potentially accessible pivotal points of the temperature in the deep Earth. Consequently the melting of iron at high pressure has been subject of extensive research (Williams et al. 1987, Boehler 1993, Shen et al. 1998, Anzolini et al. 2013, Zhang et al. 2016) but is complicated by the partitioning of unidentified light elements between outer and inner core. According to the 'redox-freezing model' (Rohrbach and Schmidt 2011, Frost and McCammon 2008) iron, taenite, and hexaferrum are potentially common accessories in the Earth's transition zone and lower mantle. In this case, iron phases could serve as carrier of siderophile elements like Re, and the platinum group elements. Hexaferrum has not been found as inclusions in diamond. Because of the nearly isochoric path that connects a residual pressure of above 13 GPa at 300 K of a hypothetical hexaferrum inclusion in diamond with the pressure and temperature of entrapment at least up to the regime of viscoelastic deformation of diamond and because of the slope of the taenite-hexaferrum phase boundary (Boehler 1986) the presence of hexaferrum as inclusion in diamond would imply entrapment below 900 km depth (see section 3.4 and Navon 1991, Navon et al. 2017, Tschauner et al. 2018).

383

384 **Complex intermetallics and quasicrystalline alloys**.

385 In the highly shocked Khatryka carbonaceous chondrite a number of hitherto unknown
386 intermetallic compounds and quasicrystalline phases with constituent Al were observed
387 such as Icosahedrite, $Al_{63}Cu_{24}Fe_{13}$ (Bindi et al.2011). Coexistence with ahrensite (Hollister et
388 al. 2014) and a subsequent experimental dynamic compression study (Asimow et al. 2016)
389 showed that their formation is bound to elevated pressures probably upon cooling of
390 metallic melt during shock-release. Elevated pressures appear to extend the formation
391 regime of quasicrystals in the Fe-Ni-Al system and allows for formation of quasicrystals
392 which have not been obtained at ambient pressure (Asimow et al. 2016). The mechanism of
393 formation of quasicrystals makes these naturally occurring phases typical examples of
394 intermediate-pressure minerals.

395 Various carbides and silicides of iron and other transition metal elements have been
396 reported from iron-meteorites and ureillites (see Rubin and Ma 2017 for a review), as
397 inclusions in diamonds (Kaminisky and Wirth 2009, Smith et al 2018), fulgurites (Essene and
398 Fisher 1986), and from various terrestrial localities including the Luobusha ultrahigh-
399 pressure metamorphic terrain (Dobrzhinetskaya et al. 2009). The formation processes of
400 some of these occurrences have involved high pressures but these phases can also be
401 synthesized at ambient pressure. Therefore, we do not discuss them here further as not
402 genuinely high-pressure minerals.

403

404

3.2 Pnictides and chalcogenides

Allabogdanite

Phosphides are minor accessories in iron-meteorites (Rubin and Ma 2017). In 2008 Dera et al. discovered that the meteorite mineral allabogdanite, Fe_2P, is the result of a pressure-induced transformation of barringerite, Fe_2P, at 8 GPa. The transition is based on a group-subgroup relation from P-62m to Pnma and involves a shift of half of the P atoms relative to the Fe sublattice (Dera et al. 2008). Allabodganite is an incipient high-pressure mineral because its formation involves pressure but no major change in bonding and coordination of P and Fe. The cause of this pressure-induced transformation is shock-compression during the break-up of the parent body of the iron-meteorites which host allobogdanite. As of yet, there is no systematic study on unreversed shock induced tranformations and reactions in pnictides and chalcogenides in iron-meteorites, although they could contribute to a shock-metamorphic scale for iron-meteorites that is as finely graded as that for stoneymeteorites.

Quingsongite and pnictides in the Earth's interior

The hypothesis of redox freezing in the deeper mantle (Rohrbach and Schmidt 2011) implies the possibility of a regime in the Earth's mantle where conditions are reducing enough to stabilize pnictides. Occurrence of pnictides as minerals in the Earth is limited by the overall low abundance of N in the mantle (Mikhail et al. 2014a). Diamonds contain up to 5000ppm N but most type-I (N-bearing) diamonds exhibit much lower concentrations (Taylor et al. 1990). Kaminsky and Wirth (2017) reported inclusions of nitrides and carbonitrides in diamonds from the deeper mantle. Dobrzhinetzkaya et al. (2014) reported the occurrence of quingsongite,

cubic BN, in the ultrahigh-pressure metamorphic rocks from the Luobusha complex in Tibet, China. The cubic sphalerite-type structure of boron nitride is the high-pressure polymorph of BN (Wentorf 1961), while at ambient conditions BN assumes a layered graphite-like structure.

3.3 Chalcogenides

A wealth of studies has been dedicated to the Fe-S system at high pressures and temperatures with the main goal of assessing the S-content in planetary cores (Fei et al. 1995, Bertka and Fei, 1997, Lin et al. 2004) These studies have revealed pressure-induced transformations in stoichiometric pyrrhotite (troillite, FeS, Fei et al. 1995) and the formation of Fe- and Ni-sulfides of stoichiometries different from those that occur at ambient pressure (Fei et al. 1997, Prewitt et al. 2002). As of yet, none of these phases has been found in nature. Sulfides are minor accessories in the Earth's mantle and take an important role in controlling the mobility of chalcophile elements as well as PGEs. Pressure-effects on sulfides beyond the Fe-S system are rarely studied. Observed phase transformations are mostly reversible (Fei et al. 1995). Pyrrhotite, pentlandite, chalcopyrite (Richardson et al. 2001, Stachel and Harris 2008), and mawkinawite (Agrosi et al. 2018) have been found as inclusions in diamonds, but possible high-pressure structures or residual pressures were not conserved or documented. Shenzhuangite, $NiFeS_2$, is isotypic to chalcopyrite and was discovered in the highly shocked Suizhou L6 chondrite (Bindi et al. 2018). At ambient pressure Ni is rather incompatible in the chalcopyrite structure and formation of shenzhuangite may have involved high pressure (Bindi et al. 2018).

3.4 Molecular compounds

General aspects: Three types of abiotic molecular solids occur on Earth: water-ice, clathrates of H_2O with other molecules like CH_4, and former fluids that are trapped in diamond, retained elevated pressure and crystallized upon ascent. These occurrences are minor in comparison with the terrestrial abundance of molecular compounds in fluid or gaseous state.

Some of these molecular phases are to be classified as incipient high-pressure minerals, because they represent sterically denser packing of their constituent molecules than the low- or ambient pressure polymorphs. Efficient packing becomes possible when librational modes are suppressed upon compression (Hemley and Dera 2000). Upon further compression these materials enter the regime of enhanced intermolecular interaction through resonance-bonding and ultimately the formation of extended network structures, which are genuine high-pressure phases or, in competition with such structures, decomposition. Examples are N_2 and CO_2 which both exhibit upon compression a sequence of molecular phases but ultimately transform into extended network structures at ~ 140 GPa (N_2, Eremets et al. 2004) and 23-25 GPa (CO_2-V, Iota et al. 1997). CO_2-V competes with decomposition to diamond and oxygen (Tschauner et al. 2001, Takafuji et al. 2006, Litasov et al. 2011). None of these high-pressure phases have been found in nature and the known abiotic molecular minerals are low-temperature or intermediate-pressure phases. We do not discuss the known methane-clathrates here since they are rather low-temperature minerals (Kvevolden 1993). Along with the few molecular intermediate pressure minerals we mention a few occurrences of dense molecular phases which are not yet approved as minerals because they elucidate processes in the Earth's interior that involve fluids.

Nitrogen

Upon compression solid N_2 undergoes a number of phase transformations which impose denser sterical arrangement of the N_2 molecules along with suppression of librational modes (Bini et al., 2000). In 2017 Navon et al. reported spectroscopic evidence for inclusions of N_2 in natural diamonds from Junia, Brazil, at residual pressures of 10 GPa. Subsequent SAEDS on of such inclusions inside FIB-milled sections of diamond is consistent with the δ-N_2-structure (Cromer et al. 1981). δ-N_2 is not yet an approved mineral. It would falls into the class of incipient high-pressure minerals because it's structure reflects marked suppression of molecule rotation compared to α-, and β-N_2 (Bini et al. 2000). Here, it is worth mentioning for two reasons: 1) δ-N_2 illustrates the potential of diamond of retaining small mineral inclusions at high residual pressures. 2) These residual pressures allow for constraining the pressure and temperatures of entrapment of the inclusions. This method has been applied to inclusions of ice-VII (Tschauner et al. 2018b) and of dense CO_2 in diamonds (Navon 1991). Figure 3 gives an overview of the current residual pressures inclusions of dense molecular mineral and phases in diamond and the reconstruction of their entrapment conditions in the Earth's mantle. N_2 as a free phase in diamond has been explained as exsolution of N from the diamond lattice within the Earth's transition zone (Navon et al. 2017).

Ice-VII

Ice-VII was approved as mineral in 2017 (Tschauner et al. 2018b). Ice-VII is the stable form of ice above 2.4 GPa and is closely related to the anti-cuprite structure (Kuhs et al. 1984). The structure can also be described as the superposition of two cristobalite-like networks translated by ¼, ¼, ¼. However, ice-VII is a H-bonded network where two protons establish mutually

molecular bonds to adjacent O though their dynamic disorder. Consequently, ice-VII is a sterically denser arrangement of an H-bonded H_2O network than it's lower- and ambient pressure polymorphs ice-Ih,-II, -III, -IV, -V, -IV, and –XI (Petrenko and Whitworth 1999). Ice-VII is, therefore, an incipient high-pressure mineral. Further compression of ice-VII does not induce sterical rearrangment of water molecules but a gradual weakening of the H-bond (Holzapfel et al. 1984, Goncharov et al. 1998) which eventually results in the transition to ice X with ionic bonds of protons ordered on Wyckoff sites 4b, along the space diagonals between the oxygen ions in an exact anti-cuprite configuration (Holzapfel et al. 1984). This phase, ice X, represents particular case of a high-pressure phase because it exhibits H-O bonding that does not exist at ambient pressure but at the same time, it is structurally nearly equal to ice-VII besides the ordering along with the shift of H from the partially occupied site 8c to fully occupied 4b. The transition from ice-VII to X had been originally estimated to occur around 40 GPa (Holzapfel et al. 1984, Goncharov et al. 1998) but subsequent studies have proposed markedly higher pressures (e.g. Guthrie et al. 2013), until recent work on annealed ice-crystals has established a pressure of 30 GPa (Grande et al. 2019).

Ice-VII has been observed as inclusions in sublithospheric diamonds. It is remnant of diamond-forming C-H-O rich fluid and occurs along with other inclusions which formed out of the fluid such as halite, and magnesian calcite, and minerals which have formed during mantle metasomatism such as ilmenite. All known ice-VII inclusions contain between 0.5-4 mol% NaCl. These ice-VII inclusions as well as other mineral inclusions in the same diamonds have high residual pressures in the range of 4 to 23(2) GPa which allow for constraining the pressures and temperatures of their entrapment (Figure 3, Tschauner et al. 2018b).

Along with the disocvery of hydrous ringwoodite (Pearson et al. 2014, see section 3.6) the natural occurrencies of ice-VII identify actual regions of past hydrous metasomatism in the Earth's mantle whereas previous experimental studies only assess the general possibility of such processes. A recent evaluation of seismic data with respect to elastic signatures of water-bearing dense silicates indicate that the average transition zone mantle is rather dry with local wet spots of ~ 0.6 wt% of chemically bound water (Houser 2016). Ice-VII inclusions are likely related to such wet spots.

Ice-VI

The melting points of ice phases –II, -III, -IV, and –V are below 300 K (Petrenko and Whitworth 1999) and these phases are not expected to be observed in natural environments on Earth although they may occur in icy moons and planets. Ice-VII and ice-VI melts above 300 K. Kagi et al. (2000) evaluated IR transmission spectra of a diamond and assigned part of the absorption bands related to the O-H asymmetric stretching vibration to ice-VI. However, no structure analysis has been reported and ice-VI is not an approved mineral. The narrow stability field of ice-VI could be instrumental in assessing the P-T conditions of aqueous fluids in the shallow sublithospheric mantle.

Carbondioxide

No solid phase of CO_2 is an approved mineral, but optical spectroscopy has provided evidence for molecular CO_2 inclusions in diamond at residual pressures of 2-5 GPa (Navon 1991, Schrauder and Navon 1993). Therefore, we discuss CO_2 here. A recent overview of the known synthetic phases of CO_2 is given in Datchi and Weck (2014). At ambient pressure CO_2 crystallizes

as dry ice (CO_2-I) at 194 K and the solid-fluid transition line crosses 300 K at about 1 GPa (Downs and Somayazulu 1996). A large number of solid phases of carbon dioxide have been synthesized and the effect of pressure can be summarized as follows: Up to about 23-25 GPa phase transformations are governed by sterical rearrangements of CO_2 molecules and through suppression of librational modes (Hanson and Jones 1981, Aoki et al. 1994). Above 23-25 GPa, CO_2 assumes network structures closely related or isotypic to cristobalite (Iota et al. 1997, Datchi et al. 2014). This major change in chemical bonding is kinetically inhibited at low temperatures and may result in changes of the CO_2 molecule configuration and intermolecular resonance bonding (Iota et al. 2007), while at high temperatures CO_2 network phases are not as stable as the equivalent silica-phases, because they decompose upon melting into diamond and oxgyen (Tschauner et al. 2001, Takafuji et al. 2006, Litasov et al. 2011). Hence, in comparison to aluminophosphate and to silica, the flexibility, and hence stability, of the tetrahedral network upon compression follows the trend $AlPO_4 > SiO_2 > CO_2$ with the former recovering their coordination upon pressure-release (Tse and Klug 1992), silica transforming to stable phase with different coordination of Si, and CO_2 breaking down into its constituents. The network-structures CO_2-V and –VI (Tschauner et al. 2001, Datchi et al. 2014) are high-pressure phases due to the marked change in extended C-O bonding from molecular to an extended network structure equivalent to the covalent network structures of SiO_2, the oxide of the next heavier group VI element in the periodic table. The dense molecular phases CO_2-II, -III, and -IV (Datchi and Weck 2014) are incipient high-pressure phases.

Both, absorption bands from the bending and asymmetric stretching related bands of molecular CO_2 are not uncommon observations in infrared spectra of fibrous diamonds. Interestingly, the IR absorption band of the C-O asymmetric stretching vibration of of CO_2 in diamonds has an energy of around 2350 cm^{-1} - 2380 cm^{-1} which implies residual pressures in the range of 2-5 GPa

564 and pressures of entrapment in diamond of 5 to 7 GPa (Figure 3, Navon 1991, Schrauder and
565 Navon 1993, Tschauner 2019, Hanson and Jones, 1981). In addition, partially resolved splitting
566 of this band indicates interaction with other phonon states which is also characteristic for CO_2
567 phases at elevated pressure (Hanson and Jones 1981). No diffraction data of these CO_2-
568 inclusions have been obtained but the energy of the vibron corresponds to those of CO_2-II (Aoki
569 et al. 1994). Hainschwang and Notari (2011) observed that the reported energies of different
570 CO_2-related modes observed in single diamonds give different pressures and do not match the
571 spectrum of any known phase of CO_2. Possibly CO_2 is not occurring as free phase in diamond
572 inclusions, but is captured in a clathrate or 'filled ice'. Similar to inclusions of ice-VII, inclusions
573 of CO_2 in diamond are not expected to represent the average composition of the diamond-
574 forming fluid but rather a by-product of the breakdown of carbonate during diamond formation.
575 Thus, CO_2 or CO_2-bearing clathrate constrains pressure-temperature conditions of diamond
576 formation from carbonaceous melts and fluids (Schrauder and Navon 1993).

577

578 **3.5 Halides**

579 Pressure-induced phase transformations in halides have been studied experimentally. The
580 transition of alkalihalides from the NaCl- to the CsCl-structure as a function of effective ionic
581 radii and pressure has been a hallmark in the understanding of the effect of strong compression
582 on solids (Born and Huang 1954, Bassett et al. 1968, Sato-Sørensen 1983). The high-pressure
583 phases of halite and sylvite form above 20 GPa and have not yet been observed in nature. As we
584 discussed above with respect to hexaferrum, their occurrence as inclusions in diamond would
585 imply entrapment in deep in the lower mantle of Earth. Halite-sylvite solid solutions have been
586 reported as inclusions in diamonds at remnant pressures as high as 10 GPa (Tschauner et al.

2018b). Also other halides have been reported as inclusions in diamond: Sylvite, $CaCl_2$, cottunite ($PbCl_2$) (Wirth et al. 2009), sellaite (MgF_2), and a compound $(Na,K)Cl{\cdot}5H_2O$ (Tschauner et al. 2018b). These phases occur in their ambient pressure structures but their occurrence within diamond reflects elevated pressure of formation. It is noteworthy that pressure favors the formation of hydrous alkalihalides such as monohydrohalite (Driesner and Heinrich 2007).

3.6 Oxides and hydroxides

General aspects: The rocky part of Earth is dominated by compounds of Mg, Si, O as the most abundant and Al,Ca, Fe as next common elements (Ringwood 1979, McDonough and Sun 1998). The Earth surface, crust, and upper mantle are predominantely composed of silicates of these elements. Oxides and hydroxides occur rather as accessory phases in these silicate rocks (Haggerty 1991). As such oxides and hydroxides operate as carriers of minor and trace elements which convey important geochemical information and influence the partitioning of minor elements upon partial melting, such as the complex spinel in spinel-peridotite. At the boundary between transition zone and lower mantle at 660 km depth and at pressures of 23-25 GPa a major structural and chemical transition of the dominant chemical compounds $(Mg,Fe)_2SiO_4$ and $(Mg,Fe)SiO_3$ transforms the rock-forming minerals ringwoodite and majorite into periclase and bridgmanite (Fig. 2, Ringwood 1979, Ringwood And Irifune 1988, Ito and Takahashi 1989). Periclase is an oxide and, as we argue below, bridgmanite is also an oxide rather than a silicate. Hereby we define silicates as constituted by covalently bounded SiO_4-units. Hence, the boundary between transition zone and lower mantle is not only a seismic discontinuity but marks the transition from fundamentally covalently bonded silicates, the salts of the silicic acid, to dominantely ionically bonded oxides of the major elements Mg,Si, Fe,Ca, and Al.

610 It was mentioned in the introduction that the partial hybridization of the Si 3d states, empty at
611 ambient pressure, with the 3s and p states at the pressures of the deeper Earth mantle causes
612 the change in coordination of Si by oxygen from four to six. The change in coordination
613 corresponds to a rearrangement of valence orbital states from sp^3 toward a 3p-dominated state
614 hybridized with 3s and 3d states (Li et al. 1993, Wu et al. 2012, Du and Tse 2017) and these
615 authors have argued for an overall more ionic Si-O bonding in these structures and at these
616 pressures. Previously, the effect of pressure on silicates was assumed to enhance covalency
617 (Prewitt and Downs 1998). However a more recent re-evaluation of the charge density
618 distribution in stishovite by Kirfel et al. (2001) is more consistent with the more spherical charge
619 distribution of increased ionic bonding. Similarly, Cohen (1991) and Metsue and Tsuchiya (2012)
620 argue for an intermediate state of ionic and covalent bonding for stishovite. This is also
621 consistent with the observation that the spherical (ionic) form factor of Si yields systematically
622 better structure refinements for X-ray diffraction data of high pressure silicate phases than the
623 covalent one (J. Smyth, personal communication. This also agrees with the author's experience).
624 It should be noted that bonds between different atomic species are usually not pure cases of
625 either ionic or covalent bonding. The discrepancy between a more ionic or more covalent bond
626 character at high pressure is mediated if one recalls that pressure favors higher probabilities of
627 occupancy of higher orbital states, which for Si are the 3d states. The hybridization of 3d with
628 the 3s and -p states favors a charge distribution which is spatially overall more even than the
629 more directional sp^3-bond state of $Si^{[4]}$. The statement that pressure favours a more ionic Si-O
630 bonding should be taken in this sense.

631 The boundary between upper mantle and transition zone marks the change from the ambient
632 pressure stable phase of magnesium orthosilicate, forsterite, to the incipient high-pressure
633 phases wadsleyite, at 410 km, and ringwoodite, at 520 km depth (Akaogi et al. 1989). The

boundary between transition zone and lower mantle marks the change from incipient to the proper high pressure phases bridgmanite and $CaSiO_3$-perovskite (out of clinopyroxene and garnet, see Fig. 2), plus periclase. Hence, the main divisions in what is commonly called bulk silicate Earth are pressure-induced changes in chemical and physical properties expressed through major structural tranformations. The correlation between depth in Earth, corresponding pressure, major seismic discontinuities and the corresponding structural and chemical changes are illustrated in Figure 2. Although the elemental composition of the mantle does not markedly change between the transition zone and the lower mantle the chemical properties of the elements change, albeit reversibly.

Besides the carrier phases of the main elements in the rocky part of the Earth, Mg,Si, Fe,Ca, Al, also phases which contain less common elements as constituents such as oxides of Ti of Cr undergo equivalent transitions to incipient- and high-pressure minerals. Most of them have been discovered in shocked meteorites or terrestrial impactites and their potential geochemical role inside Earth is not yet understood.

Periclase and wuestite

Periclase and wüstite are the monoxides of Mg and Fe in the halite-structure. Both minerals occur at ambient pressure but are stable over an extremely large pressure range: Wüstite assumes the nickeline structure above 90 GPa (Fei et al. 1994) and MgO remains in the halite-structure to beyond the pressures of the Earth's mantle (Coppari et al. 2013). Below the 660 km boundary between transition zone and lower mantle, ferromagnesian orthosilicate in the ringwoodite structure (see below) decomposes into ferrous periclase and bridgmanite (see Fig. 2 and section about perovskites below). This makes periclase the third most abundant mineral in

Earth after bridgmanite and hexaferrum and the second most abundant mineral in the rocky part of the Earth. Solid solutions between periclase and wüstite have been found as inclusions in diamond (Kesson et al. 1994, Harte et al. 1999, Stachel et al. 2000, Brey et al. 2004, Smith et al. 2018). In a few cases periclase coexists with enstatite and this paragenesis has been interpreted as retrograde transformation product of a bridgmanite-periclase assembly that was entrapped in diamond in the lower mantle (Kesson et al. 1994, Harte et al. 1999, Stachel et al. 2000, Smith et al. 2018). However, ferrous periclase also forms upon decomposition of carbonate under upper mantle conditions (Brey et al. 2004) and the conclusion from periclase inclusions in diamond onto a lower mantle source region is not always coercive.

Brucite

Brucite was reported along with magnesioferrite as lamellae in a periclase inclusion within a diamond from Juina, Brazil, (Palot et al. 2016), a locality known for diamonds with inclusions that are retrograde transformation products of transition zone and lower mantle minerals (Stachel et al. 2000, Walter et al. 2011, Navon et al. 2017) and of an inclusion of ringwoodite (Pearson et al. 2014). Palot et al (2016) took the brucite-lamellaeas indication for the former presence of aqueous fluid which altered periclase into brucite, and subsequently periclase + magnesioferrite as breakdown product of a former lower mantle phase of the feiite type (see below). Brucite itself undergoes a reversible distortive structural transition to an orthorhombic phase at 7 GPa ('brucite-II'). At higher pressures, a phase isotypic to anatase has been calculated to be stable (Hermann & Mokherjee 2016). However, geothermal temperatures destabilize brucite at mantle pressures relative to periclase and aqueous fluid (Fei et al. 1994).

Ca,-Al- and Fe- oxyhydroxides, phase Egg

679 Experimental studies on the high pressure behaviour of hydrargylite (α-AlOOH), goethite (α-
680 FeOOH), and portlandite ($Ca(OH)_2$) have revealed a number of high pressure phases, none of
681 which has yet been found in nature but may be important in retaining water to within the lower
682 mantle (Hu et al. 2016). Phase Egg is a dense hydrous alumosilicate with layered structure
683 (Eggleton et al. 1978). We note that the high-pressure polymorph of portlandite '$Ca(OH)_2$-III'
684 assumes the baddelyite-type structure above 12 GPa (Kunz et al. 1996), same as TiO_2 at above
685 20 GPa and SiO_2 above 90 GPa (see below). Recently, dense Al- and Fe-oxyhydroxides that do
686 not break down at lower mantle pressures have been synthesized (Zhang et al. 2018).

687

688 **Rutile- and post-rutile-type phases**

689 Rutile is one of the polymorphs of TiO_2 and also the structural prototype of many compounds
690 ranging from sellaite, MgF_2, to plattnerite (β-PbO_2), cassiterite, and ε-FeOOH, a high-pressure
691 polymorph of goethite (Otte et al. 2009).

692 In mineralogical textbooks, TiO_2 is commonly presented as trimorph with anatase as the stable
693 phase at reference conditions, brookite, as low-temperature-intermediate pressure, and rutile
694 as the high-pressure phase. However, srilankite, riesite, and akaogiite are further high-pressure
695 polymorphs of TiO_2 which are all approved minerals (Willgallis et al. 1983, El Goresy et al. 2001,
696 Tschauner et al. 2017). Upon compression rutile undergoes a series of transitions to phases of
697 the scrutinyite-type (α-PbO_2) above 3 GPa (Withers et al. 2003, Kojitani et al. 2018), the
698 baddeleyite-type above 12 GPa, and the cotunnite- (PbClO) type above 40 GPa (Olsen et al. 1999,
699 Sato et al. 1991). This sequence is an accordance with the general scheme of high-pressure
700 crystalline structures isotypic to ambient pressure phases of higher-Z elements. Scrutinyite-type
701 TiO_2 is the mineral srilankite, which usually contains high contents of ZrO_2 (Troitzsch et al. 2006).

The ZrO_2-component reduces the phase transformation pressure from ~ 3 GPa to less than 0.3 GPa (Troitzsch et al. 2006). Srilankite is a rare high-grade metamorphic mineral but it occurs also as minor accessory in metasomatized garnet peridotite (Wang et al. 1999). Endmember srilankite has been reported from the Ries-impact crater (ElGoresy et al. 2001) and the Luobusha complex in Tibet (Dobrzhinetskaya et al. 2019). Baddeleyite-type TiO_2 is the mineral akaogiite and has also been foound first at the Ries impact structure (El Goresy et al. 2001). Riesite is a monoclinic polymorph of titania that is structurally related to srilankite but where Ti assumes Wyckoff sites different from those in srilankite. Riesite represents probably a retrograde transformation product of akaogiite (Tschauner et al. 2017).

Rutile-type structures occur for components AX_2 with a ration rA/rX between 0.41 to 0.73 (Wyckhoff 1960) bordering to fluorite-type phases at higher ratio and at lower ratio to tetrahedral network structures, like the anti-cuprite structure, such as ice-VII, or the various low-pressure polymorphs of silica. Pyrite-type phases exhibit similar ratios of radii as rutile and the two types of structures are related. The pyrite-structure has been proposed as ultra-high pressure polymorph of silica (Kuwayama et al. 2006). Within this general scheme of structures of AX_2-compounds srilankite and riesite are incipient high-pressure minerals, whereas akaogiite is a high-pressure mineral with r_{Ti}/r_O in the field of rutile but assuming a distorted fluorite-type structure instead.

The poststrutile titania minerals establish excellent indicators for shock-metamorphic pressures in terrestrial impactites. Srilankite is a minor accessory in garnet peridotite, where it hosts Zr and Hf. Conceivably, srilankite is replaced by akaogiite at greater depth. However, neither Ti-rich srilankite nor akaogiite have yet been found as inclusions in sublithospheric diamonds, probably because of the breakdown reaction of rutile + magnesite to geikielite + CO_2 (Ferry et al. 2002).

Nano-scale crystallites of post-rutile titania phases have been reported from eclogites where they occur along interfaces of rutile lamellae but it is not yet clear if these occurrences represent free phases or rather interfacial layers of reduced symmetry.

Stishovite and seifertite

Stishovite is silica in the rutile structure. Its discovery was a hallmark in the study of astroblemes and shock metamorphism (Chao et al. 1962) and followed the synthesis of rutile-type SiO_2 by less than one year (Stishov and Popova 1961). Stishovite is a common occurrence in terrestrial impact sites such as Barringer crater (Chao et al. 1962, Ries (Chao 1967), Popigai (El Goresy et al. 2001), Vredefort (Spray and Boonsee 2018). Recently stishovite was reported from a lunar meteorite (Kaneko et al. 2015). Presence of stishovite in subducted crustal rock has been inferred but as of yet it has been not been directly observed. The rate of obduction of such rocks may not be high enough to permit conservation of stishovite but some of the coesite that has been found as inclusions in eclogitic garnets has probaby formed retrogradely from stishovite (Liou et al. 2009).

As we mentioned already in the introduction: the rA/rB ratio (whether ionic or 'covalent') places silica into the range of tetrahedral network structures. Hence the formation of a rutile-type phase implies a drastic change in chemical bonding. Stishovite is the prototype of a fundamental pressure-induced change in bonding and coordination (Li et al. 1993).

Seifertite is silica in the scrutinyite-type structure. Stishovite follows the same trend of pressure-induced phase transformations as rutile and evolves from rutile- to scrutinyite- to baddeleyite-type (Hemley et al. 1994). Seifertite is an approved mineral that was found in the Shergotty and

747 Zagami martian meteorites (Dera et al. 2002, El Goresy et al. 2008). At pressures above 30 GPa
748 stishovite can accommodate Al_2O_3 and H_2O through coupled substitution (Lakhstanov et al.
749 2007), whereas at lower pressure stishovite does not accommodate other elements beyond
750 trace level.

751 For pure SiO_2 seifertite forms at pressures in excess of 70 GPa (Hemley et al. 1994), which is
752 generally considered too high for the peak shock pressures that the Shergotty meteorite had
753 experienced prior ejection from Mars (Fritz et al. 2005). Experimental studies (Dubrovinskaya et
754 al. 2001) showed that cristobalite transforms metastably to seifferite at pressures above 30 GPa,
755 which is more in accordance with independent assessments of the peak shock pressures of the
756 Shergotty meteorite. Thus, type seiferite in the Shergotty meteorite has probably formed from
757 cristobalite as precursor (Dera et al. 2002). A baddeleyite-type silica phase has been synthesized
758 (Hemley et al. 1994) but not reported as mineral.

759 Coesite

760 Coesite is an incipient high-pressure polymorph of silica, which is, along with diamond, an
761 important indicator of pressures in the range of few GPa in ultrahigh pressure metamorphic
762 rocks (Yang et al. 2007, Schertl et al. 1991) and for terrestrial impacts (Chao 1967). The structure
763 of coesite bears similarity to the alumosilicate framework of feldspars and the Si-O bond
764 distance is nearly equal to that of quartz (Prewitt and Downs 1998).

765 Diaplectic silica

766 Quartz-bearing bedrock at terrestrial impact sites is often transformed into vitreous silica but of
767 density higher than quartz itself. This, so called, diaplectic quartz is an example of pressure-
768 induced amorphization where compression induces a collapse of the ambient-pressure structure

769 but kinetic barriers are too high to allow for conversion into a stable high-pressure structure.
770 Shock-induced vitrification of quartz has been confirmed experimentally (Ahrens and Gregson
771 1964) and was also reported for other silica phases, including coesite (Luo et al. 2003). An
772 overview and detailed discussion of relevance and occurrence of diaplectic quartz is given by
773 Grieve et al. (1996) and Hamann et al. (2018). Tschauner et al. (2006) found that exerimentally
774 generated diaplectic quartz, when statically recompressed in a diamond anvil cell at 300 K,
775 assumes the stishovite structure above 11 GPa. Because kinetic barriers for structural
776 rearrangement in silica are high, they proposed that diaplectic quartz is actually stishovite that
777 suffered local structural disordering upon shock-release. Static recompression shifts the slightly
778 displaced atoms back into their lattice-periodic sites. This hypothesis was recently confirmed by
779 in situ XRD experiments during dynamic compression of quartz and coesite (Gleason et al. 2018).
780 It remains to be noted that more longer periods of elevated temperature during and after
781 shock-release from natural impact events may shift the silica structure further and irreversibly
782 away from stishovite (Wackerle 1962) and that extended geologic time may also removes this
783 structural memory effect in diaplectic quartz (both is indicated by a decrease in density of
784 diaplectic quartz).

785 Computational studies of vitreous and molten silica also exhibit a gradual change from
786 tetrahedral network to non-bridging states with 5-,6-, and 7- fold coordinated Si which overall is
787 better described as ionically rather than covalently bonded (Du and Tse 2017) (see above).

788

789 **Rutile-derived high-pressure minerals – silicate hollandites**

790 A group of AB_3O_8 phases can be derived from rutile through a correlated rotation of octahedra
791 along the four-fold axis of the rutile structure and reconnection to edge-sharing double-chains

792 along their outer two edges (Hyde and Anderson 1989). Consequently a channel opens along the
793 four-fold axis. Since this channel can be occupied by large cations or by H_3O^+ this geometric
794 structural operation provides the template for the hollandite-series manganates (Bystrøm and
795 Bystrøm 1950). Equivalenty, the feldspars $NaAlSi_3O_8$, $KAlSi_3O_8$, and $CaAl_2Si_2O_8$, albite, orthoclase,
796 and anorthite, assume hollandite-type structures in the 10 to above 25 GPa pressure range (Liu
797 1978, Yamada et al. 1984, Yagi et al. 1987, Gautron and Madon 1994), as well as synthetic Sr-,
798 Ba- and Pb-alumosilicate (Reid and Ringwood 1975, Downs et al. 1995). The crystal-chemical
799 equivalence of Al+Si and Mn^{4+} and the rutile-like octahedral framework in these structures mark
800 the silicate-hollandites as high-pressure minerals. Generally, minerals where all Si is six-fold
801 coordinated are high-pressure minerals. There are minerals which contain both six- and four-
802 fold coordinated Si such as majoritic garnets (see section 3.8) or even the Ca-silicate thaumasite
803 whose formation does not involve pressures above ambient (Effenberger et al. 1983). A
804 representation of the structure of silicate-hollandites is shown in Figure 4.

805 All silicate-hollandites are approved minerals. Lingunite, $NaAlSi_3O_8$ was first described by Gillet
806 et al. (2000) from an occurrence in the Sixiangkou L6 chondrite. Subsequently, liebermannite
807 $KAlSi_3O_8$, and stöfflerite, $CaAl_2Si_2O_8$, were discovered in the Zagami shergottite (Ma et al. 2018,
808 Tschauner et al 2018). Langenhorst and Poirer (2000) had already reported $KAlSi_3O_8$-hollandite
809 in a TEM study on the Zagami shergottite and Spray and Boonsee (2017) had reported Raman-
810 spectra and EBSD patterns of stöfflerite from shock melt veins in bed rock from the central uplift
811 of the Manicouagan impact structure. Hollandite-type post-feldspar phases are important
812 indicators for high shock-metamorphic pressures. They allow for narrowing the dynamic
813 pressures beyond the occurrence of maskelynite in shocked feldspathic rocks, terrestrial and
814 meteoritic. Formation of silicate-hollandites is bound to locally elevated temperatures
815 ('hotspots') or the vicinity of shock-melt veins where temperature above the principal Hugoniot

of feldspars is generated (Gillet et al. 2000, Ma et al. 2018) but below peak pressures where melting occurs upon shock release (Ahrens et al. 1969, Sekine and Ahrens 1992). In the Zagami shergottite stöfflerite occurs as intermediate between bytownitic maskelynite and integrowth of zagamiite (see below) and stishovite in the center of the hotspot. Hence, stöfflerite forms in a regime of modest temperature between shock-amorphized plagioclase ('maskelynite') and the stable phase assembly. Similarly lingunite and liebermannite have been found in proximity to shock melt veins or as clasts with such veins (Gillet et al. 2000, Ma et al. 2018).

No occurrence of silicate-hollandites has been reported that is not shock-related. In the Earth's mantle the possible occurrence of silicate-hollandites is limited in composition to liebermannite with rather minor components of lingunite and stoefflerite and to a rather narrow pressure-temperature interval of stability (Yagi et al. 1987). At high pressure liebermannite breaks down to Na-ferrate type K-aluminate and stishovite, whereas at low pressure the stability range of liebermannite is separated from orthoclase by intermediate decomposition into cymrite- and wadeite-type silicates coexisting with coesite (Yagi et al. 1987). Similar intermediate decomposition prior formation of high-pressure minerals occurs also in the cases of $MgCr_2O_4$ and $FeCr_2O_4$ (see below).

A recent experimental study (Zhou et al. 2017) reported linguite80liebermannite20 to have a stability field at temperatures above the geotherm, which bears possible relevance for occurrences within shock melt veins but not for Earth. Stöfflerite had been synthesized by laser heating in diamond anvil cells (Gautron and Madon 1994) but is not stable relative to zagamiite and stishovite (Gautron et al. 1996, Liu et al. 2012).

Maskelynite

Equivalent to quartz, feldspars are also found to transform into a dense amorphous state if subjected to dynamic compression above 25 GPa (Milton & DeCarli 1962, Ahrens et al. 1969, Stöffler et al. 1991). These shock-amorphized feldspars are called maskelynite and are important indicators of high grade shock-metamorphism both in meteorites and at terrestrial impact sites (Stöffler et al. 2018). Within the present context it has to be asked if maskelynite is result of dynamic compression beyond the mechanic stability of the feldspar crystal structure but at temperatures too low to induce transformation into a crystalline high-pressure polymorph of feldspar, or, equivalent to quartz, product of disordering or retrograde transformation of such a dense polymorph. As of yet, no evidence for such a transformation has been reported. Using micro-diffraction the author has observed that synthetic maskelynite (from oligoclase) exhibits spatially isolated remnants of the feldspar structure at least up to 57 GPa. Accordingly, infrared and Raman-spectra of natural and synthetic maskelynite show feldspar-like features to this pressure (Fritz et al.2005) and therefore represent these structural remnants of feldspar rather than the bulk vitreous material. Natural maskelynite exhibits a range of density and changing vibrational features (Fritz et al. 2005) which at least in part reflect structural changes from heating upon shock release.

In the Tissint- and Zagami shergottites the following sequence of phases is observed along the temperature gradient around hot spots: maskelynite $\rightarrow$ stöfflerite $\rightarrow$ zagamiite + stishovite with the latter representing the area of highest temperature (Tschauner and Ma 2017).

Spinels and spinelloids

General

Spinels and minerals with spinel-like structures assume an important role in the Earth's mantle down to 660 km depth although they become dominant rock forming minerals only below 410 km depth (Fig. 2). Spinels are also prominent in other environments such as primitive meteorites or interstellar dust (Rubin and Ma 2017). Many transition metal oxides that occur in igneous and in some metamorphic rocks assume the spinel structure (Haggerty 1981). Spinel in spinel peridotite is a complex solid solution of chromite, hercynite, magnetite, spinel, and other spinel components. Olivine and wadsleyite, the major minerals of the Earth's upper mantle and transition zone, assume structures closely related to spinel (Bragg and Brown 1926, Horiuchi and Sawamoto 1981) and ringwoodite, the dominant phase in the lower part of the transition zone is $(Mg,Fe)_2SiO_4$ in a normal spinel structure (Binns et al. 1969, Sasaki et al. 1982). Hence, the structure and properties of silicates and oxides AB_2O_4 with spinel- and related structures exert strong influence on the geochemical and -physical evolution and properties of the mantle through their abundance. Here we are mainly concerned with the high-pressure minerals among those phases. We discuss postspinel high-pressure phases and place the important rockforming minerals wadsleyite and ringwoodite into the context of high-pressure mineralogy.

The definition of structure fields for compounds AB_2O_4 is less straightforward than for ABO_3 or ABO_4 (see below). In part this is owed to the possibility of inversion between the octahedral and tetrahedral site in the spinel structure (Gibbs et al. 2008) and in part to the marked distortion of [6]-fold coordinated polyhedra in spinelloids and post-spinel structures. Kugimiya and Steinfink (1968) defined structure fields for AB_2X_4 compounds based on more than thousand structure files. They found that by using a measure of bond strength as additional parameter structure fields can be clearly delineated over a large range of compositions and effective ionic radii. Since we are mainly concerned with oxides, a conventional plot of radii r_A versus r_B is sufficient (Fig. 5) and we prefer this here for consistency. Within this frame, tetrahedral network structures like

885 the Be-silicate phenakite are found for low r_A/r_B at low r_B. Olivine and similar spinelloids occupy
886 an intermediate range of values with r_A above 1.05 and r_B up to ~ 0.65, above which post-spinel
887 phases of the harmunite ($CaFe_2O_4$-), the marokite ($CaMn_2O_4$-), and the $CaTi_2O_4$-type are favored.
888 Spinels occur for r_A below 1.05 and radii ratios around ~ 0.8 to ~1.0. Combined high r_A and r_B
889 define the mentioned post-spinels and AB_2O_4-perovskites (Fig. 5). Harmunite ($CaFe_2O_4$-),
890 marokite- ($CaMn_2O_4$-), and $CaTi_2O_4$-type postspinel structures are assumed at high pressure by
891 many compounds that are spinels at reference conditions such as the mineral spinel itself
892 (Akaogi et al. 1999), magnesioferrite (Andrault and Bolfan-Casanova 2001, Chen et al. 2017),
893 magnetite (Fei et al. 1998, Ricolleau and Fei 2016), chromite (Chen et al. 2003, Ishii et al. 2014,
894 2016, Ma et al. 2019) and ulvospinel (Nishio-Hamame et al. 2012, Ma et al. 2018). These
895 structures establish the high-pressure phases within the AB_2O_4 system.

896

897 **Wadsleyite and olivine**

898 Olivine, the main phase of the upper mantle is the solid solution between forsterite Mg_2SiO_4 and
899 fayalite Fe_2SiO_4. The olivine structure exhibits a distorted hcp-like arrangement of the oxide-ions
900 though deviation from the regular hcp arrangement is much more pronounced (Bragg and
901 Brown 1926, Wyckoff 1960, Hyde and Anderson 1989). Similary, the anion lattice of wadsleyite
902 is best described as a distorted ccp anion lattice. Hence in comparison with olivine, the anion
903 lattice obeys an ABA- rather than ABC-stacking sequence. Wadsleyite contains edge-sharing
904 dimers of silicate-tetrahedra and is therefore a sorosilicate, whereas olivine is a nesosilicate with
905 only one tetrahedral site. In olivine the tetrahedra share sites with octahedra whereas in
906 wadsleyite they only share corners. These differences in connectivity are illustrated in Fig. 6.
907 More detailed discussions of these structures are found in (Prewitt 1980). Properly spoken, the

908 two octahedral units in olivine (M1 and M2-sites) are combinations of orthorhombic sphenoids
909 (symmetry 22) and in wadsleyite the three M-sites, are combinations of domata (symmetry mm),
910 whereas in ringwoodite (Mg_2SiO_4-spinel) the single equivalent site is a proper octahedron. One
911 notes the decreases in distortion of the M-sites from olivine over wadsleyite to ringwoodite
912 along with the pressure of the stability fields. The distortion of the M-sites reflects the deviation
913 of the anion lattice from hcp (olivine), and ccp (wadsleyite and ringwoodite). In cubic spinels like
914 ringwoodite, the anion lattice is very close to a regular ccp lattice (Hyde and Anderson 1989).

915 The olivine structure does not gradually approach the denser spinel structure upon compression
916 (Hazen 1976). Instead, above 13-15 GPa and temperatures sufficiently high to overcome kinetic
917 barriers, olivine transforms through a first order transition into wadsleyite (Rubie 1984, Yagi et
918 al. 1987, Akaogi et al. 1989). The actual transition pressure depends on the Fe-content and
919 obeys a positive Clapeyron slope (Akaogi et al. 1989). In the Earth's mantle wadsleyite replaces
920 olivine as principal rock-forming mineral below the 410 km discontinuity. This discontinuity in
921 seismic velocities is believed to be directly caused by this structural transition. The transition
922 influences the rheology of mantle rock (Rubie 1984).

923 Compression of olivine at 300 K to 40 and to above 80 GPa induces a sequence of transitions to
924 other spinelloid phases (Finkelstein et al. 2014), which have not been observed in nature. Guyot
925 and Reynard (1992) reported a phase with olivine composition, closer to regular hcp anion
926 lattice, and with cation disorder in TEM studies of a highly shocked meteorite but this phase
927 may be identical or similar to forsterite-III (Finkelstein et al. 2014). Xie et al. (2014) reported a
928 phase with olivine structure but composition $(Mg,Fe)SiO_3$ from the highly shocked Tenham L6
929 chondrite, also based on TEM studies. These interesting phases are not approved minerals.

930

Wadsleyite is an approved mineral and was discovered by Price et al. (1983) in the Peace River L6 chondrite. Thereafter, it has been found in numerous shocked chondrites. Although entrapment conditions of high-pressure inclusions observed in terrestrial diamonds extend well within the stability of field of wadsleyite (Navon et al. 2017, Tschauner et al. 2018) this major rock-forming mineral of the transition zone has not yet been found as terrestrial mineral. Endmember wadsleyite is 7.6% denser than forsterite. By its range of stability as well as by our schematics of structure fields, wadsleyite is an incipient high-pressure mineral (Fig. 5). In thin sections of standard thickness wadsleyite is noticeable through its strong emerald-green color in transmission (with Fe-contents of less than 10 at%). Wadsleyite-II is a polytype of wadsleyite that can accommodate chemically bound water (Smyth et al. 2005) but has not yet been found in nature.

Crystal chemical aspects and related phases: The wadsleyite structure is less compatible for Fe_2SiO_4 than olivine and ringwoodite (see below) and Fe-contents above 20-30mol% Fe_2SiO_4 result in coexistence with more Fe-rich phases, which are either olivine at lower or ahrensite (see below) at higher pressure (Akaogi et al. 1989). Even shock-metamorphic iron-rich olivine has been found to transform into assemblies of wadsleyite (>52) and ahrensite (>50) rather than Fe-dominant wadsleyite (Hu et al. 2017). However, recently Bindi et al. (2019) reported the discovery of Fe-dominant wadsleyite, defining the endmember asimowite (Table 1), At higher fO_2 and within the wadsleyite stability field Fe-rich orthosilicate exsolves magnetite or transforms into other ferric spinelloids, depending on pressure and temperature (Woodland et al. 2000). These Fe-rich silicate spinelloids have not yet been found in nature.

Hydrous wadsleyite

953 In 1987 J. Smyth (Smyth 1987) discovered that wadsleyite can dissolve H_2O up to several mol%.
954 The magnesium-silicate structure adapts to the water content through a transition governed by
955 a direct group-subgroup transition (Imma $\rightarrow$ I2/m). Smyth (1987) proposed that the transition
956 zone is much more hydrous than the upper mantle of the Earth. Ever thereafter this proposition
957 has been matter of active debate. A gobal stratification of the mantle along a scheme of relative
958 water abundance: 'dry' (upper mantle) – 'wet'(transition zone) – 'dry' (lower mantle) would
959 control water- and, generally, incompatible element recycling in the mantle (Bercovici and
960 Karato 2003, Hirschmann 2006). While the actual abundance of water in the deeper mantle is
961 not yet well understood, a combination of mineralogical, seismic, and experimental results
962 places increasingly better constraints on this parameter: Huang et al. (2005) provided
963 constraints of the water content of the transition zone based on mantle electrical conductivity.
964 Houser (2016) correlated experimentally determined sound velocities in hydrous and dry
965 wadsleyite and ringwoodite with seismic velocities and concluded on a generally dry transition
966 zone (comparable to the upper mantle) with few wet regions. The observation of hydrous
967 ringwoodite (Pearson et al. 2014) and ice-VII (Tschauner et al. 2018b) as inclusions in diamond
968 show that at least some regions of the transition zone mantle, which are also involved in
969 diamond formation, are quite hydrous. On the other hand diamond formation in the mantle
970 inevitably involvesmetasomatism through fluids and we cannot safely conclude the entire
971 transition zone to be subject to continuous hydrous metasomatism.

972 In shocked meteorites, wadsleyite represents shock-metamorphic levels S4 or higher (Stöffler et
973 al. 2018). In meteorites where wadsleyite is found, peak shock pressures and temperatures
974 were too low to allow for bulk rock olivine transformation. Shock compression is superadiabatic.
975 Hence, temperatures which are high enough to permit bulk rock transformation of olivine into
976 wadsleyite cause back-transformation or bulk rock melting upon adiabatic release. This is the

977 reason why incipient- and high-pressure minerals are never found as bulk rock phases in shock-
978 metamorphic environments. Instead, minerals like wadsleyite are found at locations of high
979 local temperature such as shock-melt veins and -pockets (Sharp and DeCarli 2016). Wadsleyite is
980 the only silicate mineral that has been synthesized in shock-recovery experiments (Tschauner et
981 al. 2009). Its formation on experimental sub-microsecond time scales implies crystal growth
982 rates of the order 1 – 10 m/s.

983

984 **Ringwoodite and Ahrensite**

985 Whereas olivine and wadsleyite are spinelloids, ringwoodite and ahrensite are Mg_2SiO_4 and
986 Fe_2SiO_4 in the proper spinel structure (Akimoto et al. 1965, Akimoto and Fujisawa 1968).
987 Endmember ringwoodite is 16% denser than forsterite. The degree of inversion in ringwoodite is
988 less than 4 mol% (Hazen et al. 1993). Type ahrensite and all occurrences of ahrensite that the
989 author is aware of have not shown inversion beyond uncertainty (Ma et al. 2016). Hence, both
990 phases should properly be written as $SiMg_2O_4$ and $SiFe_2O_4$ with $A^{[4]}B^{[6]}{}_2O_4$ as the structure
991 formula of normal spinel. Si-O bond distances increase from 1.63 $\pm$0.02 Å in olivine and
992 wadsleyite to 1.67 Å in ringwoodite. Yet, Si-O bond distances in bridgmanite, akimotoite, and
993 stishovite are in the range of 1.7-1.8 Å which may serve to define predominantely ionic Si-O
994 bonding in phases with constituent Si (see introductory paragraph of section 3.6 and the
995 paragraph about perovskites below). Of course, the coordination of Si by O is six-fold in
996 akimotoite and bridgmanite whereas in ringwoodite it is four-fold. This already implies an
997 extension of the bond for sterical reasons (Shannon and Prewitt 1969). However, a vacancy-
998 stabilized silicate spinel with partial inversion was recently described from shock-melt vein
999 matrices and exhibits Si-O bond distances of 1.72-1.75 Å (Ma et al. 2017, 2019) – similar to

akimotoite and bridgmanite. Taken together, ringwoodite and ahrensite are at the border between incipient- and high-pressure minerals. However, the strong preferrence for the normal spinel structure in ringwoodite and ahrensite places these two minerals rather into the class of incipient high-pressure minerals. Accordingly, the shift from ambient conditions structure stability fields in the r_A/r_B plot (Fig. 5) is less pronounced for the transition from forsterite and fayalite to ringwoodite and ahrensite respectively, than from enstatite to akimotoite or bridgmanite (see below, Fig. 8). At around 23 GPa ringwoodite decomposes into periclase and bridgmanite whereas endmember ahrensite decomposes above 15 GPa into wuestite and stishovite (Ito and Yamada, 1982, Ito and Takahashi 1989) .

Ringwoodite has been discovered in the Tenham L6-chondrite (Binns 1969) and subsequently been found in many highly shocked meteorites (for an overview: see Stöffler et al. 2018, Langenhorst and Deutsch 2012, Rubin and Ma 2017). Its occurrence is bound to the immediate vicinity of clasts within shock melt veins where the temperature at high dynamic pressure was sufficient to overcome the kinetic barrier of transforming shock-compressed olivine into its high-pressure polymorphs (Sharp and deCarli 2006). In thin sections of standard thickness ringwoodite is distinguished by a cornflower blue to purple color (when using parallel polarizers, see Fig. 7). This intense color is observed even for ringwoodite with bulk composition corresponding to chrysolith olivine (Fa < 10 mol%). Synthetic ringwoodite of similar thickness and composition has a deep green to bluish green color (e.g. in Schmandt et al. 2014). Similarly, the one observed terrestrial hydrous ringwoodite inclusion in diamond had a deep green color (Pearson et al. 2014). The reason for both, the deep color, and the difference in color between natural and synthetic ringwoodite is unknown.

Ahrensite, γ-Fe_2SiO_4, has been approved as mineral based on chemical and structural occurrence of this phase in the Tissint shergottite at the rim of shock-melt pockets which border to fayalitic rims of olivine crystals (Ma et al. 2016) but there is an earlier report about the occurrence of γ-Fe_2SiO_4 in the Umbarger L4 chondrite based on TEM analysis (Xi et al. 2002). In standard thin sections ahrensite has a bluish- to emerald green color (Ma et al. 2016).

Crystal chemical aspects: The solid solution between ringwoodite and ahrensite appears to be gapless (Fei et al. 1991): Solid solutions in the 30-60 mol% Ahr range have been found in nature and samples with 5-20 mol% Ahr have been syntheszied. The solid solution follows a symmetric mixing model. Since this has not been reported for the full set of known synthetic and natural occurrences, we show this relation here in Figure 6.

Co_2SiO_4, and Liebenbergite (Ni_2SiO_4) also transform into spinel phases at elevated pressure (Yagi et al. 1974, Morimoto et al. 1974) and break down into constituent oxides at higher pressures. A general thermodynamic assessment of silicate-spinels and their transformations can be found in Navrotski (1987).

Hydrous ringwoodite

Smyth et al. (2003) found that ringwoodite can dissolve up to 5mol% H_2O in its structure. In 2014 Pearson et al. reported the discovery of a natural hydrous ringwoodite in a sublithospheric diamond from the Juina locality in Brazil. Hydrous ringwoodite was primarily identified through its Raman-spectrum. The relevance of hydrous ringwoodite has been discussed above already.

1043

1044 Vacancy-stabilized silicate spinel with high degree of inversion

1045 As mentioned above inversion is a very minor parameter for the silicate spinels ringwoodite and
1046 ahrensite, yet, in 2017 Ma et al. (2017, 2019) found in the matrix of shock melt veins in the
1047 Tenham L6-chondrite a tetragonally distorted phase with spinel structure but composition
1048 $Mg_2Si_3O_7$. Since the structure is exactly that of a spinel mapped onto subgroup $I4_2/mnn$ the
1049 structural formula has to be written as $(Si,\square_\delta)_2(Mg,Si)O_{4-\delta}$. Interatomic distances imply that
1050 inversion is achieved through correlation of Si on the M-site with vacancies on the T-site rather
1051 than with Mg (Ma et al. 2019). Hence the hypothetic endmember of the inverted component is
1052 $(Si,\square)_2Si(O,\square)_4$. The presence of ~ 25 mol% of this component causes a spontaneous
1053 deformation of the unit cell of ringwoodite from cubic to tetragonal. A second occurrence of this
1054 phase has been found in the Sinxian L6-chondrite (Ma et al. 2019). In both meteorites this phase
1055 accounts for ~ 40vol% of the shock melt matrix. It does not occur in the similarly highly shocked
1056 Acfer040 L6-chondrite. This phase is considered a tetragonal variety of ringwoodite because the
1057 endmember component $(Si,\square)_2Si(O,\square)_4$ is below 50 mol% in all known occurrences.

1058

1059 **Post-spinel phases of transition metal oxides**

1060 In igneous and in some metamorphic rocks at ambient pressure and within the pressures range
1061 of the spinel-peridotite stability field transition metal elements like Fe, Cr, Ti, Mn often occur as
1062 spinel-type oxides. usually in complex solid solution. Magnetite and magnesiochromite have also
1063 been found as inclusions in lithospheric diamonds and in fibrous rims of diamonds (Sobolev et al.
1064 1997). Experimental studies have shown these spinels to break down in a complex fashion by

formation of simple oxides like periclase or sesquioxides like eskolaite plus ludwigite-type oxides (Akaogi et al. 1999, Ishii et al. 2014, 2015) which, at higher pressure recombine into AB_2O_4-compounds of the Ca-ferrate (harmunite), Ca-titanate, and Ca-manganite (marokite) type (Fig. 9a,b). However, not all of these structures occur for each spinel composition. For $MgAl_2O_4$ (Akaogi et al.1999) and $MgCr_2O_4$ (Ishii et al. 2015) only the Ca-titanate, but not the Ca-ferrate type structure appears to have a stability field but for $FeCr_2O_4$ both phases have been observed experimentally (Ishii et al. 2014) and in nature (Chen et al. 2003, Ma et al. 2019). In experiments the postspinel phase of $MgFe_2O_4$ has been reported to assume the marokite-type structure (Andrault and Bolfan-Casanova 2001) but the $MgFe_2O_4$-postspinel mineral maohokite assumes the Ca-titanate structure (Chen et al. 2017). For magnetite a marokite- (Fei et al. 1999) and a harmunite-type high-pressure phase are known but the former may be metastable (Ricolleau and Fei 2009).

Spinel grains in shocked martian and lunar meteorites which border to shock melt pockets and –veins have been transformed into some of these post-spinel phases. In particular, maohokite ($MgFe_2O_4$ in the Ca-titanate type structure (Chen et al. 2017)), xieite (Ca-titanate type $FeCr_2O_4$, Chen et al. 2003), chenmingite (Ca-ferrate type $FeCr_2O_4$ (Ma et al. 2019, Chen et al. 2003), and tschaunerite (Ca-titanate type $FeTi_2O_4$, Ma et al. 2018) have been found and approved as minerals. Vestaite and schreyerite are titanates with constituent Cr and V where edge-sharing dimers of face-sharing titanate octahedra establish a network similar to the postspinels but can also be described as a polysome of the α-PbO_2-type post-rutile and the pseudobrookite structure (Döbelin et al. 2006). Schreyerite forms at GPa-level pressures in the roots of orogens formed through continent-continent collisions (Döbelin et al. 2006) and vestaite is a shock-metamorphic mineral found in an H-chondrite (Pang et al. 2017).

Xieite is found right at the border of shock melt pockets and replaces chromite through incongruent growth (Chen et al. 2003). Chenmingite occurs as lamellae in shocked chromite grains in the proximity of shock melt pockets and is replaced by xieite closer to the melt, in accordance with the experimental phase diagram (Ma et al.. 2019). Tschaunerite has been found in the kernel of a transformed ulvospinel-imenite grain trapped in a shock melt pocket in the Tissint shergottite (Ma et al. 2018). The outer part of this grain was oxidized to feiite (see below) and ilmenite had reacted with melt and transformed into liuite (see below).

In a plot of r_A versus r_B the stability fields of the marokite-, harmunite-, and $CaTi_2O_4$-structures border the spinel stability field toward larger cation radii, following the general trend of pressure-induced transformations (Fig. 5). As discussed above we consider these postspinel phases of chromite, magnesiochromite, and ulvospinel as high-pressure minerals.

Feiite

Structurally related to the AB_2O_4 postspinel phases but of different stoichiometry is the X_4O_5 series of oxides with X = Fe (Lavina et al. 2011), Mg (Ballaran et al. 2015), and Ti, Cr (Ishii et al. 2014, 2015, Ma et al. 2018). AB_2O_4-postspinels are composed of rows of corner-sharing octahedra which run along the short axis of the unit cell and are connected through corner-sharing dimers in the plane perpendicular to the short axis (Fig.8a,b). The interstitial channels are also filled by a transition metal cation which assumes a rather irregular polyhedron with high coordination. The octahedra in these structures are more or less strongly distorted. In feiite and in ludwigite-type X_4O_5 these rows of corner-sharing octahedra are linked to adjacent rows through joined corners into corrugated sheets with two- and three-member rows, respectively (Fig. 9c,d). Similar structural patterns as in the postspinel transition metal oxides are assumed by pseudobrookite and related minerals, where, however, the rows of corner-sharing distorted

1111 octahedra are offset as dimers (Wyckhoff 1960). In 2018 feiite, $(Fe,Ti,Cr)_4O_5$ was approved as
1112 mineral (Ma et al. 2018). It occurs at the rim of a fromer ulvospinel-ilmenite grain that was
1113 trapped in a shock-melt pocket in the Tissint shergottite and transformed into tschaunerite,
1114 liuite, and feiite.

1115 **Crystal chemical aspects:** The natural $(Fe,\ldots)_4O_5$ shows that this type of structure is quite
1116 compatible with Ti and Cr (Ma et al. 2018). Experimental studies (Ballaran et al. 2015) showed
1117 the existence of a series of intermediate structures and solid solutions along the Fe_4O_5-MgO
1118 joint.

1119 High-pressure polymorphism and sensitivity to compositional parameters makes the postspinel
1120 and the X_4O_5 transition metal oxides interesting probes of temperature at high pressure: For
1121 instance the occurrence of chenmingite in shocked shergottites is bound to lower temperatures
1122 than xieite (Ishii et al. 2014, 2015, Ma et al. 2018). Since the solubility fo Ti and Cr in majoritic
1123 garnet increases with pressure, the occurrences of free postspinel phases in DMM appears not
1124 likely. However, the recent observation of an ilmenite inclusion in a sublithospheric diamond at
1125 a residual pressure of 10(2) GPa (Tschauner et al. 2018b) indicates that elements like Ti can be
1126 enriched sufficiently to form free phases in diamond-bearing mantle in the transition zone. If
1127 found as mantle-derived mineral inclusions in diamond these postspinel phases and feiite are
1128 potential probes of redox conditions through their ferric components. Inclusions with lamellar
1129 intergrowth of periclase with magnesioferrite have been suggested to have formed retrogradely
1130 from Mg-bearing feiite (Wirth et al. 2011).

1131 In an intermediate pressure regime transition metal spinels decompose into sesquioxides and
1132 ludwigite-type oxides (Ishii et al. 2014, 2015). Ludwigite-type oxides have not been observed so
1133 far in nature. Presently, their relevance is based on this absence of observation since it indicates

that pyroxene lamellae in chromites from podiform chromitite bodies in ultrahigh pressure terrains are unlikely to reflect a former silicate-component in precursor xieite or chenmingite in the transition zone: Upon ascent xieite and chenmingite would have decomposed into eskolaite and ludwigite-type oxides but none of these phases have been observed in those rocks (Ishii et al. 2014, 2015, Akaogi et al. 2018). We note a single observation of eskolaite (Cr_2O_3) as inclusion in diamond (Sobolev et al. 1997) which may be product of break down of chromite to eskolaite and a ludwigite-type oxide at pressures of the deep upper mantle. However, the corresponding ludwigite-like oxide has not been observed. The mineral ludwigite, $Mg_2Fe^{3+}(BO_3)O_2$, is not a high pressure mineral but its structure is closely related to the oxides discussed in this section (Figure 9d).

Dense hexagonal oxide structures with octahedral layers

Corundum is the stable phase of Al_2O_3 at reference conditions (α-Al_2O_3), it is also a phase of extremely high relative electron density (ρ/Z), similar to diamond and to periclase. Consequently, corundum does not undergo any structural transition up to ~ 70 to 90 GPa (Lin et al. 2005).At these high pressures Al_2O_3 is not expected to occur as a free phase. However, corundum is also the prototype of a large structure family of sesquioxides with ratio of cation-anion radii larger or equal to 1.0. At larger ratios sesquioxides assume the bixbyite- or related structures (Roth 1957). The corundum structure is composed of layers of octahedra, with trigonal faces oriented along 6-axis, equivalent to hcp but with central octahedron on the 6_3 axis missing ('dioctahedral' layering). This arrangement is also the basic pattern of many hydroxides and oxyhydroxides and of the dioctahedral hydroxide sheets in phyllosilicates. Coupled substitution of the trivalent by a

1156 di- and a tetravalent cation comes in most cases with ordering and breaking of mirror symmetry
1157 perpendicular to 6-axis such as in case of ilmenite , R-3m.

1158 The occurrence of these dense octahedral phases at high pressure is rather limited by
1159 geochemical than structural constraints. Eskolaite had been reported as inclusion in a diamond
1160 (Sobolev et al. 1997) but the unit cell volume was not measured prior to extraction and the
1161 pressure of entrapment is therefore unknown. Ilmenite has been found in xenoliths from garnet
1162 peridotites, as exsolution in Cpx and olivine from deep lithospheric mantle (Griffin et al. 1992)
1163 and as inclusion in diamonds (Sobolev et al. 1997). Recently, an ilmenite inclusion was found
1164 that has been entrapped in a metasomatized, diamond-bearing region in the transition zone of
1165 Earth (Tschauner et al. 2018b).). This ilmenite was a 90-10 ilmenite geikielite solid solution. The
1166 entrapment path implies that upon release this inclusion transformed from liuite above 1000K
1167 14.6 GPa to > 18 GPa and <1500 K depending on the slope of the transition boundary (Fig. 11,
1168 Ming et al. 2006, Nishio-Hamame et al. 2012). Thus, the ilmenite inclusion is a retrograde
1169 transformation product of a (Fe,Mg)TiO_3-perovskite. Generally, the mixing gap between
1170 geikeilite and ilmenite closes at pressures of a few GPa (Linton et al. 1999) and geikielite-
1171 dominated solid solution may be expected at conditions where sublithospheric mantle is
1172 subjected to infiltration by melts or fluids. However, inclusions in diamonds may not reflect the
1173 bulk composition of surrounding mantle or fluid. Incorporation of chemically bound water in
1174 iron-titanate results in formation of minerals of the hoegbohmite series (Heiny and Armbruster
1175 2002). LIL elements are too large to be adapted by the ilmenite or hoegbohmite structures.
1176 However, carmichealite and pyrochlor-related titanates of the crichtonite series are found in
1177 garnet peridotite xenoliths in kimberlites (Haggerty et al. 1983, Wang et al. 1999) and may
1178 replace ilmenite under conditions of extensive fluid metasomatism at lithospheric mantle
1179 pressures

This is a preprint, the final version is subject to change, of the American Mineralogist (MSA)
Cite as Authors (Year) Title. American Mineralogist, in press.
DOI: https://doi.org/10.2138/am-2019-6594

1180

1181

1182 **Akimotoite and hemleyite**

1183 Akimotoite is $MgSiO_3$ isotypic to ilmenite (Horiuchi et al. 1982). It's formation in the $MgSiO_3$
1184 system at pressures above 10 GPa was shown experimentally (Kawaii et al. 1974, Ito and Matsui
1185 1979) prior to its discovery as mineral in shock-melt veins of the Tenham- and the Acfer 040 L6-
1186 chondrites (Tomioka and Fujino 1997, Sharp et al. 1997, Ohtani et al. 2004, Ferroir et al. 2008).
1187 Subsequently, akimotoite has been found in many chondrites which have experienced high-
1188 grade shock metamorphism. Its occurrence is always bound to shock-induced melting: In the
1189 Tenham, Suizhou, and Yamato chondrites akimotoite occurs in transformed opx clasts that were
1190 trapped in shock melt veins (Tomioka and Fujino 1997, Ohtani et al. 2004, Ferroir et al. 2008,
1191 Tschauner et al. 2014, 2018). In difference to those occurrences, akimotoite in Acfer040 occurs
1192 within the melt matrix (Sharp 1997). Bindi et al. (2018) reported the occurrence of $FeSiO_3$ in the
1193 ilmenite structure in the Sinxian L6-chondrite. This phase was named hemleyite. Both
1194 akimotoite and hemleyite are approved minerals. The thermodynamic stability of akimotoite is
1195 limited to rather low hemleyite-content. In fact, synthesis of akimotoite with more than 3 mol%
1196 hemleyite has consistently failed (Ito and Takahashi 1989). Tschauner et al. (2018) refined
1197 structure and unit cells of shock-generated akimotoites and obtained a binary mixing model
1198 which is nearly ideal. Hence, within the MFS system Fe prefers available energetically favorable
1199 solid solutions over dissolution in akimotoite. Based on the structure refinements the low
1200 compatibility of Fe in the akimotoite structure has been related to the rigidity of the AO_6
1201 octahedra which are egde- and corner-sharing with the SiO_6-octahedra (Tschauner et al. 2018)
1202 and the same argument has been brought forward in explaining the transition of akimotoite to

bridgmanite above 23-24 GPa based on the compressibility and evolution of the compressed structure of endmember akimotoite (Horiuchi et al. 1982).

The r_A/r_B cation ratio and the r_A radii of akimotoite and hemleyite are far below the structure field of ilmenite- and corundum type phases (Fig. 10). Instead, magnesium and iron-metasilicates are within the range of tetrahedral chain structures, which is exactly what the stable phases at low pressures are (Fig. 10). Thus, akimotoite and hemleyite are high-pressure phases. Their formation reflects a major change in chemical bonding – notably of Si-O. The Si-O bond distances in akimotoite are 1.8 Å, which compares to the Si-O bond distances in stishovite and brigdmanite, whereas in ringwoodite the distance is 1.7 Å and and olivine and wadsleyite 1.6-1.68 Å. The same observation holds for $CaSiO_3$ which also assumes an ilmenite-type structure at 7-11 GPa (Ito and Matsui 1979) but has not been found in nature. Akimotoite is an important marker of high shock metamorphic pressures in chondrites. Its occurrence in Earth appears to be limited by a) its narrow stability field, b) incompatibility of Fe. Both parameters disfavor akimotoite relative to majoritic garnet and bridgmanite in mantle rock. Stixrude and Lithgow-Bertelloni (2011) modeled pyrolitic mantle by including this mineral based on the work by Hirose and Fei (2002) which reported ~5 vol% akimotoite in transformed MORB in the 20-23 GPa range but other experimental studies on similar systems did not report formation of akimotoite (Lee et al. 2004, Ishii et al. 2018).

Zagamiite

Zagamiite is a dense layered structure of Ca-Si-Al oxide. The type material (Ma et al. 2016) and other natural occurrences (Beck et al. 2004) contain an appreciable amount of Na but an alkaline-free phase with same structure has been synthesized (Gautron et al. 1969, 1999, Akaogi et al. 2010). This phase was originally reported in experimental studies as CAS phase (Gautron et al. 1996, 1999), then observed in the Zagami martian meteorite by Beck et al. (2004) based on Raman spectroscopy and SEM-EDS. It was approved as mineral based on X-ray diffraction based structure analysis and electron microprobe analysis with the name zagamiite in 2016 (Ma et al. 2016). Zagamiite appears to be common in shock-melt pockets of shergottites. Its rather narrow stability range (Akaogi et al. 2010, Liu et al. 2019) makes it a good pressure indicator for shock-metamorphism in feldspar-bearing rocks.

Crystal chemistry: The structure is composed of dioctahedral SiO_2-layers with intermittant layers of face-sharing octahedra and larger polyhedra (Fig. 4a). The latter are occupied by Ca and alkalines whereas the face-sharing inter-layer octahedra are predominantely occupied by Al but with partial occupancy. The potentially extremely dense packing of the zagamiite structure is limited by close intercation distances in adjacent interlayer polyhedra. Mutual exclusion from these short distances results in partial occupancy and compositional variance with potential of accommodating protons.

In the CAS system zagamiite breaks down into Na-ferrate type Ca-aluminate plus stishovite above 20 GPa. In Earth the occurrence of zagamiite would be constrained to basaltic crust subducted into the transition zone but in competition with aluminous phase D (Liu et al. 2019). We note that the stability range of zagamiite-like layered oxides has not been studied beyond the CAS system and its stability may vary in a more extended compositional space.

Perovskite-type high-pressure minerals

Bridgmanite

The seismic discontinuity at 660 km depth represents the boundary between transition zone and lower mantle of the Earth. As we discussed, this boundary marks a major change in chemical and physical properties of the rock forming minerals from structures based on tetrahedrally coordinated silicate-units to oxides of Mg, Si, Fe, Ca, and Al (Fig. 2). This change is accompanied by an increase in density (Dziewonski and Anderson 1981) and in rock viscosity (Forte and Mitrovica 2000). Moroever, the high solubility of water that characterizes transition zone minerals is probably not conveyed to lower mantle minerals (Schmandt et al. 2014). Both factors together make the transition zone-lower mantle boundary a division line where a substantial portion of subducted material becomes stagnant, releases fluid and causes extensive metasomatism in the transition zone and the shallow lower mantle (Schmandt et al 2014). The deeper parts of the lower mantle are suspected to contain ancient geochemical reservoirs although their spatial scale is not known (Helffrich and Wood 2001).

The major mineral of the lower mantle is bridgmanite, $(Mg,Fe)SiO_3$ in a $GdFeO_3$-type perovskite structure (Fig. 12). This makes bridgmanite the most abundant mineral in Earth because it comprises ~ 80->90 mass% of the lower mantle, which by itself is 50 mass% of Earth (Ringwood 1979). As in the case of akimotoite, $(Mg,Fe)SiO_3$ is far outside the structure field of perovskites (Fig. 10). Starting with the low pressure pyroxene phases of $MgSiO_3$ and $FeSiO_3$, enstatite and ferrosilite, a pressure-induced trend across the ilmenite- and into the perovskite-type field can be constructed similar to the trends for ABO_4-type compounds (Manjon et al. 2007). This trend

1269 continues with the $CaIrO_3$-type postperovskite phases (Murakami et al. 2004, Ono and Oganov
1270 2004).

1271 Ringwood was the first to show that the 660 km boundary implies existence of a 'postspinel'
1272 silicate phase (see Ringwood 1979). Based on chrystal chemical reasoning and high-pressure
1273 experiments on aluminate-perovskites Reid and Ringwood (1975) proposed decomposition of
1274 ringwoodite into periclase and a perovskite- type $MgSiO_3$ phase. This hypothesis was confirmed
1275 by Liu (1975, 1976) through laser heating experiments on pyrope in a diamond anvil cell and
1276 subsequently by Ito and Matsui (1978), followed by studies of crystal structure (Ito et al. 1987),
1277 the phase boundary between ringwoodite and bridgmanite + periclase (Ito et al., 1981,
1278 Ringwood and Irifune 1988, Fei et al. 1996, Irifune et al. 1998), thermal expansion (Ross and
1279 Hazen, 1989), crystal chemical relations (Yagi et al. 1994), melting (Heinz et al. 1992, Zerr and
1280 Boehler 1994) and a wealth of other studies on structure, compressibility, elastic tensor, and
1281 thermoelastic properties which we cannot review here. The slope of the boundary between
1282 ringwoodite + garnet $\leftrightarrow$ bridgmanite + periclase is slightly negative and, thus, the reaction
1283 endothermic (Irifune et al 1998). McCammon et al. (1997) observed that bridgmanite contains
1284 appreciable amounts of ferric iron. Subsequent experimental work under different redox
1285 conditions indicated that the presence of ferric iron in bridgmanite is result of a pressure-
1286 induced disproportionation of ferrous iron into metallic iron and ferric iron (Frost et al. 2004,
1287 Frost and McCammon 2008). The volume of the ferric Fe-O polyhedra in bridgmanite experience
1288 marked reduction at lower mantle pressures due to the high spin- low spin transition of ferric
1289 iron. This effect has been analyzed in a number of studies which are summarized by McCammon
1290 et al. (2013).

Due to the high pressure of its stability field and the low kinetic barrier of back transformation to pyroxenes at lower pressure, the search for natural occurrences (and therfore, approval as a mineral) had focused on highly shocked meteorites (Mori 1994, Tomioka and Fujino 1997, Sharp et al. 1997) where release from high pressures and temperatures is fast (see below). Other than akimotoite, bridgmanite rapidly vitrifies in the beam of the electron microscope and direct structural information has to be obtained with different means.

Ultimately $MgSiO_3$-perovskite was proved to exist in the highly shocked Tenham L6 chondrite by using synchrotron-micro diffraction in combination with electron microprobe analysis and named bridgmanite after Percy W. Bridgman (Tschauner et al. 2014). Bridgmanite occurs along with akimotoite in transformed enstatite clasts trapped in shock melt veins in the Tenham meteorite. Ma et al. (2016) also reported an occurrence in shock melt pockets of the Tissint shergottite where olivine and fayalite grains in the vicinity of the melt pockets were transformed into ringwoodite and ahrensite and at the immediate border have broken down to periclase plus bridgmanite and wuestite plus bridgmanite, respectively (Fig. 13).

Subsequently, vitrified or vitrifying metasilicate intergrown with periclase in Tissint and other meteorites was identified as former bridgmanite (Miyahara et al. 2016, Hu and Sharp 2017). Direct observation of the terrestrial occurrence of bridgmanite is extant. Periclase-enstatite assemblies as inclusions in diamonds have been interpreted as former bridgmanite-periclase aggregates from the Earth's lower mantle (Kesson and Fitz Gerald 1991, Harte and Harris 1994, Harte et al. 1999, Stachel et al. 2000, 2008, Kaminsky 2012).

Jeffbenite (Harris et al. 1997, Nestola et al. 2016), see section 3.6), a silicate phase with unique structure and garnet-like composition along the pyrope-almandine joint (Finger and Conrad

2000), has been interpreted as retrograde transformation product of aluminous bridgmanite, based on experimental studies in the pyrope-almandine system (Armstrong et al. 2012).

Crystal chemistry: As a $GdFeO_3$-type perovskite, bridgmanite exhibits tilt of the corner-sharing SiO_6-octahedra to a degree where the polyhedron of the A-cation approaches a 6+6 arrangement rather than the dodecahedron of the cubic perovskites (see Fig. 12 and for detailed discussion Ito et al. 1987, Ross and Hazen 1989). This strong distortion of the perovskite structure is rather pressure- and temperature-invariant (Stixrude and Cohen 1993, Fiquet et al. 2000) and controls some of the crystal chemical properties of brigdmanite. For instance, the rigid inter-octahedral bonding probably accounts for the high Debye temperature of ~ 1000K and the high elastic moduli (Sturhahn et al. 2005), the high melting temperature (Zerr and Boehler 1994) and plastic deformation limit, and the absence of distortive phase transitions. As phase within the MFS system bridgmanite is not a binary but at least ternary solid solution because of the presence of ferric Fe. Ferric iron can be suppressed only for less than 4at% Fe in bridgmanite (Parise et al. 1990). Vanpethegem et al. (2006) presented structure analyses which showed ferric Fe to reside only on the A site. Crystal field splitting of ferric bridgmanite require more than one site for Fe^{3+} (Sturhahn et al. 2005). Hummer (2012) compared volume data for synthetic Fe-bearing bridgmanites and concluded that some ferric iron resides on the B-site as well. Natural bridgmanite is comparatively Fe-rich and follows the trend that Hummer proposed (Tschauner et al. 2014). The compatibility of ferric iron with the brigdmanite structure is relevant for the apparent, if not effective, redox state of the lower mantle. This compatibility for ferric iron has to be placed in context with the proposed disproportionation of ferrous iron at lower mantle pressures (Frost et al. 2004): In a static system the actual redox state could remain

as reducing as bulk silicate Earth composition suggests but segregation of metallic iron could shift the redox state of the lower mantle toward more oxidized conditions.

Al_2O_3 dissolves in bridgmanite up to few mol% through coupled substitution on both A- and B-site (Andrault et al. 2003). It has been observed that Al- and Fe-solubility strongly correlate through the presence of ferric iron in the bridgmanite lattice (Vanpetheghem et al. 2006b, Frost and McCammon 2008). A ferric endmember $Fe(Fe,Si)O_3$ has been reported by Bykova et al. (2017).Ca and Ti have been found rather incompatible in bridgmanite but as we indicate below, type liuite, $FeTiO_3$ perovskite, contains ~ 40% bridgmanite.

Transition metal elements in bridgmanite

The solubility of Ni and Co in bridgmanite increases with pressure in chemical exchange with metallic iron (Tschauner et al. 1998). The pressure-dependence of the Ni-solubility scales with the reaction volume of the nickel-bunsenite system normalized by FeO (Campbell et al. 2006) and is therefore a general phenomenon that is probably related to the high-spin-low spin transition of ferric iron and the disproportionation of ferrous iron (Frost and McCammon 2008). Ohtani et al. (1997) reported partition coefficients of Ni, Co, Cr, Mn, V for brigdmanite and silicate melts at 24 GPa.

Above 120-140 GPa bridgmanite transforms into a $CaIrO_3$-type postperovskite phase (Murakami et al. 2004, Ono and Oganov 2004, Hirose 2006) following a positive Clapeyron slope. The possible effect of this transition onto the petrology of the lowermost lower mantle, the D”-layer (Fig. 2), is subject of active debate (for a review see Hirose 2006)

As shock-metamorphic mineral, bridgmanite constraints dynamic compression processes in three ways: 1) through the high pressure of formation above 23 GPa, 2) through the steep

increase of solidus and liquidus of brigdmanite-bearing rock above 23 GPa, 3) through the low kinetic barrier of back transformation into low pressure metasilicate phases or into glass. Combining these three parameters it could be shown that the peak shock pressures of the Tenham meteorite were 24-27 GPa at 2500-2700 K, and that the release path involves a regime of rapid cooling on the order of 100K/μs at pressures above 20 GPa (Tschauner et al. 2014).

$CaSiO_3$-perovskite

$CaSiO_3$ follows a similar trend of pressure-induced transformation as $MgSiO_3$. At ambient pressure calcium metasilicate assumes a pyroxenoid structure (wollastonite, see Fig. 10) As in the case of $MgSiO_3$ a high-pressure ilmenite and a perovskite phase become stable above 10 and 15 GPa, respectively (Ito and Matsui 1982). Upon release to ambient conditions both high-pressure phases vitrify sponteneously and consequently they have not been observed in shocked meteorites. Conservation as inclusions in diamonds at elevated residual pressure seems possible. Nestola et al. (2018) showed that inclusions with intergrowth of perovskite and wollastonite in diamonds from Juina, Brazil shoud be interpreted as former Ca $(Si,Ti)O_3$ perovskite. A number of mixed Ca silicate-titanate-ferrate perovskites occur within the Ca-Ti-Fe-Si-O system at high pressures (Leineweber et al. 1995, 1997).

$CaSiO_3$ perovskite is a cubic or pseudocubic tetragonal ABO_3 perovskite (Fig 11 a, recently re-evaluated by Chen et al. 2018). As figure 10 shows, the sequence wollastonite $\rightarrow$ CaSi-ilmenite $\rightarrow$ CaSi-perovskite does not follow a monotonous trend of r_A/r_B relations, such as $MgSiO_3$. In fact, $CaSiO_3$ does not transform directly from a pyroxenoid to ilmenite. Both phases are separated by a region of partial decomposition into coesite and breyite (see 3.9) (Ito and Matsui 1982). $CaSiO_3$ perovskite has been synthesized in experimental studies on MORB-like bulk compositions at

lower mantle pressures (Hirose and Fei 2002, Lee et al. 2004, Liu et al. 2012, 2019, Ishii et al. 2018) where it owes its presence to the high compatibility fo Al in bridgmanite which, by mass balance, inhibits formation of dense Ca-aluminates. Minor accessory $CaSiO_3$-perovskite may be important in the mantle as host of K as heat-generating element through the decay of ^{40}K into ^{40}Ca.

The $FeTiO_3$-perovskites liuite and wangdaodeite

Wangdaodeite is $FeTiO_3$ in the $LiNbO_3$-type rhombohedral perovskite structure (Fig. 12c). It was discovered in the highly shocked Suizhou L6-chondrite by Xie et al. (2016) and is an approved mineral. The transformation of pure $FeTiO_3$ from the ilmenite to the $LiNbO_3$-type rhombohedral perovskite at 15 GPa was reported in an experimental study by Leineweber et al. (1995) and the transition was found to be reversible. The natural wangdaodeite appears to be stabilized by vacancies or minor chemical components that appear to inhibit back-transformation (Berry et al. 2000). Experimental work (Ming et al. 2006, Akaogi et al. 2017) showed that above 20 GPa $FeTiO_3$ transforms from the rhombohedral $LiNbO_3$- to an orthorhombic $GdFeO_3$-type perovskite structure but upon reversal the $GdFeO_3$-type perovskite phase transforms directly back into ilmenite. Hence, wangdaodeite is a metastable structure. Its observation in shocked meteorites indicates that it can form at high stress rates and stress-release rates. The $GdFeO_3$-type perovskite phase was recently discovered in the Tissint meteorite and is also approved as a mineral with the name liuite (Ma et al. 2018). As in the case of wangdaodeite, pure endmember liuite is expected to transform back into ilmenite at ambient pressure but the type material contains ~ 40 mol% bridgmanite. Both liuite and wandaodeiite are high-pressure minerals since their rFe/rTo ratio is far outside the structure field of perovskites (Fig. 10).

1404 As mentioned above, ilmenite as inclusion in diamond at 10-12 GPa remnant pressure is very
1405 likely a retrograde transformation product of liuite because the release path from mantle
1406 conditions intersects the ilmenite-liuite phase boundary (Figure 12, Tschauner et al. 2018b). We
1407 cannot anticipate a more detailed description of these new minerals here but point out the
1408 interesting fact that type liuite contains almost 40 mol% bridgmanite (Ma et al. 2018).

1409

1410 **3.7. Carbonates, Sulfates, and other minerals with complex anions.**

1411 The pressure effects on salts of complex anions have been studied experimentally to some
1412 extend (see for instance Manjon et al. 2007 for ABO_4 phases). Many of them, such as borates,
1413 tungstates, and molybdates are constituted by elements geochemically too rare to be expected
1414 to form free phases within the mantle although the partitioning of these elements between
1415 mantle phases is of geochemical interest. Sulfates are not expected in the mantle because the
1416 redox conditions support sulfides over sulfates or sulfites.Wirth et al. (2009) reported an
1417 inclusion of anhydrite from a diamond, probably reflecting local oxidizing conditions.

1418 Carbonates are of particular interest in the Earth's mantle because they take part in the deep
1419 carbon cycle (see for instance Shirey et al. 2013, Thomson et al 2016). High-pressure phase
1420 transformations of calcite and aragonite have been observed in experiments (Merlini et al. 2013,
1421 2014, Smith et al. 2018b), others have been predicted (Oganov et al. 2013). Navon (1991)
1422 reported infrared spectra of carbonate-bearing diamonds where the energy of the CO_3^-
1423 assymetric stretching vibration indicates elevated remnant pressure of carbonate inclusions.
1424 Tschauner et al. (2018b, 2019) reported X-ray diffraction data of magnesian calcite inclusions
1425 and determined remnant pressures as high as 7.0 ± 0.5 GPa but no high-pressure polymorph of
1426 calcite or aragonite has been found so far. The absence of high-pressure polymorphs of calcite is

1427 due to the magnesite-component in solid solution, which generates a large negative excess
1428 volume thus stabilizing the calcite structure relative to high-pressure polymorphs. Under mantle
1429 conditions carbonates break down through reaction with enstatite. In eclogitic environments
1430 carbonates are stabilized to higher pressure and temperature (Thomson et al. 2016) as cation-
1431 disordered dolomite. It is not yet clear why calcite inclusions in diamond contain rather high
1432 magnesite concentrations where disordered $(Ca,Mg)CO_3$ is expected to decompose into
1433 magnesite and aragonite (Buob et al. 2006) upon cooling during ascent of their host diamonds in
1434 the mantle.

1435

1436 **3.8 Silicates**

1437 The most important rock forming silicates and silicic high-pressure oxides have already been
1438 discussed in the section about oxides and do not need to be recapitulated. Generally, silicates in
1439 the proper sense are based on covalently bonded SiO_4 or alumosilicate as building blocks.
1440 Therefore silicates in the proper sense belong to the class of low- to intermediate-pressure
1441 minerals because their formation does not involve a major change in this fundamental chemical
1442 bonding pattern. Because of the abundance of Si and O , and the manifold topological
1443 possibilities of arranging isolated or corner-sharing alumosiicate or silicate tetrahedral along
1444 with other ions, silicates are the dominant phases in the Earth's crust and upper mantle (Fig. 2)
1445 and occur in a vast number of mineral species. A general effect of pressure can be distinguished
1446 here as well: Structures assumed by silicates with constituent high-Z cations are assumed by
1447 silicates with smaller, less heavy cations at higher pressure. For example, walstroemite and
1448 cymrite are Ba-silicate minerals, wadeite is a K-Zr silicate. Breyite, the isotypic 'Ca-walstroemite'
1449 has been found as inclusions in diamonds that originate in the sublithospheric mantle (Stachel et

al. 2000,2008, Anzolini et al. 2016, Brenker et al. 2018). Experimental studies show existence of K-Al cymrite and –wadeite phases (Yagi et al. 1994, Yong et al. 2006) which well could exist in deep subducted slabs but have not yet been found as minerals. This trend is in accordance with the direction of pressure-driven transformation observed for other chemical classes of minerals such as the elements and oxides (see Introduction). However, the structural flexibility of silicates also permits formation of a wealth of incipient high-pressure phases which have no equivalent at ambient pressure such as the minerals lawsonite, jeffbenite (see below) and of synthetic phases which potentially occur in Earth such as the 'NAL-phase' (Pamato et al. 2014), 'phase Egg' (Eggleton et al. 1978), and a high pressure post-kaolin phase (Hwang et al. 2017).

Dense hydrous Mg-silicates

Dense hydrous Mg-silicates are expected to occur in mantle peridotite dragged along with subducted slabs and metasomatized by hydrous fluid released from the slabs . Presently they have not been reported as minerals. Structurally they are not members of one family. Some, like phase B and E, are spinelloids, whereas phase A and G are layered structures composed of octahedral sheets with intermittent tetrahedra, and phase F is a dense octahedral layer structure (Prewitt and Downs 1998, Angel et al. 2001). The so called '10-Ångstroem phase' is a mica closely related to phlogopite but with H_2O substituting for K and with much lower Al content (Comodi et al. 2005).

Reidite

Silicates with high field strength elements as constituting cations undergo mainly reversible continuous transformations such as the transformation from zircon to reidite ($ZrSiO_4$ in the scheelite-type structure, Reid and Ringwood 1969, Glass et al. 2002). Reidite is important in identifying and dating terrestrial and martian impacts (Glass et al. 2002, Cavosie et al. 2015). The transition from zircon to reidite is caused by sublattice shift and subsequent loss of the mirror-symmetry perpendicular to the 4-fold axis. Thus, reidite is an incipient high-pressure mineral despite it's relatively high pressure of formation. At higher pressure $ZrSiO_4$ and other silicates of high field strength elements ultimately break down into oxides (Tange and Takahashi 2004).

Pyroxenes

Like the minerals of the olivine series pyroxenes have one tetrahedral and two distorted octahedral sites. However, pyroxenes are inosilicates and tilting or twisting of the chains of corner-sharing tetrahedra allows for accommodating a much larger range of structural and compositional variations than olivine. In particular, pyroxenes accommodate coupled substitution of monovalent ions on their M-sites along with Al substitution on the T-site or the substitution of two Al on M1 and T-site (Tschermak-component), which both is not possible in olivine. In addition to proper pyroxenes there are also pyroxenoids which exhibit different periodicities of the tetrahedral chains and amphiboles where two chains are combined to ribbons. Pyroxene-type silicates, pyroxenoids and amphiboles are low- to intermediate pressure minerals (Fig. 2) whereas high-pressure pyroxene-type polycarbonates (Oganov et al. 2013) have not been found as minerals. Hence, detailed account on pyroxenes and related structures in not within the scope of this paper and can be found elsewhere (Prewitt 1980). Pyroxenes react to elevated and high pressure through three principal mechanisms:

1) Volume reduction through structural modification. Pyroxenes undergo reversible transitions upon compression. In particular above 5 -7 GPa enstatite undergoes a transition to a C2/c-type clinopyroxene, which is different for high-temperature clinoenstatite at ambient pressure (Angel et al. 1992). This high-pressure clinoenstatite is expected to occur in fertile mantle peridotite but has not yet been found as a mineral. It may be captured as inclusion with sufficiently high remnant pressure in P-type (peridotitic) diamonds. A large number of structural transitions in pyroxenes and pyroxenoids of different composition have been observed in experiments and are mostly confined to a regime of low-temperatures compared to the mantle geotherm but their occurrence in cold slabs has been discussed (Woodland and Angel 1997, Dera et al. 2013, Plonka et al. 2012, Xu et al. 2018).

2) New endmembers such as jadeite $NaAlSi_2O_6$ occur at elevated pressure. Omphacite, a complex solid solution with dominant jadeite-component is a rock-forming mineral in eclogite (e.g. Liou et al. 2009).

3) Coupled substitution which involves vacancies on the M1 site. This partial vacancy permits additional compression of the pyroxene structure. Thus, this mechanism combines chemical and structural aspects of the first and the second mechanism. The most prominent vacancy-based high-pressure pyroxene is the Ca-Eskola endmember Ca (Al,.) Si_2O_6, which dominates over kushiroite (the Tschermak endmember Ca Al $(Si,Al)_2O_6$,) at elevated pressures (McCormick 1980). Tissintite is a Ca-Eskola rich pyroxene which occurs in shocked meteorites (Ma et al. 2016) and terrestrial impactites (Walton et al. 2018). Tissintite defines regimes of intermediate dynamic pressure and temperatures during shock-metamorphism (Walton et al. 2018, Ma et al. 2016, Herd et al. 2011,Sharp et al. 2018).

Garnets

Garnets are compounds with composition $X_3Y_2T_3O_{12}$, where T can be Si, Ge, Al, Ga, P, As, and even Li (in synthetic materials). Site X is a large, roughly dodecahedral site, Y is a smaller octahedral, and T is a tetrahedral site. Silicate-garnets are nesosilicates because the Si-tetrahedra are isolated although the Y-T sites form strong cage-like networks around site X, if Y is occupied by Al or Si. Sites X and Y can accommodate a large variety of cations with full or partial occupancy and consequently, there is a large number of silicate garnet endmembers (Grew et al. 2012). Pyrope-dominated complex garnet solid solutions are rock forming minerals in garnet-peridotite and in eclogite. High pressure favors Si substitution on site Y through coupled substitution (Na+ Si) = Al + Cr (Collerson et al. 2010). In addition the combined substitution of ferrous and ferric iron on sites X and Y is favoured by pressure (at given O-activity) and defines the skiagite-endmember which is not stable at ambient pressure (Woodland et al. 1999). Pressure favours accommodation of Si on the Y-site as majorite-component defined through the endmember majorite, $Mg_3(Mg,Si)_2Si_3O_{12}$, (Smith and Mason 1970) and Ca $_3(Mg,Si)_2Si_3O_{12}$ (Hazen et al. 1994). Majorite is a mineral which was discovered by Smith and Mason (1970) in the Coorara L6 chondrite but has been known as synthetic phase earlier (Ringwood 1967). Majorite and garnets with high majorite component have been found in shocked meteorites (Langenhorst and Deutsch 2012, Rubin and Ma 2017), terrestrial impactites (Staehle et al. 2011, Walton et al 2018) and as inclusions in terrestrial diamonds that have formed in the transition zone or lower mantle (Stachel&Harris 2008, Collerson et al. 2010).

Ca $_3(Mg,Si)_2Si_3O_{12}$ has been synthesized but not yet been described as mineral but is a minor component in majorite and other garnets that formed at high pressures. This phase exhibits a tetragonal distortion of its unit cell from site ordering of Si and Mg (Hazen et al. 1994). Recently

the time-scale of this site ordering has been used to assess time scales of temperature-release in shock melt veins (Tomioka et al 2017) in agreement with the assessments based on the occurrence of bridgmanite in similar highly shocked meteorites (Tschauner et al. 2014). Tetragonal distortion was also found in an almandine-majorite solid solution that occurred in a shock-melt pocket of the Shergotty martian meteorite (Ma et al. 2016).

The stability of majorite-rich garnets extends to about 30 GPa where they transform into aluminous bridgmanite (Irifune et al. 1998). Containing both four- and six-fold coordinated Si majorite is an incipient high-pressure mineral. This is reflected in the gradually increasing occupancy of the Y-site by Si along with increasing pressure and its ultimate transformation into bridgmanite.

Jeffbenite is a silicate with composition along the almandine-pyrope joint but of a structure very different from garnets (Conrad and Finger, Nestola et al. 2018). We have discussed it's possible relation to alminouns bridgmanite further above.

3. 9 Phosphates

The general statements about silicates can be extended to phosphates which are also based on tetrahedral PO_4 building blocks with the possibility of polymerization (Huminicki and Hawthorne 2002). One interesting difference between silicates and phosphates is the much larger flexibility of intertetrahedral P-O-P bonds. For instance, berlinite $AlPO_4$ can be compressed by about 50 GPa without structural rearrangment other than a gradual approximation of adjacent tetrahedra (Klug and Tse 1994). Consequently, high pressure phase transformation in phosphates are mostly reversible and between structures related through group-subgroup relations (see for

instance Errandonea and Manjon 2008). Tuite is a polymorph of anhydrous Ca triphosphate that forms above 10 GPa and occurs in shocked chondrites and shergottites (Xie et al. 2003). It's structure represents a denser rearrangement of a tetrahedral phosphate network with central channel, filled by Ca. Thus, tuite is an intermediate-pressure mineral. Similarly, merrillite forms through shock-induced dehydration of whitlockite above 5 GPa and this experimentally obtained finding may explain the dominance of merrillite over whitlockite in many extraterrestrial environments such as martian, lunar, and primitie meteorites (Adcock et al. 2017).

Finally, we note an extensive isotypism or homoiotypism between phosphates and silicates (Huminicki and Hawthorne 2002). The larger flexibility of intertetrahedral bonds or bonds between tetrahedra and other polyhedra in phosphates then accounts for more variability in chemical substitution than in the structurally equivalent silicates (e.g. olivine cannot accommodate coupled substitution of alkalines plus Al above trace level, in contrast to the olivine-like phosphates triphylite and lithiophorite). This larger flexibility also accounts for the observation that many phosphates assume structures at low or ambient pressure which are isotypic or closely related to incipient high-pressure silicates such as phosphate-ellenbergerite and ellenbergerite, phosphates of the mozartite- chopinite series and Mg-silicate spinelloids. However, for the same reason phopshates with octahedrally cordinated P do not exist.

4. Summary

High-pressure minerals are a minor subset of the known minerals but they are key in understanding the deep Earth, shock-metamorphism, and in modeling other planets. Over the

1584 past decade the number of known high pressure minerals has largely increased. Therefore a
1585 comprehensive overview and a definition of high-pressure minerals is a timely matter.

1586 The pressures of the deeper interior of Earth are sufficient to cause noticeable differences in
1587 chemical behaviour of elements, notably in Si and Fe. These changes induce structural
1588 transformations of rock forming minerals, which mark the major divisions in the Earth's mantle:
1589 Upper mantle, transition zone, and lower mantle. The pronounced effect of pressure on the
1590 chemical and, consequently, the physical properties and structures of minerals makes Earth
1591 different from smaller rocky planets like Mars.

1592 Not only the major divisions in the Earth mantle but also structures and properties of many
1593 accessory minerals as well as those of the iron-rich metal in the core are controlled by the effect
1594 of pressure. Accessory high-pressure minerals reflect the differentiation of less and
1595 incompatible elements in the deeper mantle. This large array of pressure-induced structural
1596 changes and phases make it important to examine if high-pressure minerals can be defined as a
1597 distinct category of solid phases which differ from their equivalents at low or ambient pressure.
1598 We define high-pressure minerals by the general notion that their stability fields do not
1599 intersect ambient pressure. However, this criterion is insufficient and does not capture the
1600 effect of pressure-induced changes in chemical properities of the constituent elements.
1601 Therefore, we complement this criterion with two others: 1) that their structures place the high-
1602 pressure minerals clearly outside the structure tolerance fields defined through their ambient
1603 pressure ionic radii. 2) that their structures follow the correlation between pressure of phase
1604 stability and the nuclear charge number. Minerals whose stability field is beyond ambient
1605 pressure but whose structures are within the tolerance fields of their ionic radii are defined as
1606 incipient high-pressure minerals. Their structures reflect sterical rearrangements of atoms and

polyhedral units under the effect of pressure but without basic changes in chemical bond states which occur in proper high-pressure minerals. The distinction between low-, incipient- and high-pressure minerals reflects the principal divisions in the Earth's mantle into upper mantle transition zone, and lower mantle and lower mantle and is therefore useful in correlating mineralogical observations with the geochemistry and –physics of the deep Earth.

We discuss all currently known high-pressure minerals and a number of incipient high-pressure minerals and indicate their relevance in the study of the deep Earth, impacts, meteorites, and planetary interiors.

Acknowledgements:

This work was supported through NSF EAR-1838330. The author thanks two anonymous reviewers, the editor D. Baker, and the associate editor M. Ballmer for their helpful comments, R. Russell and K. Bailey for their technical support, and K. Putrika for the suggestion and encouragement to write this paper.

References:

Adcock, C.T., Tschauner, O., Hausrath, E.M., Udry, A., Luo, S.N., Cai, Y., Ren, M., Lanzirotti, A., Newville, M., Kunz, M., and Lin, C. (2017) Shock-transformation of whitlockite to merrillite and the implications for meteoritic phosphate. Nature Communications, 8, 14667.

Agrosi, G. et al. (2017) Non-destructive, multi-method, internal analysis of multiple inclusions in a single diamond: First occurrence of mackinawite (Fe,Ni)(1+x)S. American Mineralogist, 102, 2235-2243.

Ahrens, T.J., and Gregson, V.G. (1964) Shock compression of crustal rocks – data for quartz, calcite + plagioclase rocks. Journal of Geophysical Research, 69, 4839.

Ahrens, T.J., Petersen, C.F., and Rosenberg, J.T. (1969) Shock compression of feldspars. Journal of Geophysical Research, 74, 2727.

Ahrens, T.J. (1986) Application of shock wave data to earth and planetary science, in Shock Waves in Condensed Matter, edited by Y.M. Gupta, pp. 571-588, Plenum, New York.

Akaogi, M. Ito, E., Navrotsky, A. (1989) Olivine-modified spinel-spinel transitions in the system Mg2SiO4-Fe2SiO4 – calorimetric measurements, thermochemical calculation, and geophysical application. Journal of Geophysical Research – Solid Earth and Planets, 94, 15671 – 15685.

Akaogi, M., et al. (1999) High pressure transitions in the system MgAl2O4-CaAl2O4: a new hexagonal aluminous phase with implication for the lower mantle. Physics of the Earth and Planetary Interiors, 115, 67-77.

Akaogi, M. et al. (2010) High-pressure phase relations in the system CaAl4Si2O11-NaAl3Si3O11 with implication for Na-rich CAS phase in shocked Martian meteorites. Earth and Planetary Science Letters, 289, 503-508.

Akaogi, M., et al. (2017) High-pressure high-temperature phase relations in $FeTiO_3$ up to 35 GPa and 1600 A degrees C. Physics and Chemisty of Minerals, 44, 63-73.

Akaogi, M. et al. (2018). High-pressure phase transitions in MgCr2O4.Mg2SiO4 composition: Reactions between olivine and chromite with implications for ultra-high chromitites. American Mineralogist, 103, 161-170.

1651 Akimoto, S.I., Fujisawa, H., and Katsura, T. (1965) Olivine-spinel transition in Fe2SiO4 and
1652 Ni2SiO4. Journal of Geophysical Research, 70, 1969.
1653 Andrault, D. and Bolfan-Casanova, N. (2001) High-pressure phase transformations in the
1654 MgFe2O4 and Fe2O3-MgSiO3-systems. Physics and Chemistry of Minerals, 28, 211-217.
1655 Andrault, D., Bolfan-Casanova, N., and Guignot. N. (2001) Equation of state of lower mantle
1656 (Al,Fe)-MgSiO3 perovskite. Earth and Planetary Science Letters, 193, 501-508.
1657 Angel. R.J., Chopelas. A., and Ross, N.L. (1992) Stability of high-density clinoenstatite at upper-
1658 mantle pressures. Nature, 358, 322-324.
1659 Angel, R.J., Frost, D.J., Ross, N.L., Hemley, R. (2001) Stability and equations of state of dense
1660 hydrous magnesium silicates. Physics of the Earth and Planetary Interiors, 127, 181-196.
1661 Angel, R.J., Mazzucchelli M.L., Alvaro, M. Nimis, P. and Nestola, F. (2014) Geobarometry from
1662 host-inclusion systems: The role of elastic relaxation. American Mineralogist, 99, 2146-
1663 2149.
1664 Anzellini, S., Dewaele, A., Mezouar, M., Loubeyre, P., and Morard. G. (2013) Melting of iron at
1665 Earth's inner core boundary based on fast X-ray diffraction. Science, 340, 464-466.
1666 Anzolini, C., et al. (2016) Depth of formation of CaSiO3-walstromite included in super-deep
1667 diamonds. Lithos, 265, 138-147.
1668 Aoki, K., Yamawaki, H., Sakashita, M., Gotoh, Y., Takemura, K. Crystal-structure of the high-
1669 pressure phase of solid CO2. Science, 263, 356-358.
1670 Armstrong, L.S. and Walter M.J. (2012) Tetragonal almandine pyrope phase (TAPP): retrograde
1671 Mg-perovskite from subducted oceanic crust? European Journal of Mineralogy, 24, 587-
1672 597.
1673 Armstrong, L.S. et al. (2012) Perovskite phase relations in the system CaO-MgO-TiO2-SiO2 and
1674 implications for deep mantel lithologies. Journal of Petrology, 53, 611-635.

Asimow, P.D., Lin. C, Bindi. L, Ma, C., Tschauner, O., Hollister, L.S., and Steinhardt, P.J. (2016) Shock synthesis of quasiecrystals with implications for their origin in asteroid collisions. Proceedings of the National Academy of Sciences of the United States of America, 113, 7077-7081.

Ballaran, T.B., Uenver-Thiele, L., and Woodlang, A.B. (2015) Complete substitution of Fe2+ by Mg in Fe4O5: The crystal structure of the Mg2Fe2O5 end-member. American Mineralogist, 100, 628-632.

Bassett, W.A., Takahashi, T., Mao, H.K., and Weaver, J.S. (1968) Pressure-induced phase transformation in NaCl. Journal of Applied Physics, 39, 319 -325.

Beck, P., Gillet, P. Gautron, L., Daniel, I., and El Goresy, A. (2004). A new nat- ural high-pressure (Na,Ca)-hexaluminosilicate [(CaxNa1 x)Al3+xSi3 xO11] in shocked Martian meteorites, Earth and Planetary Science Letters, 219, 1–12.

Bercovici, D., and Karato, S. (2003). Whole-mantle convection and the transition-zone water filter. Nature, 425, 39-44.

Berry, F.J., Greaves, C., Helgason, O., McManus, J., Palmer, H.M., and Williams, R.T. (2000) Structural and magnetic properties of Sn-, Ti-, and Mg-substituted alpha-(Fe2O3): a study by neutron diffraction and Mossbauer spectroscopy. Journal of Solid State Chemistry 151(2):157-162

Bertka, C.M. and Fei, Y.W. (1997) Mineralogy of the Martian interior up to core-mantle boundary pressures. Journal of Geophysical Research – Solid Earth, 102, 5251-5264.

Biller, A.Y., Logvinova, A.M., Babushkina, S.A., Oleynikov, O.B., Sobolev, N.V. (2018) Srilankite inclusions in garnets from kimberlite bodies and diamondiferous volcanic-sedimentary rocks of the Yakution kimberlite province, Russia. Doklady Earth Science, 478, 15-19.

1698 Bindi, L. et al. (2011) Icosahedrite, Al63Cu24Fe13, the first natural quasicrystal. American
1699 Mineralogist, 96, 928-931.
1700 Bindi, L. and Xie, X.D. (2018) Shenzhuangite, NiFeS2, the Ni-analogue of chalcopyrite from the
1701 Suizhou L6 chondrite, European Journal of Mineralogy, 30, 165-169.
1702 Bindi, L., Chen, M., and Xie, X.D. (2017) Discovery of the Fe-analogue of akimotoite in the
1703 shocked Suizhou L6 chondrite. Scientific Reports, 7, article number: 42674.
1704 Bindi, L., Brenker, F.E., Nestola, F., Koch, T.E., Prior, D.J., Lilly, K., Krot A.N., Bizzarro, M. and Xie,
1705 X. (2019) Discovery of asimowite, the Fe-analog of wadsleyite, in shock-melted silicate
1706 droplets of the Suizhou L6 and the Quebrada Chimborazo 001 CB3.0 chondrites.
1707 American Mineralogist, 104, 775-778.
1708
1709 Bini, R., Ulivi, L., Kreutz, J., and Jodl. H.J. (2000) High-pressure phases of solid nitrogen byRaman
1710 and infrared spectroscopy. Journal of Chemical Physics, 112, 8522-8529.
1711 Binns, R.A., Davis, R.J., and Reed, S.J.B. (1969) Ringwoodite, natural (Mg,Fe)2SiO4 spinel in
1712 Tenham meteorite. Nature, 221, 943.
1713 Boehler R (1986) The phase diagram of iron to 430 kbar. Geophysical Research Letters, 13,
1714 1153–1156.
1715 Boehler R (1993) Temperatures in the Earth's core from melting-point measurements of iron at
1716 high static pressures. Nature, 363, 534-536.
1717 Born, M., and Huang, K. Dynamical Theory of Crystal Lattices, chpt. 2,§ 4 (Oxford University
1718 Press, U.K 1954, 1998 printing).
1719 Bragg, W.L. and Brown, G.B. (1926) The structure of Olivine. Zeitschrift fuer Kristallographie, 63,
1720 538-556.

1721 Brey, G.P., Bulatov, V., Girnis, A., Harris, J.W., Stachel, T. (2004) Ferropericlase - a lower mantle
1722 phase in the upper mantle. Lithos, 77, 655-663.
1723 Bridgman, P.W. (1924) The thermal conductivity and compressibility of several rocks under high
1724 pressures. American Journal of Science, 7, 81-102.
1725 Brown, J.M., and Shankland, T.J. (1981) Thermodynamic parameters in the Earth as determined
1726 from seismic profiles. Geophysical Journal of the Royal Astronomical Society, 66, 579-
1727 596.
1728 Bukowinski, M.S.T. (1994) Quantum Geophysics. Annual Review of Earth and Planetary Sciences,
1729 22, 167-205.
1730 Buob, A., Luth, R. W., Schmidt, M. W., and Ulmer, P. (2006) Experiments on CaCO3-MgCO3 solid
1731 solutions at high pressure and temperature. American Mineralogist, 91, 435-440.
1732 Buseck, P.R., Tsipursky, S.I., and Hettich, R. (1992) Fullerenes from the geological environment.
1733 Science, 257, 215-217.
1734 Buseck, P.R. (2002) Geological fullerenes: review and analysis. Earth and Planetary Science
1735 Letters, 203, 781-792.
1736 Bystrom, A., and Bystrom, A.M. (1950) The crystal structure of hollandite, the related
1737 manganese oxide minerals, and alpha-MnO2. Acta Crystallographica, 3, 146-154.
1738 Campbell, A.J., Danielson, L., Righter, K., Seagle, C.T., Wang, Y.B.,and Prakapenka, V.B. (2009)
1739 High pressure effects on the iron-iron oxide and nickel-nickel oxide oxygen fugacity
1740 buffers. Earth and Planetary Science Letters, 286, 556-564.
1741 Cavosie, A.J., Erickson, T.M. , and Timms, N.E.(2015) Nanoscale records of ancient shock
1742 deformation: Reidite (ZrSiO4) in sandstone at the Ordovician Rock Elm impact crater.
1743 Geology, 43, 315-318.

1744 Chao, E.C.T., Fahey, J.J., Littler, J., and Milton, D.J. (1962) Stishovite, SiO2, a very high pressure
1745 new mineral from meteor crater, Arizona. Journal of Geophysical Research, 67, 419.
1746 Chao, E.C.T. (1967). Shock effects, in certain rock-forming minerals. Science, 156, 192.
1747 Chen, M., Shu, J.F., Mao, H.K., Xie, X.D., and Hemley, R.J.(2003) Natural occurrence and synthesis
1748 of two new postspinel polymorphs of chromite. Proceedings of the National Academy of
1749 Sciences of the United States of America, 100, 14651-14654.
1750 Chen, M., Shu, J., Xie, X. and Tan, D. (2017) Maohokite, IMA 2017-047. CNMNC Newsletter No.
1751 39, October 2017, 1281; Mineralogical Magazine, 81, 1279-1286
1752 Chen, H.W., Shim, S.H., Leinenweber, K., Prakapenka, V., Meng, Y., and Prescher, C. (2018)
1753 Crystal structure of CaSiO3 perovskite at 28-62 GPa and 300 K under quasi-hydrostatic
1754 stress conditions. American Mineralogist, 103, 462-468.
1755 Chen, M., Shu, J., Xie, X. and Tan, D. (2019) Maohokite, a post-spinel polymorph of MgFe2O4 in
1756 shocked gneiss from the Xiuyan crater in China. Meteoritics and Planetary Science, 54,
1757 495-502.
1758 Cohen, R.E. (1991) Bonding and elasticity of stishovite at high-pressure – lineared augmented
1759 plane-wave calculations. American Mineralogist, 76, 733-742.
1760 Comodi, P. Fumagalli, P. S. Nazzareni, S. and Zanazzi, P.F. (2005) The 10 Å phase Crystal structure
1761 from single-crystal X-ray data. American Mineralogist, 90, 1012–1016.
1762 Collerson, K.D., Williams, Q., Kamber, B.S., Omori, S., Arai, H., and Ohtani, E. (2010) Majoritic
1763 garnet: A new approach to pressure estimation of shock events in meteorites and the
1764 encapsulation of sub-lithospheric inclusions in diamond. Geochimica et Cosmochimica
1765 Acta, 74, 5939-5957.

1766 Coppari, F., Smith, R.F., Eggert, J.H., Wang, J, Rygg, J.R., Lazicki, A., Hawreliak, J.A., Collins, G.W.,
1767 and Duffy, T.S. (2013) Experimental evidence for a phase transition in magnesium oxide
1768 at exoplanet pressures. Nature Geoscience, 6, 926-929.
1769 Cromer, D.T. et al. (1981) The structure of N2 at 46 kbar and 299 K. Acta Crystallographica, 37, 8-
1770 11.
1771 Datchi, F., Mallick, B., Salamat, A., and Ninet, S. (2012) Structure of Polymeric Carbon Dioxide
1772 CO2-V. Physical Review Letters, 108, Article Number: 125701.
1773 Datchi, F. and Weck. G. (2014) X-ray crystallography of simple molecular solids up to megabar
1774 pressures: application to solid oxygen and carbon dioxide. Zeitschrift fuer
1775 Kristallographie Crystalline Materials, 229 (SI), 135-157.
1776 Dera, P., Prewitt, C.T., Boctor, N.Z., and Hemley, R.J. (2002) Characterization of a high-pressure
1777 phase of silica from the Martian meteorite Shergotty. American Mineralogist, 87, 1018-
1778 1023.
1779 Dera, P. et al. (2008) High-pressure polymorphism of Fe2P and its implications for meteorites
1780 and Earth's core. Geophysical Research Letters, 35, Article Number: L10301.
1781 Dera, P. , Finkelstein, G.J., Duffy, T.S., Downs, R.T., Meng, Y., Prakapenka, V., and Tkachev, S.
1782 (2013). Metastable high-pressure transformations of orthoferrosilite Fs(82). Physics of
1783 the Earth and Planetary Interiors, 221, 15-21.
1784 Dobrzhinetskaya, L.F. et al. (2009) High-pressure highly reduced nitrides and oxides from
1785 chromitite of a Tibetan ophiolite. Proceedings of the National Academy of Sciences of
1786 the United States of America, 106, 19233-19238 .
1787 Dobrzhinetskaya, L.F., Wirth, R., Yang, J.S., Green, H.W., Hutcheon, I.D., Weber, P.K., and Grew,
1788 E.S. (2014) Qingsongite, natural cubic boron nitride: The first boron mineral from the
1789 Earth's mantle. American Mineralogist, 99, 764-772.

1790 Döbelin, N., Reznitsky, L.Z., Sklyarov, E.V., Armbruster, T., and Medenbach, O. (2006) Schreyerite,
1791 V2Ti3O9: New occurrence and crystal structure. American Mineralogist, 91, 196-202.
1792 Downs, R.T., Hazen, R.M., Finger, L.W., and Gasparik. T. (1995) Crystal-chemistry of lead
1793 aluminosilicate hollandite – a new high-pressure synthetic phase with octahedral Si.
1794 American Mineralogist, 80, 937-940.
1795 Downs, R.T. and Somayazulu, M.S. (1998) Carbon dioxide at 1.0 GPa. Acta Crystallographica
1796 Section C, 54, 897-898.
1797 Driesner, T., and Heinrich, C. A. (2007). The system H2O-NaCl. Part I: Correlation formulae for
1798 phase relations in temperature-pressure-composition space from 0 to 1000 degrees C, 0
1799 to 5000 bar, and 0 to 1 X-NaCl. Geochimica et Cosmochimica Acta, 71, 4880-4901.
1800 Du, X.P. and Tse, J.S. (2017) Oxygen Packing Fraction and the Structure of Silicon and
1801 Germanium Oxide Glasses. Journal of Physical Chemistry B, 121, 10726-10732.
1802 Dubrovinskaia, N.A., Dubrovinsky, L.S., Saxena, S.K., Tutti, F., Rekhi, S., and Le Bihan, T. (2001)
1803 Direct transition from cristobalite to post-stishovite alpha-PbO2-like silica phase.
1804 European Journal of Mineralogy, 13, 479-483.
1805 Dubrovinsky LS, Dubrovinskaia NA, Narygina O et al (2007) Bodycentered cubic iron–nickel alloy
1806 in Earth's core. Science, 316, 1880–1883.
1807 Duffy, T.S. et al. (1999) High-pressure phase-transitions in brucite, Mg(OH)2. American
1808 Mineralogist, 80, 222-230.
1809 Duthie, J.C., and Pettifor, D.G. (1977) Correlation between d-band occupancy and crystal
1810 structure in rare-earths. Physical Review Letters, 38, 564-567.
1811 Dziewonski, A.M., and Anderson, D.L. (1981) Preliminary Reference Earth model. Physics of the
1812 Earth and Planetary Interiors, 25, 297-356.

1813 Effenberger, H., Kirfel, A., Will, G., and Zobetz, E. (1983) A further refinement of the crystal-
1814 structure of thaumasite Ca3Si(OH)6CO3SO4-12H2O. Neues Jahrbuch fuer Mineralogile –
1815 Monatshefte, 2, 60-68.
1816 Eggleton, R.A., Boland. J.N., and Ringwood, A.E. (1978) High-pressure synthesis of a new
1817 aluminum silicate Al5Si5O17(OH). Geochemical Journal, 12, 191-194.
1818 El Goersy, A. and Donnay, G. (1968). A new allotropic form of carbon from Ries crater. Science,
1819 161, 363.
1820 El Goresy, A., Chen, M., Gillet, P., Dubrovinsky, L., Graup, G., and Ahuja, R. (2001) A natural
1821 shock-induced dense polymorph of rutile with alpha-PbO2 structure in the suevite from
1822 the Ries crater in Germany. Earth and Planetary Science Letters, 192, 485-495.
1823 El Goresy, A. et al. (2003). A new natural, super-hard, transparent polymorph of carbon from the
1824 Popigai impact crater, Russia. Comptes Rendus Geoscience, 335, 889-898.
1825 El Goresy, A. et al. (2008) Seifertite, a dense orthorhombic polymorph of silica from the Martian
1826 meteorites Shergotty and Zagami. European Journal of Mineralogy, 20, 523-528.
1827 Eremets, M. I. (1996) High pressure experimental methods, Oxford University Press, Oxford UK.
1828 Eremets, M.I. et al. (2004) Single-bonded cubic form of nitrogen. Nature Materials, 3, : 558-563.
1829 Errandonea, D. and Manjon, F.J. (2008) Pressure effects on the structural and electronic
1830 properties of ABX(4) scintillating crystals. Progress in Materials Science, 53, 711-773.
1831 Essene. E.J., and Fisher, D.C. (1986) Lightning strike fusion – extreme reduction and metal-
1832 silicate immiscibility. Science, 234, 189-193.
1833 Fei, Y.W., Mao, H.K., and Mysen, B.O. (1991) Experimental determination of element
1834 partitioning and calculation of phase-relations in the MgO-FeO-SiO2 system at high-
1835 pressure and high-temperature. Journal of Geophysical Research – Solid Earth and
1836 Planets, 96, 2157-2169.

1837 Fei, Y.W. and Mao, H.K. (1993) Static compression of Mg(OH)2 to 78-GPa at high-temperature
1838 and constraints on the equation of state of fluid H2O. Journal of Geophysical Research –
1839 Solid Earth, 98, 11875-11884.
1840 Fei, Y.W. and Mao, H.K. (1994) In-situ determination of the NiAs phase of Feo at high-pressure
1841 and temperature. Science 266, 1678-1680.
1842 Fei, Y.W. et al. (1995) Structure and density of FeS at high-pressure and high-temperature and
1843 the internal structure of Mars. Science 268, 1892-1894.
1844 Fei, Y., Wang, Y., and Finger, L.W. (1996) Maximum solubility of FeO in (Mg,Fe)SiO3 perov- skite
1845 as a function of temperature at 26 GPa: implication for FeO content in the lower mantle.
1846 Journal of Geophysical Research 101, 11525–11530.
1847 Fei, Y.W., Bertka, C.M. and Finger, L.W. (1997) High-pressure iron sulfur compound, Fe3S2, and
1848 melting relations in the Fe-FeS system. Science 275, 1621-1623 .
1849 Fei, Y.W. et al. (1999) In situ structure determination of the high-pressure phase of Fe3O4.
1850 American Mineralogist, 84, 203-206.
1851 Ferroir T. et al. (2008). Akimotoite in the Tenham meteorite: Crystal chemistry and high-
1852 pressure transformation mechanisms. Earth and Planetary Science Letters 275: 26–31.
1853 Ferry, J.M., Newton, R.C., and Manning, C.E. (2002) Experimental determination of the equilibria:
1854 rutile plus magnesite equals geikielite plus CO2 and zircon plus 2 magnesite equals
1855 baddeleyite plus forsterite plus 2 CO2. American Mineralogist, 87, 1342-1350.
1856 Finger, L.W. and Conrad, P.G. (2000) The crystal structure of “Tetragonal Almandine-Pyrope
1857 Phase” (TAPP): a reexamination. American Mineralogist, 85, 1804–1807.
1858 Finkelstein, G.J., Dera, P.K., Jahn, S., Oganov, A.R., Holl, C.M., Meng, Y., and Duffy, T.S. (2014)
1859 Phase transitions and equation of state of for-sterite to 90 GPa from single-crystal X-ray
1860 dif-fraction and molecular modeling. American Mineralogist, 99, 35-43.

1861 Fiquet, G., Dewaele, A., Andrault, D., Kunz, M., and Le Bihan, T. (2000) Thermoelastic properties
1862 and crystal structure of MgSiO3 perovskite at lower mantle pressure and temperature
1863 conditions. Geophysical Research Letters, 27, 21-24.Forte, A.M. and Mitrovica, J.X. (2001)
1864 Deep-mantle high-viscosity flow and thermo-chemical structure inferred from seismic
1865 and geodynamic data. Nature, 410, 1049-1056.
1866 Fritz, J., Artemieva, N., Greshake, A. (2005) Ejection of Martian meteorites (Greshake, A).
1867 Meteoritics & Planetary Science, 40, 1393-1411.
1868 Fritz, J., Greshake, A., and Stöffler, D. (2005) Micro-Raman spectroscopy of plagioclase and
1869 maskelynite in Martian meteorites: Evidence of progressive shock metamorphism.
1870 Antarctic Meteorite Research, 18, 96-116.
1871 Frost, D.J. et al. (2004). Experimental evidence for the existence of iron-rich metal in the Earth's
1872 lower mantle. Nature, 428, 409-412.
1873 Frost, D.J. and McCammon, C.A.(2008) The redox state of Earth's mantle. Annual Review of
1874 Earth and Planetary Sciences, 36, 389-420.
1875 Gautron, L. and Madon, M. (1994) A Study of the stability of anorthite in the PT conditions of
1876 Earth’s transition zone. Earth and Planetary Science Letters, 125, 281-291.
1877 Gautron, L., Kesson, S.E., and Hibberson, W.O. Phase relations for CaAl2Si2O8 (anorthite
1878 composition) in the system CaO-Al2O3-SiO2 at 14 GPa. Physics of the Earth and
1879 Planetary Interiors, 97, 71-81.
1880 Gautron, L., Angel, R.J., and Miletich, R. (1999) Structural characterisation of the high-pressure
1881 phase CaAl4Si2O11. Physics and Chemistry of Minerals, 27, 47-51.
1882 Gibbs, G.V. et al. (2008) Bonded interactions and the crystal chemistry of minerals: a review.
1883 Zeitschrift fuer Kristallographie, 223, 1-40.

1884 Gillet, P. et al.(2000) Natural NaAlSi3O8-hollandite in the shocked Sixiangkou meteorite. Science,
1885 287, 1633-1636.
1886 Glass, B.P., Liu, S.B. , and Leavens, P.B.(2002) Reidite: An impact-produced high-pressure
1887 polymorph of zircon found in marine sediments. American Mineralogist, 87, : 562-565.
1888 Gleason, A.E. et al. (2017) Time-resolved diffraction of shock-released SiO2 and diaplectic glass
1889 formation. Nature Communications, 8, Article Number: 1481.
1890 Goldschmidt, V.M. (1937) The principles of distribution of chemical elements in minerals and
1891 rocks. The seventh Hugo Muller Lecture, delivered before the Chemi-cal Society on
1892 March 17th, 1937. Journal of the Chemical Society, 655-673.
1893 Goncharov, A. F., Struzhkin, V. V., Mao, H.-k., and Hemley, R. J. (1998) Raman spectroscopy of
1894 dense H2O and the transition to symmetric hydrogen bonds. Physical Review Letters, 83,
1895 1998.
1896 Grande. Z. et al. (2019) Bond strengthening in dense H_2O and implications to planetary
1897 composition. arXiv:1906.11990 [cond-mat.mtrl-sci].
1898 Grew, E.S., Locock, A.J., Mills, S.J., Galuskina, I.O., Galuskin, E.V., and Halenius, U. (2012) Nomen-
1899 clature of the garnet supergroup. American Mineralogist; preprint December 2012.
1900 Grieve, R.A.F., Langenhorst, F., and Stoffler, D. (1996) Shock metamorphism of quartz in nature
1901 and experiment .2. Significance in geoscience. Meteoritics & Planetary Science, 31, 6-35.
1902 Griffin, W.L., Gurney, J.J., and Ryan, C.G. (1992). Variations in trapping temperatures and trace-
1903 elements in peridotite suite inclusions from African diamonds – evidence for 2 inclusion
1904 suites and implications for lithosphere stratigraphy. Contributions to Mineralogy and
1905 Petroligy, 110, 1-15.

1906 Guthrie, M., Boehler, R., Tulk, C. A., Molaison, J. J., dos Santos, A. M., Li, K., and Hemley, R. J.
1907 (2013). Neutron diffraction observations of interstitial protons in dense ice. Proceedings
1908 of the National Academy of Sciences, 110, 10552–10556.
1909 Guyot, F. and Reynard, B. (1992) Pressure-induced structural modifications and amorphization in
1910 olivine compounds. Chemical Geology, 96, 411-420.
1911 Haggerty, S.E. (1991) Oxide Mineralogy of the Upper Mantle. Reviews in Mineralogy, 25, 355-
1912 416.
1913 Harris, J. , Hutchison, M.T., Hursthouse, M., Light, M., and Harte, B. (1997) A new tetragonal
1914 silicate mineral occurring as inclusions in lower-mantle diamonds. Nature, 387, 486-488.
1915 Harte, B. and Harris, J.W.(1994) Lower mantle mineral association preserved in diamonds.
1916 Mineralogical Magazine 58A, 384–385.
1917 Harte, B., Harris, J.W., Hutchison, M.T., Watt, G.R., and Wilding, M.C. (1999) Lower mantle
1918 mineral associations in diamonds from Sao Luiz, Brazil. In: Fei, Y., Bertka, C.M., Mysen,
1919 B.O. (Eds.), Mantle Petrology: Field Observations and High Pres-sure Experimentation: A
1920 Tribute to Francis R. (Joe) Boyd: Geochemical Society Special Publication No. 6, 125–153.
1921 Hazen, R.M. (1976) Effects of temperature and pressure on crystal-structure of forsterite.
1922 American Mineralogist, 61, 1280-1293.
1923 Hazen, R.M., Downs, R.T., Finger, L.W., and Ko, J.D. (1993). Crystal-chemistry of ferromagnesian
1924 silicate spinels – evidence for Mg-Si disorder. American Mineralogist, 78, 1320-1323.
1925 Hazen, R.M., Downs, R.T., Finger, L.W., Conrad, P.G., and Gasparik, T. (1994) Crystal-chemistry of
1926 Ca-bearing majorite. American Mineralogist, 79, 581-584.
1927 Heinz, D.L. and Jeanloz, R. (1987) Measurement of the melting curve of Mg0.9Fe0.1SiO3 at
1928 lower mantle conditions and its geophysical implications. Journal of Geophysical
1929 Research – Solid Earth and Planets, 92, 11437-11444.

1930 Hejny, C. and Armbruster, T. (2002) Polysomatism in hogbomite: The crystal structures of 10T,
1931 12H 14T, and 24R polysomes. American Mineralogist, 87, 277-292.
1932 Helffrich, G.R. and Wood, B.J. (2001) The Earth's mantle. Nature, 412, 501-507.
1933 Hemley, R.J., Prewitt, C.T., and Kingma, K.J. (1994) High-pressure behavior of silica. Reviews in
1934 Mineralogy, 29, 41-81.
1935 Hemley, R.J. and Dera. P. (2000). Molecular crystals. Reviews in Mineralogy & Geochemistry, 41,
1936 335-419.
1937 Herd, C.D.K. et al. (2017) The Northwest Africa 8159 martian meteorite: Expanding the martian
1938 sample suite to the early Amazonian. Geochimica et Cosmochimica Acta, 218, 1-26.
1939 Hermann, A. and Mookherjee, M. (2016). High-pressure phase of brucite stable at Earth's
1940 mantle transition zone and lower mantle conditions. Proceedings of the National
1941 Academy of Sciences of the United States of America, 113, 13971-13976 .
1942 Hirose, K. and Fei, Y.W. (2002) Subsolidus and melting phase relations of basaltic composition in
1943 the uppermost lower mantle. Geochimica et Cosmochimica Acta, 66, 2099-2108.
1944 Hirose, K. (2006) Postperovskite phase transition and its geophysical implications. Reviews in
1945 Geophysics, 44, RG3001.
1946 Hirschmann, M.M. (2006) Water, melting, and the deep Earth H2O cycle. Annual Review of Earth
1947 and Planetary Sciences, 34, 629-653.
1948 Hollister, L.S. et al. (2014) Impact-induced shock and the formation of natural quasicrystals in
1949 the early solar system. Nature Communications, 5, Article Number: 4040.
1950 Holzapfel, W.B., Seiler, B., and Nicol, M.F. (1984) Effect of pressure on infrared-spectra of ice VII.
1951 Journal of Geophysical Research: Solid Earth, 89.
1952 Holzapfel, W.B. (1995) Structural Systematics of 4F and 5F elements under pressure. Journal of
1953 Alloys and Compounds, 223, 170-173.

1954 Horiuchi, H., Ito, E., and Weidner, D.J. (1987) Perovksite-type MgSiO3 – single crystal X-ray
1955 diffraction study. American Mineralogist, 72, 357-360.
1956 Horiuchi, H. et al. (1987) MgSiO3 (ilmenite-type) – single crystal X-ray diffraction study.
1957 American Mineralogist, 67, 788-793.
1958 Houser, C. (2016) Global seismic data reveal little water in the mantle transition zone. Earth and
1959 Planetary Science Letters, 448, 94-101.
1960 Hu, J.P. and Sharp, T.G. (2017) Back-transformation of high-pressure miner-als in shocked
1961 chondrites: Low-pressure mineral evidence for strong shock. Geochimica et
1962 Cosmochimica Acta, 215, 277-294.
1963 Hu, Y., Kiefer, B., Bina, C.R., Zhang, D.Z., and Dera, P.K. (2017) High-Pressure gamma-CaMgSi2O6:
1964 Does Penta-Coordinated Silicon Exist in the Earth's Mantle? Geophysical Research
1965 Letters, 44, 11340-11348.
1966 Huang, X.G., Xu, Y.S., and Karato, S.I.(2005) Water content in the transition zone from electrical
1967 conductivity of wadsleyite and ringwoodite. Nature, 434, 746-749.
1968 Huminicki, D.M.C. and Hawthorne, F.C. (2002) The crystal chemistry of the phosphate minerals.
1969 Reviews in Mineralogy & Geochemistry, 48, 123-253.
1970 Hummer, D.R. and Fei, Y.W. (2012) Synthesis and crystal chemistry of Fe3+-bearing
1971 (Mg,Fe3+)(Si,Fe3+)O-3 perovskite. American Mineralogist, 97, 1915-1921.
1972 Hund, F. (1936) Overview of the relationship of matter in very pressure and temperature.
1973 Physikalische Zeitschrift, 37, 853-853.
1974 Hwang, H. et al. (2017) A role for subducted super-hydrated kaolinite in Earth's deep water cycle.
1975 Nature Geoscience, 10, 947.
1976 Iota, V. , Yoo, C.S. , and Cynn, H. (1999) Quartzlike carbon dioxide: An optically nonlinear
1977 extended solid at high pressures and temperatures. Science, 283, 1510-1513.

1978 Iota, V., Yoo, C.S. , Klepeis, J.H., Jenei, Z., Evans, W., and Cynn, H. (2007) Six-fold coordinated
1979 carbon dioxide VI. Nature Materials, 6, 34-38.
1980 Ishii, T. et al. (2014) High-pressure phase transitions in FeCr2O4 and structure analysis of new
1981 post-spinel FeCr2O4 and Fe2Cr2O5 phases with meteorit-ical and petrological
1982 implications. American Mineralogist, 99, 1788-1797.
1983 Ishii, T. et al. (2015) High-pressure high-temperature transitions in MgCr2O4 and crystal
1984 structures of new Mg2Cr2O5 and post-spinel MgCr2O4 phases with implications for
1985 ultrahigh-pressure chro-mitites in ophiolites. American Mineralogist, 100, 59-65.
1986 Ishii, T., Kojitani, H., and Akaogi, M. (2018) Phase relations and mineral chemistry in pyro-litic
1987 mantle at 1600-2200 degrees C under pressures up to the uppermost lower mantle:
1988 Phase transitions around the 660-km discontinuity and dynamics of upwelling hot
1989 plumes. Physics of the Earth and Planetary Interiors, 274, 127-137.
1990 Ito, E., and Matsui, Y. (1979) High-pressure transformations in silicates, germanates, and
1991 titanates with ABO3 stoichiometry. Physics and Chemistry of Minerals, 4, 265-273.
1992 Ito, E., and Takahashi, E. (1989) Postspinel transformations in the system Mg2SiO4 – Fe2SiO4
1993 and some geophysical implications. Journal of Geophysical Research – Solid Earth and
1994 Planets, 94, 10637-10646.
1995 Ito, E. and Matsui, Y. (1978) Synthesis and crystal-chemical characterization of MgSiO3
1996 perovskite. Earth and Planetary Science Letters, 38, 443-500.
1997 Ito, E. and Yamada H. (1982). Stability relations of silicatespinels, ilmenites and perovskites. in
1998 High Pressure Research in Mineral Physics, edited by S. Akamoto and M. H. Manghnani,
1999 pp. 405–419, Terra Sci., Tokyo.
2000 Jamieson, J.C. (1963) Crystal structures at high pressures of metallic modifications of silicon and
2001 germanium. Science, 139, 762.

2002 Kagi, H., Lu, R., Davidson, P., Goncharov, A.F., Mao, H.K., and Hemley, R.J. (2000) Evidence for
2003 ice VI as an inclusion in cuboid diamonds from high P-T near infrared spectroscopy.
2004 Mineralogical Magazine, 64, 1089-1097.
2005 Kaminsky, F. (2012) Mineralogy of the lower mantle: A review of 'super-deep' mineral in-
2006 clusions in diamond. Earth-Science Reviews, 110, 127-147.
2007 Kaminsky, F. V. and Wirth, R. (2011). Iron-carbide inclusions on lower-mantle diamond from
2008 Juina, Brazil. Canadian Mineralogist, 49, 555-572.
2009 Kaminsky, F. V. and Wirth, R. (2017). Nitrides and carbonitrides from the lowermost mantle and
2010 their importance in the search for Earth's "lost" nitrogen. American Mineralogist, 102,
2011 1667-1676.
2012 Kaneko, S., Miyahara, M., Ohtani, E., Arai, T., Hirao, N., and Sato, K. (2015) Discovery of
2013 stishovite in Apollo 15299 sample. American Mineralogist, 100, 1308-1311.
2014 Kawai, N. and Tachimori, M. (1974) High-pressure hexagonal form of MgSiO3. Proceedings of
2015 the Japan Academy, 50, 378-380.
2016 Kennedy, C.S., and Kennedy, G.C. (1976) Equilibrium boundary between graphite and diamond.
2017 Journal of Geophysical Research, 81, 2467-2470.
2018 Kesson, S.E. and Fitz Gerald, J.D. (1991) Partitioning of MgO, FeO, NiO, MnO and Cr2O3 between
2019 magnesian silicate perovskite and magnesiowustite: implications for the origin of
2020 inclusions in diamond and the composition of the lower mantle. Earth and Planetary
2021 Science Letters, 111, 229–240.
2022 Kirfel, A., Krane, H.G., Blaha, P., Schwarz, K., and Lippmann, T. (2001) Electron-density
2023 distribution in stishovite, SiO2: a new high-energy synchrotron-radiation study. Acta
2024 Crystallographica Section A, 57, 663-677.

2025 Korenaga, J. (2008) Urey ratio and the structure and evolution of Earth's mantle. Reviews of
2026 Geophysics, 46, Article Number: RG2007.
2027 Kubo, T. et al. (2017) Formation of a metastable hollandite phase from amorphous plagioclase: A
2028 possible origin of lingunite in shocked chondritic meteorites. Physics of the Earth and
2029 Planetary Interiors, 272, 50-57.
2030 Kugimiya, K. and Steinfink, H. (1968) The Influence of Crystal Radii and Electronegativities on the
2031 Crystallization of AB2X4 Stoichiometries. Inorganic Chemistry, 7, 9
2032 Kuhs, W.F., Finney, J.L. ,Vettier C., and Bliss, D.V.(1984) Structure and hydrogen ordering in ices
2033 VI, VII, and VIII by neutron powder diffraction, Journal of Chemical Physics, 81, 3612–
2034 3623.
2035 Kunz, M. et al. (1996) The baddeleyite-type high pressure phase of Ca(OH)(2). High Pressure
2036 Research, 14, 311-319.
2037 Kuwayama, Y., Hirose, K., Sata, N. , and Ohishi, Y. (2007) The pyrite-type high-pressure form of
2038 silica. Science, 309, 923-925.
2039 Kvenvolden, K.A. (1993) Gas Hydrates – Geological Perspective and Global Change. Reviews of
2040 Geophysics, 31, 173-187.
2041 Landau, L.D. and Lifshitz, E.M. (1978) Theoretical Physics, Vol V, Statistical Physics, Chpt 7,
2042 Paragr 80, Academie Verlag, Berlin.
2043 Langenhorst, F. and Poirier, J.P. (2000) 'Eclogitic' minerals in a shocked basaltic meteorite. Earth
2044 and Planetary Science Letters, 176, 259-265.
2045 Langenhorst, F. and Deutsch, A. (2012) Shock Metamorphism of Minerals. Elements, 8, 31-36.
2046 Lakshtanov, D.L. et al. (2007) The post-stishovite phase transition in hy-drous alumina-bearing
2047 SiO2 in the lower mantle of the earth. Proceedings of the National Academy of Sciences
2048 of the United States of America, 104, 13588-13590.

2049 Lavina, B. et al. (2011) Discovery of the recoverable high-pressure iron oxide Fe4O5. Proceedings
2050 of the National Academy of Sciences of the United States of America, 108, 17281-17285.
2051 Lee, K.K.M., O'Neill, B., Panero, W.R., Shim, S.H., Benedetti, L.R., and Jeanloz, R. (2004)
2052 Equations of state of the high-pressure phas-es of a natural peridotite and implications
2053 for the Earth's lower mantle. Earth and Planetary Science Letters, 223, 381-393.
2054 Leinenweber, K., Utsumi, W., Tsuchida, Y., Yagi, T., and Kurita, K. (1991) Unquenchable High-
2055 Pressure Perovskite Polymorphs of MnSnO3 and FeTiO3. Physics and Chemistry of
2056 Minerals, 18, 244-250.
2057 Leinenweber, K. , Linton, J., Navrotsky, A., Fei, Y.W., and Parise, J.B. (1995) High-pressure
2058 perovskites on the join CaTiO3-FeTiO3. Physics and Chemistry of Minerals, 22, 251-258.
2059 Li, D. Bancroft, G.M., Kasrai, M., Fleet, M.E., Feng, X.H., Tan, K.H., and Yang, B.X. (1993). High-
2060 resolution Si K-egde and L2,3-edge XANES of alpha-quartz and stishovite. Solid State
2061 Communications, 87, 613-617.
2062 Li, J. and Agee, C.B. (1996) Geochemistry of mantle-core differentiation at high pressure. Nature,
2063 381, 686-689.
2064 Lin J.-F., et al. (2002) Iron–nickel alloy in the Earth's core. Geophysical Research Letter, 29,109–
2065 111.
2066 Lin, J.F., Degtyareva, O., Prewitt, C.T., Dera, P., Sata, N. , Gregoryanz, E. , Mao, H.K. , and Hemley,
2067 R.J. (2005) Nature Materials, 3, 389-393.
2068 Lin, J.F. et al. (2013) Effects of the electronic spin transitions of iron in lower mantle minerals:
2069 Implications for deep mantle Geophysics and geochemistry. Review s of Geophysics. 51,
2070 244-275.
2071 Linton, J.A., Fei, Y.W., and Navrotsky, A. (1995) The MgTiO3-FeTiO3 join at high pressure and
2072 temperature. American Mineralogist, 84, 1595-1603.

2073 Liou, J.G., Ernst, W.G., Zhang, R.Y., Tsujimori, T., and Jahn, B.M. (2009) Ultrahigh-pressure
2074 minerals and metamorphic terranes - The view from China.Journal of Asian Earth
2075 Sciences, 35, 199-231.
2076 Liu, L.-g. (1974) Silicate perovskite from phse transformations of pyrope-garnet at high pressure
2077 and temperture. Geophysical Research Letters, 1, 277-280.
2078 Liu, L.-g. and Ringwood, A.E.(1975) Synthesis of a perovskite polymorph of CaSiO3. Earth and
2079 Planetary Science Letters, 28, 209-211.
2080 Liu, L.-g. (1978) High-pressure phase-transformations of albite, jadeite, and nepheline. Earth and
2081 Planetary Science Letters, 37, 438-444.
2082 Liu, L.-g. and El Gorsey, A. (2002) High-pressure phase transitions of the feld-spars, and further
2083 characterization of lingunite. International Geology Review, 49, 854-860.
2084 Liu, X., Ohfuji, H., Nishiyama, N., He, Q., Sanehira, T., and Irifune, T. (2012) High-P behavior of
2085 anorthite composition and some phase relations of the CaO-Al2O3-SiO2 system to the
2086 lower mantle of the Earth, and their geophysical implications. Journal of Geophysical
2087 Research – Solid Earth, 117, Article Number: B09205.
2088 Luo, S.-N., Ahrens, T.J., Asimow, P.D. (2003) Polymorphism, superheating, and amorphization of
2089 silica upon shock wave loading and release. Journal of Geophysical Research – Solid
2090 Earth, 108, Article Number: 2421.
2091 Luo, S.-N., Tschauner, O., Tierney, T.E., Swift, D.C., Chipera, S.J., and Asimow, P.D. (2005) Novel
2092 crystalline carbon-cage structure synthesized from laser-driven shock wave loading of
2093 graphite. Journal of Chemical Physics, 123, Article Number: 024703.
2094 Ma, C., Tschauner, O., Beckett, J.R., Liu, Y., Rossman, G.R., Zhuravlev, K. Prakapenka, V. B., Dera,
2095 P., Taylor, L.A. (2015) Tissintite, (Ca, Na, square)AlSi2O6, a highly-defective, shock-

induced, high-pressure clinopy-roxene in the Tissint martian meteorite. Earth and Planetary Science Letters, 422, 194-205.

Ma, C., Tschauner, O., Beckett, J.R., Liu, Y., Rossman, G.R., Sinogeikin, S.V., Smith, J.S., and Taylor, L.A. (2016) Ahrensite, gamma-Fe2SiO4, a new shock-metamorphic mineral from the Tissint meteorite: Im-plications for the Tissint shock event on Mars. Geochimica et Cosmochimica Acta, 184, 240-256.

Ma, C. and Tschauner O. (2016) Discovery of tetragonal almandine, (Fe,Mg,Ca,Na)(3)(Al,Si,Mg)(2)Si3O12, a new high-pressure mineral in Shergotty. Meteoritics and Planetary Science, 51, A434-A434.

Ma, C. and Tschauner, O. (2017) Zagamiite, IMA 2015-022a. CNMNC Newsletter No. 36, April 2017, page 409; Mineralogical Magazine, 81, 403–409.

Ma, C. and Tschauner, O. (2018) Liuite, IMA 2017-042a. CNMNC Newsletter No. 46, Decem-ber 2018, page xxxx; Mineralogical Magazine, 82, xxxx–xxxx.

Ma, C. et al. (2018) Liebermannite, KAlSi3O8, a new shock-metamorphic, high-pressure mineral from the Zagami Martian meteorite. Meteoritics and Planetary Science, 53, 50-61.

Ma, C. and Prakapenka, V.(2018) Tschaunerite, IMA 2017-032a. CNMNC Newsletter No. 46, December 2018, page xxxx; Mineralogical Magazine, 82, xxxx–xxxx.

Ma, C., Tschauner, O., Bindi. L. Beckett. J., Greenberg, E., and Prakapenka, V.B. (2019) A vacancy-rich, partially inverted spinelloid silicate, (Mg,Fe,Si)2(Si,□)O4, as a major matrix phase in shock melt veins of the Tenham and Suizhou L6 chondrites. Meteoritics and Planetary Science, accepted June 2019.

Ma, C., Tschauner, O., Beckett, J., Greenberg, E., and Prakapenka, V.B. (2019) Chenmingite, FeCr2O4 in the CaFe2O4-type structure, a shock-induced, high-pressure mineral in the Tissint Martian meteorite. American Mineralogist, accepted July 2019

2120 Ma, Y.M. et al. (2009) Transparent dense sodium. Nature, 458, 182-U3.

2121 Mailhiot, C. and McMahan, A.K. (1991) Atmospheric-pressure stability of energetic phases of
2122 carbon. Physical Review B, 44, 11578-11591.

2123 Mao, H.K., Wu, Y., Chen, L.C., Shu, J.F., and Jephcoat, A.P. (1990) Static compression of iron to
2124 300 GPa and Fe0.8Ni0.2 alloy to 260 GPa – Implications for composition of the core. .
2125 Journal of Geophysical Research – Solid Earth and Planets, 95, 21737-21742.

2126 Mao, H.K., Chen, X.J., Ding, Y., Li, B., Wang, L. (2018) Solids, liquids, and gases under high
2127 pressure. Reviews of Modern Physics, 90, Article Number: 015007.

2128 Mao, W.L. et al. (2003) Bonding changes in compressed superhard graphite. Science, 302, 425-
2129 427.

2130 Manjon, F.J. et al. (2007) Crystal stability and pressure-induced phase transitions in scheelite
2131 AWO(4) (A = Ca, Sr, Ba, Pb, Eu) binary oxides. II: Towards a systematic understanding.
2132 Physical Status Solidi B – Basic Solid State Physics, 244, 295-302.

2133 McCammon, C. (1997) Perovskite as a possible sink for ferric iron in the lower mantle. Nature,
2134 387, 694-696.

2135 McCammon, C., et al. (2013) Iron spin state in silicate perovskite at conditions of the Earth's
2136 deep interior. High Pressure Research, 33, 663-672.

2137 McCormick, T.C. (1986) Crystal-chemical aspects of nonstoichiometric pyroxenes. American
2138 Mineralogist, 71, 1434-1440.

2139 Merlini, M. et al. (2012). CaCO3-III and CaCO3-VI, high-pressure polymorphs of calcite: Possible
2140 host structures for carbon in the Earth's mantle. Earth and Planetary Science Letters,
2141 333, 265-271.

2142 Merlini, M.et al. (2014). Evidence of interspersed co-existing CaCO3-III and CaCO3-IIIb structures
2143 in polycrystalline CaCO3 at high pressure. Mineralogical Magazine, 78(2), 225-233.

2144 Metsue, A., and Tsuchiya, T. (2012) Ab initio investigation into the elasticity of ultrahigh-
2145 pressure phases of SiO2. Physics and Chemistry of Minerals, 39, 177-187.
2146 Mikhail, S. et al. (2014) Constraining the internal variability of the stable isotopes of carbon and
2147 nitrogen within mantle diamonds. Chemical Geology, 366, 14-23.
2148 Mikhail, S. et al. (2014) Empirical evidence for the fractionation of carbon isotopes between
2149 diamond and iron carbide from the Earth's mantle. Geochemistry Geophysics
2150 Geosystems, 15, 855-866.
2151 Milton, D.J., and DeCarli, P.S. (1962) Maskelynite – formation by explosive shock. Science, 140,
2152 670-673.
2153 Ming, L.C., Kim, Y.H., Uchida, T., Wang, Y., and Rivers, M. (2006) In situ X-ray diffraction study of
2154 phase transitions of FeTiO3 at high pressures and temperatures using a large-volume
2155 press and synchrotron radiation. American Mineralogist, 91, 120-126.
2156 Miyahara, M., Ohtani, E., El Goresy, A., Ozawa, S., and Gillet, P. (2016) Phase transition
2157 processes of olivine in the shocked Martian meteorite Tissint: Clues to origin of
2158 ringwoodite-, bridgmanite- and magnesiowilstite-bearing assemblages. Physics of the
2159 Earth and Planetary Interiors, 259, 18-28.
2160 Mochalov, A. G. et al. (1998) Hexaferrum (Fe, Ru), (Fe, Os), (Fe, Ir)-A new mineral. Zap Vseross
2161 Mineral Obshch, 127, 41-51.
2162 Morimoto, N., Tokonami, M., Watanabe, M., and Koto, K. (1974) Crystal-structures of 3
2163 polymorphs of Co2SiO4. American Mineralogist, 59, 475-485.
2164 Murakami, M. et al. (2004) Post-perovskite phase transition in MgSiO3. Science, 304, 855.
2165 Murakami, M., Sinogeikin, S.V., Hellwig, H., Bass, J.D., and Li, J. (2007) Sound velocity of MgSiO3
2166 perovskite to Mbar pressure. Earth and Planetary Science Letters, 256, 47-54.Navon, O.

(1991) High internal pressures in diamond fluid inclusions determined by infrared absorption. Nature 353, 746 – 748.

Navon, O., Wirth, R., Schmidt, C., Jablon, B.M., Schreiber, A., and Emmanuel, S. (2017) Solid molecular nitrogen (delta-N-2) inclusions in Juina diamonds: Exsolution at the base of the transition zone. Earth and Planetary Science Letters, 464, 237-247.

Navrotsky, A. (1987) High-pressure transitions in silicates. Progress in Solid State Chemistry, 17, 53-86.

Nellis, W.J., et al. (1988) Metal physics at ultrahigh pressure – aluminum, copper, and lead as prototypes. Physical Review Letters, 60, 1414-1417.

Nemeth, P. et al. (2014). Lonsdaleite is faulted and twinned cubic diamond and does not exist as a discrete material. Nature Communications, 5, Article Number 5447.

Nestola, F. et al. (2016) Tetragonal Almandine-Pyrope Phase, TAPP: finally a name for it, the new mineral jeffbenite. Mineralogical Magazine, 80, 1219-1232.

Nestola, F. et al. (2018) CaSiO3 perovskite in diamond indicates the recycling of oceanic crust into the lower mantle. Nature, 555, 237.

Nickel, E.H. and Grice, J.D. (1998). The IMA commission on new minerals and mineral names: Procedures and guidelines on mineral nomenclature. Canadian Mineralogist, 36, 913-926.

Nimis, P. et al. (2019) Fe-rich ferropericlase and magnesiowustite inclusions reflecting diamond formation rather than ambient mantle. Geology, 47, 27-30.

Nishio-Hamane, D., Zhang, M.G., Yagi, T., and Ma, Y.M. (2012) High-pressure and high-temperature phase transitions in FeTiO3 and a new dense FeTi3O7 structure. American Mineralogist, 97, 568-572.

Oganov, A.R. et al. (2010) Exotic behavior and crystal structures of calcium under pressure. Proceedings of the National Academy of Sciences of the United States of America, 107, 7646-7651.

Oganov, A.R. et al. (2013). Structure, Bonding, and Mineralogy of Carbon at Extreme Condi-tions. Carbon in Earth, Book Series: Reviews in Mineralogy & Geochemistry, 75, 47-77.

Ohtani, E., Yurimoto, H., and Seto, S. (1997) Element partitioning between metallic liquid, silicate liquid, and lower-mantle minerals: Im-plications for core formation of the Earth. Physics of the Earth and Planetary Interiors, 100, 97-114.

Ohtani E. et al. (2004). Formation of high-pressure minerals in shocked L6 chondrite Yamato 791384: Constraints on shock conditions and parent body size. Earth and Planetary Science Letters 227: 505–515.

Olijnyk, H., and Holzapfel, W. B. 1984, J. Phys. (Paris), Colloq. 45, Suppl. 11, C8-153.

Olsen, J.S., Gerward, L., and Jiang, J.Z. (1999) On the rutile/alpha-PbO2-type phase boundary of TiO2. Journal of Physics and Chemistry of Solids, 60, 229-233.

Ono, S. and Oganov, A.R.(2004) Theoretical and experimental evidence for a post-perovskite phase of MgSiO3 in Earth's D '' layer. Nature 430, 445-448. Otte, K. et al. (2009) Pressure-induced structural and electronic transitions in FeOOH from first principles. Physical Review B, 80, Article Number: 205116.

Palot, M. et al. (2016) Evidence for H2O-bearing fluids in the lower mantle from diamond inclusion. Lithos, 265, 237-243.

Pamato, M.G.,, Kurnosov, A., Ballaran, T.B., Trots, D.M., Caracas, R., and Frost, D.J. (2014) Hexagonal Na-0.41[Na0.125Mg0.79Al0.085](2)[Al0.79Si0.21](6)O-12 (NAL phase): Crystal structure refinement and elasticity. American Mineralogist, 99, 1562-1569.

Pang, R.L., Harries, D., Pollok, K., Zhang, A.C., and Langenhorst, F. (2018) Vestaite, (Ti4+Fe2+)Ti34+O9, a new mineral in the shocked eucrite Northwest Africa 8003. American Mineralogist, 103, 1502-1511.

Parise, J.B., Wang, Y., Yeganeh-Haeir, A., Cox, D.E., and Fei, Y.W. (1990) Crystal-structure and thermal-expansion of (Mg,Fe)SiO3 perovskite. Geophysical Research Letters, 17, 2089-2092.

Pauling, L. (1960) Nature of the Chemical Bond, 3rd edition, 1960, Cornell Univ. Press.

Pearson, D. G. et al. (2014). Hydrous mantle transition zone indicated by ringwoodite included within diamond. Nature, 507, 221-223.

Petrenko, V. F. and Whitworth, R. W. (1999) Physics of Ice (Oxford Univ.Press, 1999), p. 253.

Plonka, A.M., Dera, P., Irmen, P., Rivers, M.L., Ehm, L., and Parise, J.B. (2012) beta-diopside, a new ultrahigh-pressure polymorph of CaMgSi2O6 with six-coordinated silicon. Geophysical Research Letters, 39, Article Number: L24307.

Prewitt C.T (editor) Reviews in Mineralogy and Geochemistry January 01, 1980, Vol.7, 5-92, ISSN 1529-6466.

Prewitt, C.T. and Downs, R.T. (1998) High-pressure crystal chemistry. Reviews in Mineralogy, 37, 283-317.

Prewitt, C.T., Gramsch, S.A., and Fei, Y.W. (2002) High-pressure crystal chemistry of nickel sulphides. Journal of Physics – Condensed Matter, 14, 11411-11415.

Price, G.D. et al. (1983) Wadsleyite, natural beta-(Mg,Fe)2SiO4 from the Peace River Meteorite. Canadian Mineralogist, 21, 29-35.

Reid, A.F., and Ringwood, A.E. (1969) Newly observed high pressure transformations on Mn3O4, CaAl2O4, and ZrSiO4. Earth and Planetary Science Letters, 6, 205-208.

Reid, A.F., and Ringwood, A.E. (1975) High-pressure modification of ScAlO3 and some geophysical implications, Journal of Geophysical Research, 80, 3363-3370.

Richardson, S.H., Shirey, S.B., Harris, J.W., and Carlson, R.W. (2001) Archean subduction recorded by Re-Os isotopes in eclogitic sulfide inclusions in Kimberley diamonds. Earth and Planetary Science Letters, 191, 257-266.

Ricolleau, A. and Fei, Y.W. (2016) Equation of state of the high-pressure Fe3O4 phase and a new struc-tural transition at 70 GPa. American Mineralogist, 101, 719-725.

Ringwood. A.E. (1967) Pyroxene-garnet transformation in Earth's mantle. Earth and Planetary Science Letters, 2, 255-257.

Ringwood AE (1979) Origin of the Earth and Moon. Springer, Berlin.

Ringwood, A.E. and Irifune, T. (1988) Nature of the 650-km seismic discontinuity: implications for mantle dynamics and differentiation. Nature, 331, 131–136.

Rohrbach, A. and Schmidt, M. W. (2011) Redox freezing and melting in the Earth's deep mantle resulting from carbon-iron redox coupling. Nature, 472, 209-212.

Ross, N.L., and Hazen, R.M. (1989) Single-crystal X-ray-diffraction study of MgSiO3 perovskite from 77K to 400K. Physics and Chemistry of Minerals, 16, 415-420.

Roth, R.S. (1957) Classification of perovskite and other ABO3-type compounds. Journal of Research of the National Bureau of Standards, 58, 75-88.

Rubie, D.C. (1984) The olivine-spinel transformation and the rheology of subducting lithosphere. Nature, 308, 505-508.

Rubin, A.E. and Ma, C. (2017) Meteoritic minerals and their origins. Chemie der Erde – Geochemistry, 77, 325-385.

Sato, H. et al. (1991) Baddeleyite-type high-pressure phase of TiO2. Science, 251, 786-788.

2259 Sato-Sorensen, Y. (1983) Phase transitions and equations of state for the sodium halides: NaF
2260 NaCl, NaBr, and NaI. Journal of Geophysical Research – Solid Earth, 88, 3543-3548.
2261
2262 Schertl, H.P, Schreyer, W., and Chopin, C. (1991) The pyrope-coesite rocks and their country
2263 rocks at Parigi, Dora Maira Massif, Western Alps – Detailed petrography, mineral
2264 chemistry, and P-T path. Contributions to Mineralogy and Petrology, 108, 1-21.
2265 Schmandt, B., Jacobsen, S.D. Becker, T.W., Liu, Z. , and Dueker, K.G. (2014) Dehydration melting
2266 at the top of the lower mantle. Science, 344, 1265-1268.
2267 Schrauder, M., and Navon, O. (1993) Solid carbon-dioxide in a natural diamond. Nature, 365, 42-
2268 44.
2269 Scott, E.R.D, Keil, K., and Stöffler, D. (1992) Shock metamorphism of carbonaceous chondrites.
2270 Geochimica et Cosmochimica Acta, 56, 4281-4293.
2271 Sekine, T., and Ahrens, T.J. (1992) Shock-induced transformations in the system NaAlSiO4-SiO2 –
2272 A new interpretation. Physics and Chemistry of Minerals, 18, 359-364.
2273 Shannon, R.D. and Prewitt, C.T. (1969) Coordination and volume changes accompanying high-
2274 pressure phase transformations of oxides. Materials Research Bulletin, 4, 57-59.
2275 Shannon, R.D. (1976) Revised effective ionic-radii and systematic studies of interatomic
2276 distances in halides and chalcogenides. Acta Crystallographica Section A, 32, 751-767.
2277 Sharp T.G., Lingemann C.M., Dupas C., and Stöffler D. (1997). Natural occurrence of MgSiO3-
2278 ilmenite and evidence for MgSiO3-perovskite in a shocked L chondrite. Science, 280,
2279 352-355.
2280 Sharp T.G. and DeCarli, P.S. (2006). Shock effects in meteorites, in: Meteorites and the Early
2281 Solar System II, 653- 677. Publisher: University of Arizona Press, Tucson.

2282 Sharp, T.G., Walton, E.L., Hu, J.P., and Agee, C. (2019) Shock conditions recorded in NWA 8159
2283 martian augite basalt with implications for the impact cratering history on Mars.
2284 Geochimica et Cosmochimica Acta, 246, 197-212.
2285 Shen, G.Y., Mao, H.K., Hemley, R.J., Duffy, T.S., and Rivers, M.L. (1998) Melting and crystal
2286 structure of iron at high pressures and temperatures. Geophysical Research Letters, 25,
2287 373-376.
2288 Shoemaker, E. and Chao, E.C.T. (1961) New evidence for impact origin of Ries Basin, Bavaria,
2289 Germany. Journal of Geophysical Research, 66, 3371-3378.
2290 Smith, J.V. and Mason, B. (1970) Pyroxene-garnet transformation in Coorara meteorite. Science,
2291 168, 832-834.
2292 Smith, E. M. et al. (2018). Blue boron-bearing diamonds from Earth's lower mantle. Nature, 560,
2293 84-85.
2294 Smyth, J.R. (1987) Beta-Mg2SiO4 – a potential host for water in the mantle. American
2295 Mineralogist, 72, 1051-1055.
2296 Smyth, J.R., Holl, C.M., Frost, D.J., Jacobsen, S.D., Langenhorst, F.,and McCammon, C.A. (2003)
2297 Structural systematics of hydrous ringwoodite and water in Earth's interior. American
2298 Mineralogist, 88, 1402-1407.
2299 Smyth, R.J. et al. (2005) Crystal chemistry of wadsleyite II and water in the Earth's interior.
2300 Physics and Chemistry of Minerals, 31, 691-705.
2301 Sobolev, N.V. et al. (1997) Mineral inclusions in diamonds from the Sputnik kimberlite pipe,
2302 Yakutia. Lithos, 39, 135-157.
2303 Spray, J.G., Kelley, S.P. and Reimold, W.U. (1995) Laser probe Ar-40Ar-39 dating of coesite-
2304 bearing and stishovite-bearing pseudotachylites and the age of the Verdefort impact
2305 event. Meteoritics, 30, 335-343.

2306 Spray, J.G. and Boonsue, S. (2016) Monoclinic and tetragonal plagioclase (An54) in shock veins
2307 from the central uplift of the Manicouagan impact structure. Meteoritics & Planetary
2308 Science, 51, A590-A590.
2309 Stachel, T. et al. (2000). Kankan diamonds (Guinea) II: lower mantle inclusion parageneses.
2310 Contribution to Mineralogy and Petrology, 140, 16-27.
2311 Stachel, T. and Harris, J.W. (2008) The origin of cratonic diamonds - Constraints from mineral
2312 inclusions. Ore Geology Reviews, 34, 5-32.
2313 Stachel, T. and Luth R.W. (2015). Diamond formation — Where, when and how? Lithos, 220–223,
2314 200–220.
2315 Staehle, V., Altherr, R. Nasdala, L., and Ludwig, T. (2011) - Ca-rich majorite derived from high-
2316 temperature melt and thermally stressed hornblende in shock veins of crustal rocks
2317 from the Ries impact crater (Germany). Contributions to Mineralogy and Petrology, 161,
2318 275-291.
2319 Stishov, S.M. and Popova, S.V. (1961) New dense polymorphic modification of silica. Geokhimiya,
2320 10, 837-839.
2321 Stixrude, L. and Cohen, R.E. (1993) Stability of orthorhombic MgSiO3 perovskite in the Earth's
2322 lower mantle. Nature 364, 613-616 (1993).
2323 Stixrude, L. and Lithgow-Bertelloni, C. (2011) Thermodynamics of mantle minerals - II. Phase
2324 equilibria. Geophysical Journal International, 184, 1180-1213.
2325 Stöffler, D, Keil, K., and Scott, E.R.D. (1991) Shock metamorphism of ordinary chondrites.
2326 Geochimica et Cosmochimica Acta, 55, 3845-3867.
2327 Stöffler, D, Hamann, C., and Metzler, K. (2018) Shock metamorphism of planetary silicate rocks
2328 and sediments: Proposal for an updated classification system. Meteoritics & Planetary
2329 Science, 53, 5-49.

2330 Sturhahn, W., Jackson, J.M., and Lin, J.F. (2005) The spin state of iron in minerals of Earth's lower
2331 mantle. Geophysical Research Letters, 32, Article Number: L12307.
2332 Sundqvist, B. (1999) Fullerenes under high pressures. Advances in Physics, 48, 1-134.
2333 Tackley, P.J., Stevenson, D.J., Glatzmaier, G.A., and Schubert, G. (1993) Effects of an
2334 endothermic phase-transition at 670 km depth in a spherical model of convection in the
2335 Earth's mantle. Nature, 361, 699-704.
2336 Taggart, J. E, Foord. E., Rosenzweig, A., and Hanson, T. (1988) Scrutinyite, natural occurrences of
2337 alpha PbO 2 from Bingham, New Mexico. Canadian Mineralogist, 26, 905- 910.
2338 Tange, Y. and Takahashi, E. (2004) Stability of the high-pressure polymorph of zircon (ZrSiO4) in
2339 the deep mantle. Physics of the Earth and Planetary Interiors, 143, 223-229.
2340 Takahashi, T., Mao, H.K., and Bassett, W.A. (1969) Lead – X ray diffraction study of a high-
2341 pressure polymorph. Science, 165, 1352-1353.
2342 Tateno, S. et al. (2010) The Structure of Iron in Earth's Inner Core. Science, 330, 359-361.
2343 Taylor, W.R., Jaques, A.L., and Ridd, M. (1990) Nitrogen-defect aggregation characteristics of
2344 some Australasian diamonds – time-temperature constraints on the source regions of
2345 pipe and alluvial diamonds. American Mineralogist, 75, 1290-1310.
2346 Thomson, A. R. et al. (2016). Slab melting as a barrier to deep carbon subduction. Nature,
2347 529(7584), 76-78.
2348 Tomioka, N. and Fujino, K. (1997) Natural (Mg,Fe)SiO3-ilmenite and -perovskite in the Tenham
2349 meteorite. Science, 277, 1084-1086.
2350 Tomioka, N. and Fujino, K. (1999) Akimotoite, (Mg,Fe)SiO(3), a new silicate mineral of the
2351 ilmenite group in the Tenham chondrite. American Mineralogist, 84, 267-271.
2352 Tomioka, N., Miyahara, M., and Ito, M. (2016) Discovery of natural MgSiO3 tetragonal garnet in
2353 a shocked chondritic meteorite. Science Advances, 2, Article Number: UNSP e1501725.

2354 Tomioka, N. and Miyahara, M. (2017) High-pressure minerals in shocked meteorites. Meteoritics
2355 & Planetary Science, 52, 2017-2039.
2356 Troitzsch U., Christy A. G., and Ellis D. J. (2005) The crystal structure of disordered (Zr,Ti)O2 solid
2357 solution. Physics and Chemistry of Minerals, 32, 504-514.
2358 Tschauner, O., Mao, H.K., and Hemley, R.J. (2001) New transformations of CO2 at high pressures
2359 and temperatures. Physical Review Letters, 87, Article Number: 075701.
2360 Tschauner, O., Luo, S.-N., Asimow, P.D., and Ahrens, T.J. (2006) Recovery of stishovite-structure
2361 at ambient conditions out of shock-generated amorphous silica. American
2362 Mineralogist,91, 1857-1862.
2363 Tschauner, O. et al. (2009) Ultrafast growth of wadsleyite in shock-produced melts and its
2364 implications for early solar system impact processes. Proceedings of the National
2365 Academy of Sciences of the United States of America, 106, 13691-13695.
2366 Tschauner, O. and Ma, C. (2017) Riesite, IMA 2015-110a. CNMNC Newsletter No. 35, February
2367 2017, page 213; Mineralogical Magazine, 81, 209–213.
2368 Tschauner, O. and Ma, C. (2017) Stöfflerite, IMA 2017-062. CNMNC Newsletter No. 39, October
2369 2017, page 1285; Mineralogical Magazine, 81, 1279-1286.
2370 Tschauner, O., Ma, C., Prescher, C., and Prakapenka, V.B. (2018) Structure analysis and
2371 conditions of formation of akimotoite in the Tenham chondrite. Meteoritics and
2372 Planetary Science, 53, 62-74.
2373 Tschauner, O. et al. (2018) Ice-VII inclusions in diamonds – evidence for aqueous fluid in
2374 the Earth's deep mantle. Science, 359, 1136-1139.
2375 Tse, J.S., and Klug, D.D. (1992) Structural memory in pressure-amorphized AlPO4. Science, 255,
2376 1559-1561.

2377 Vanpeteghem, C.B., Zhao, J., Angel, R.J., Ross, N.L., and Bolfan-Casanova, N. (2006) Crystal
2378 structure and equation of state of MgSiO3 perovskite. Geophysical Research Letters, 33,
2379 Article Number: L03306.
2380 Vanpeteghem, C.B., Angel, R.J., Ross, N.L., Jacobsen, S.D, Dobson, D.P., Litasov, K.D., and Ohtani,
2381 E. (2006) Al, Fe substitution in the MgSiO3 perovskite structure: A single-crystal X-ray
2382 diffraction study. Physics of the Earth and Planetary Interiors, 155, 96-103.
2383 Wackerle, J. (1962) Shock-wave compression of quartz. Journal of Applied Physics, 33, 922–937.
2384 Walter, M.J. et al. (2011) Deep Mantle Cycling of Oceanic Crust: Evidence from Diamonds and
2385 Their Mineral Inclusions. Science, 334, 54-57.
2386 Walton, E.L., Sharp, T.G., Hu, J., and Tschauner, O. (2018) Investigating the response of biotite
2387 to impact metamorphism: Examples from the Steen River impact structure, Canada.
2388 Meteoritics & Planetary Science, 53, 75-92.
2389 Wang, L.P., Essene, E.J., and Zhang, Y.X. (1999) Mineral inclusions in pyrope crystals from Garnet
2390 Ridge, Arizona, USA: implications for processes in the upper mantle. Contributions to
2391 Mineralogy and Petrology, 135, 164-178.
2392 Wentorf, R.H. (1961) Synthesis of cubic form of boron nitride. Journal of Chemical Physics, 34,
2393 809-812.
2394 Willgallis, A., Siegmann, E. and Hettiaratchi, T. (1983) Srilankite, a new Zr-Ti-oxide mineral.
2395 Neues Jahrbuch fuer Mineralogie – Monatshefte, 4, 151-157.
2396 Williams Q. et al. (1987) The melting curve of iron to 250 gigapascals: a constraint on the
2397 temperature at the Earth's center. Science, 236, 181–182.
2398 Wirth, R., Kaminsky, F., Matsyuk, S., and Schreiber, A. (2009) Unusual micro- and nano-inclusions
2399 in diamonds from the Juina Area, Brazil. Earth and Planetary Science Letters, 286, 292-
2400 303.

2401 Wirth R., Dobrzhinetskaya, L.F., Harte, B., Schreiber, A., Green, H.W. (2011) High-Fe (Mg, Fe)O
2402 inclusion in diamond apparently from the lowermost mantle. Earth and Planetary
2403 Science Letters, 404, 365-375.
2404 Withers, A.C., Essene, E.J., and Jhang, Y. (2003) Rutile/TiO2II phase equilibria. Contributions to
2405 Mineralogy and Petrology, 145, 199–204.
2406 Woodland, A.B. and Angel, R.J. (1997) Reversal of the orthoferrosilite-high-P clinoferrosilite
2407 transition, a phase diagram for FeSiO3 and implications for the mineralogy of the Earth's
2408 upper mantle. European Journal of Mineralogy, 9, 245-254.
2409 Woodland, A.B., Angel, R.J., Koch, M., Kunz, M., and Miletich, R. (1999) Equations of state for
2410 Fe32+Fe23+Si3O12 "skiagite" garnet and Fe2SiO4-Fe3O4 spinel solid solutions. Journal
2411 of Geophysical Research – Solid Earth, 104, 20049-20058.
2412 Woodland, A.B. and Angel, R.J. (2000) Phase relations in the system fayalite-magnetite at high
2413 pressures and temperatures. Contributions to Mineralogy and Petrology, 139, 734-747.
2414 Woodland, A.B., Schollenbruch, K., Koch, M., Ballaran, T.B., Angel, R.J., and Frost, D.J. (2013)
2415 Fe4O5 and its solid solutions in several simple systems. Contributions to Mineralogy and
2416 Petrology, 166, 1677-1686.
2417 Wu, M., Liang, Y.F., Jiang, J.Z., and Tse, J.S. (2012) Structure and Properties of Dense Silica Glass.
2418 Scientific Reports, 2, Article Number: 398.
2419 Wyckoff, R.W.G. (1963) Crystal Structures, vol 1, 2nd ed. Interscience Publishers NY 1963
2420 Xie X. D., Chen M. and Wang D. Q. (2001). Shock-related mineralogical features and P-T history
2421 of the Suizhou L6 chondrite. European Journal of Mineralogy 13: 1177–1190.
2422 Xie, Z.D., Tomioka, N., and Sharp, T.G. (2002) Natural occurrence of Fe2SiO4-spinel in the
2423 shocked Umbarger L6 chondrite. American Mineralogist, 87, 1257-1260.

Xie, X.D., Minitti, M.E., Chen, M., Mao, H.K., Wang, D.Q., Shu, J.F., and Fei, Y.W. (2003) Tuite, gamma-Ca-3(PO4)(2): a new mineral from the Suizhou L6 chondrite. European Journal of Mineralogy, 15, 1001-1005.

Xie, Z.D., Sharp, T.G., Leinenweber, K., DeCarli, P.S., and Dera, P. (2011) A new mineral with an olivine structure and pyroxene composition in the shock-induced melt veins of Tenham L6 chondrite. American Mineralogist, 96, 430-436.

Xie, X., Gu, X., Yang, H., Chen, M. and Li, K. (2016) Wangdaodeite, IMA 2016-007. CNMNC Newsletter No. 31, June 2016, page 695; Mineralogical Magazine, 80, 691–697.

Xu, Y.N., and Ching, W.Y. (1991) Electronic and optical properties of all polymorphic forms of silicon dioxide. Physical Review B, 44, 11048-11059.

Xu, J.G., Zhang, D.Z., Fan, D.W., Zhang, J.S., Hu, Y., Guo, X.Z., Dera, P., and Zhou, W.G. (2018) Phase Transitions in Orthoenstatite and Subduction Zone Dynamics: Effects of Water and Tran-sition Metal Ions. Journal of Geophysical Research – Solid Earth, 123, 2723-2737.

Yagi, T., Marumo, F., and Akimoto, S.I. (1974) Crystal-structures of spinel polymorphs of Fe2SiO4 and Ni2SiO4. American Mineralogist, 59, 486-490.

Yagi, T., Mao, H.K., and Bell, P.M. (1978) Structure and crystal-chemistry of perovskite-type MgSiO3. Physics and Chemistry of Minerals, 3, 97-110.

Yagi, T., Suzuki, T., and Akaogi, M. (1994) High-pressure transitions in the system KAlSi3O8-NaAlSi3O8. Physics and Chemistry of Minerals, 21, 12-17.

Yamada, H., Matsui, Y., and Ito, E. (1984) Crystal-chemical characterization of KAISi,O, with the hollandite structure. Mineralogical Journal, 12, 29-34.

2446 Yamanaka, T., Kyono, A., Nakamoto, Y., Meng, Y., Kharlamova, S., Struzhkin, V.V., Mao, H. (2013)
2447 High-pressure phase transitions of Fe3-xTixO4 solid solution up to 60 GPa correlated
2448 with electronic spin transition. American Mineralogist, 98, 736–744.
2449 Yang, J.-S., et al. (2007) Diamond- and coesite-bearing chromitites from the Luobusa ophiolite,
2450 Tibet. Geology, 35, 875-878.
2451 Yong, W.J., Dachs, E., Withers, A.C., and Essene, E.J. (2006) Heat capacity and phase equilibria of
2452 hollandite polymorph of KAlSi3O8. Physics and Chemistry of Minerals, 33, 167-177.
2453 Zerr, A., and Boehler, R. (1993) Melting of (Mg,Fe)SiO3-perovskite to 625 kbars – indication of a
2454 high melting temperature in the lower mantle. Science, 262, 553-555.
2455 Zhang, D.Z. et al. (2016) Temperature of Earth's core constrained from melting of Fe and
2456 Fe0.9Ni0.1 at high pressures. Earth and Planetary Science Letters, 447, 72-83.
2457 Zhang, L., Yuan, H.S., Meng, Y., and Mao, H.K. (2018) Discovery of a hexagonal ultradense
2458 hydrous phase in (Fe,Al)OOH. Proceedings of the National Academy of Sciences of the
2459 United States of America, 115, 2908-2911.
2460 Zhou, Y.M., Irifune, T., Ohfuji, H., Shinmei, T., and Du, W. (2017) Stability region of
2461 K0.2Na0.8AlSi3O8 hollandite at 22 GPa and 2273 K. Physics and Chemistry of Minerals,
2462 44, 33-42.

2463

2464

2465

2466

2467

Table 1.

List of all approved high-pressure minerals and sone incipient high-pressure minerals which are discussed in this paper. Incipient high-pressure minerals are printed in italics. Endmember composition, first reference of the approved mineral or announcement by the CNMNC, density of endmembers and the density of the stable polymorph at reference conditions are given. The reported densities of the type specimens of these minerals may be different if they contain noticeable amounts of other components.

Name	**Composition**	**Reference**	**Density (Density of stable polymorph at ref. conditions) g/cm^3**
Elements and alloys			
Diamond	C	-	3.516 (graphite: 2.26)
Hexaferrum	Fe	Mochalov et al.	8.26 (iron: 7.88)

		1998	
δloc-N_2	N_2	Navon et al. 2017	1.767[1] (-)
Pnictides and Chalcogenides			
Allabogdanite	Fe_2P		6.86 (barringerite: 5.90)
Quingsongite	BN	Dobrzhinetzkaya et al. 2014	3.488 (g-BN: 2.298)
Shenzhuangite	$NiFeS_2$	Bindi et al. 2018	[2]
Molecular Minerals			
Ice-VII	H_2O	Tschauner et al. 2018b	2.07 (ice-Ih: 0.95)
(CO_2-I)	CO_2	Schauder&Navon 1993	1.76[1] (-)
Oxides and Hydroxides			
Coesite	SiO_2	Chao	3.04 (quartz: 2.65)
Stishovite	SiO_2	Chao et al. 1962	4.28 (quartz: 2.65)

Seifertite	SiO_2	Dera et al. 2002	4.37 (quartz: 2.65)
Srilankite	TiO_2	Willgallis et al. 1983	4.39 (rutile: 4.25)
Riesite	TiO_2	Tschauner et al. 2017	4.20 (rutile: 4.25)
Akaogiite	TiO_2	ElGoresy et al. 2001	4.26 (rutile: 4.25)
Scrutinyite	PbO_2	Taggart et al. 1988	9.87 (plattnerite: 9.70)
Lingunite	$NaAlSi_3O_8$	Gillet et al. 2000	3.6 (albite: 2.6)
Liebermannite	$KAlSi_3O_8$	Ma et al. 2018a	3.9 (orthoclase: 2.7)
Stöfflerite	$CaAl_2Si_2O_8$	Tschauner et al. 2018	4.0 (anorthite:2.7)
Wadsleyite	Mg_2SiO_4	Price et al. 1983	3.6 (forsterite: 3.2)
Asimowite	Fe_2SiO_4	Bindi et al. 2019	4.8[2] (fayalite: 4.4)
Ringwoodite	Mg_2SiO_4	Binns et al. 1969	3.8 (forsterite: 3.2)

Ahrensite	Fe_2SiO_4	Ma et al. 2016	4.85 (fayalite: 4.4)
Maohokite	$MgFe_2O_4$	Chen et al. 2017	5.33 (magnesioferrite: 4.5)
Chenmingite	$FeCr_2O_4$	Ma et al. 2019	5.6 (chromite: 5.1)
Xieite	$FeCr_2O_4$	Chen et al. 2003	5.8 (chromite: 5.1)
Tschaunerite	$FeTi_2O_4$	Ma et al. 2018	5.5 (ulvøspinel: 5.0)
Feiite	$(Fe,Ti)_4O_5$	Ma et al. 2018	5.4 (wüstite + ulvøspinel: 5.6)
Akimotoite	$MgSiO_3$	Tomioka&Fujino 1997, Sharp et al. 1997	3.8 (enstatite:3.2)
Hemleyite	$FeSiO_3$	Bindi et al. 2017	4.8[3] (ferrosilite:3.6)
Wangdaodeite	$FeTiO_3$	Xie et al. 2016	4.9 (ilmenite: 4.8)
Liuite	$FeTiO_3$	Ma et al. 2018	5.5 (ilmenite: 4.8)
Zagamiite	$CaAl_2Si_{3.5}O_{11}$	Ma et al. 2017, Beck et al. 2006	3.4-3.6
Bridgmanite	$MgSiO_3$	Tschauner et al.	4.1 (enstatite:3.2)

		2014	
Silicates			
Reidite	$ZrSiO_4$	Glass et al. 2002	5.16 (zircon: 4.67)
Majorite	$Mg_3(Mg,Si)_2Si_3O_{12}$	Smyth&Mason 1970	3.8 (enstatite: 3.2)
Jeffbenite	$Mg_3Al_2Si_3O_{12}$	Harris et al. 1997, Nestola et al. 2016	3.55 (pyrope: 3.55)
Breyite	$Ca_3Si_3O_9$	Brenker et al. 2018	3.52 (wollastonite: 2.9)
Jadeite	$NaAlSi_2O_6$		3.47
Tissintite	$Ca(Al,.)Si_2O_6$	Ma et al. 2016	3.4 (kushiroite: 3.4)
Phosphates			
Tuite	$Ca_3[PO_4]_2$		3.47

2480 1: Gaseous at reference conditions

2481 2: No endmember volume assessable.

2482 3: Based on assessment of endmember volume by Tschauner et al. (2018a)

2483

2484

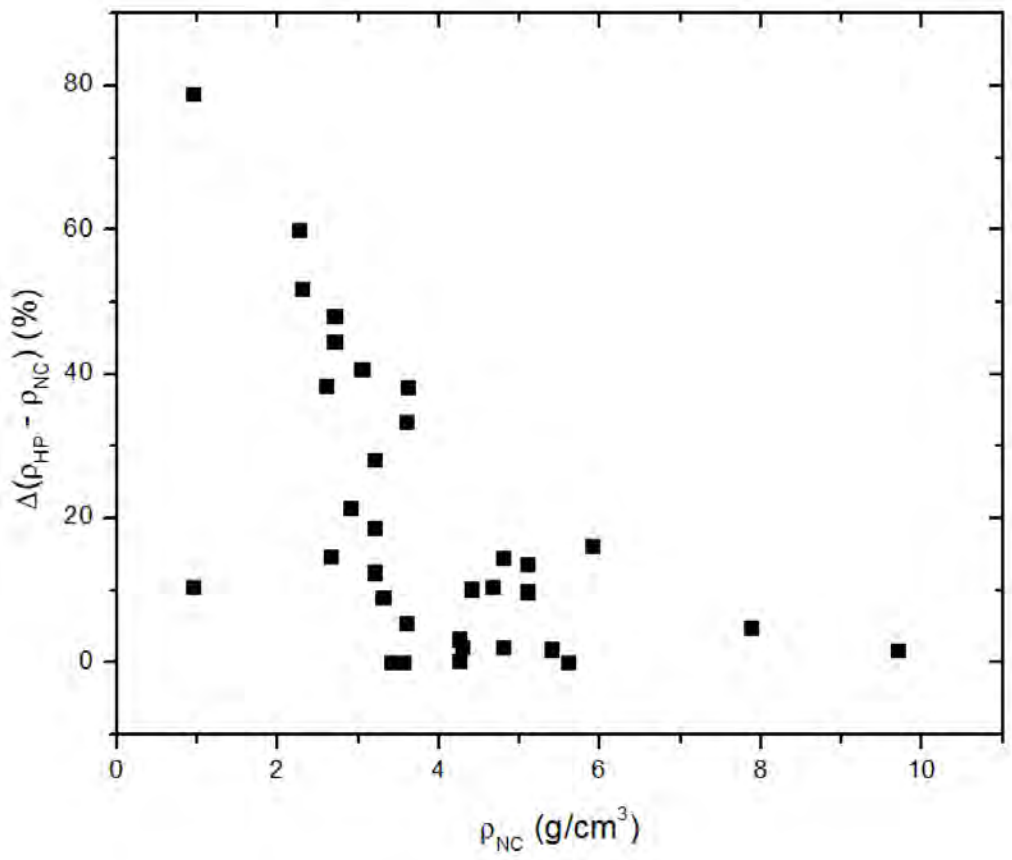

2485

2486 Figure 1: Difference in density of high- and ambient pressure mineral polymorphs in % as
2487 function of density of the polymorph stable at reference conditions. One notices that with
2488 increasing density at reference conditions, the density gain upon pressure-induced phase
2489 transformation decreases. This shows that absolute pressure or absolute density does not serve
2490 as a good criterion for defining high-pressure minerals. The Figure can also be read as
2491 illustration of the effect of pressure upon structures in general: High-pressure phases tend to be

This is a preprint, the final version is subject to change, of the American Mineralogist (MSA)
Cite as Authors (Year) Title. American Mineralogist, in press.
DOI: https://doi.org/10.2138/am-2019-6594

equivalent to low-pressure phases of compounds constituted by higher Z elements. For instance, taking a polymorphic series such as SiO_2 or TiO_2, and use the density of each subsequent higher-pressure polymorph as new reference point, the correlation of density-gain upon transition moves along the depicted trend. The plotted data are taken from Table 1.

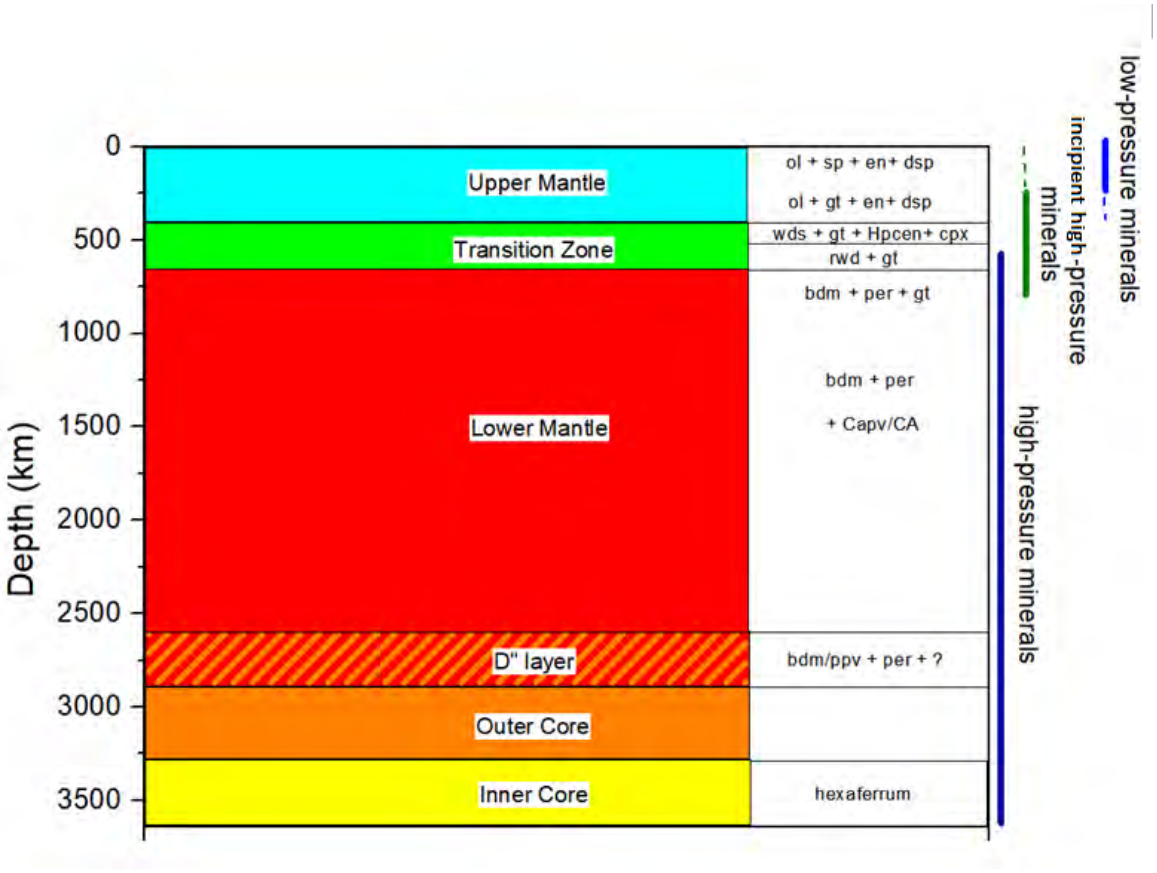

Figure 2: Schematic overview of the major divisions in Earth, their major rock-forming minerals, and their classification as low-, intermediate-, and high-pressure minerals. The division between core and mantle is primarily a change in bulk chemistry from compounds of Mg,Si, Al,Fe with O in the mantle to a metallic iron-rich alloy in the core, liquid in the outer, and solid in the inner core. The divisions of the mantle are primarily the result of pressure-induced changes in crystal structures whereas the composition of upper-, lower-mantle, and transition zone are very

similar. The Earth's crust is distinct from the mantle in both composition and basic structural features of its major minerals.

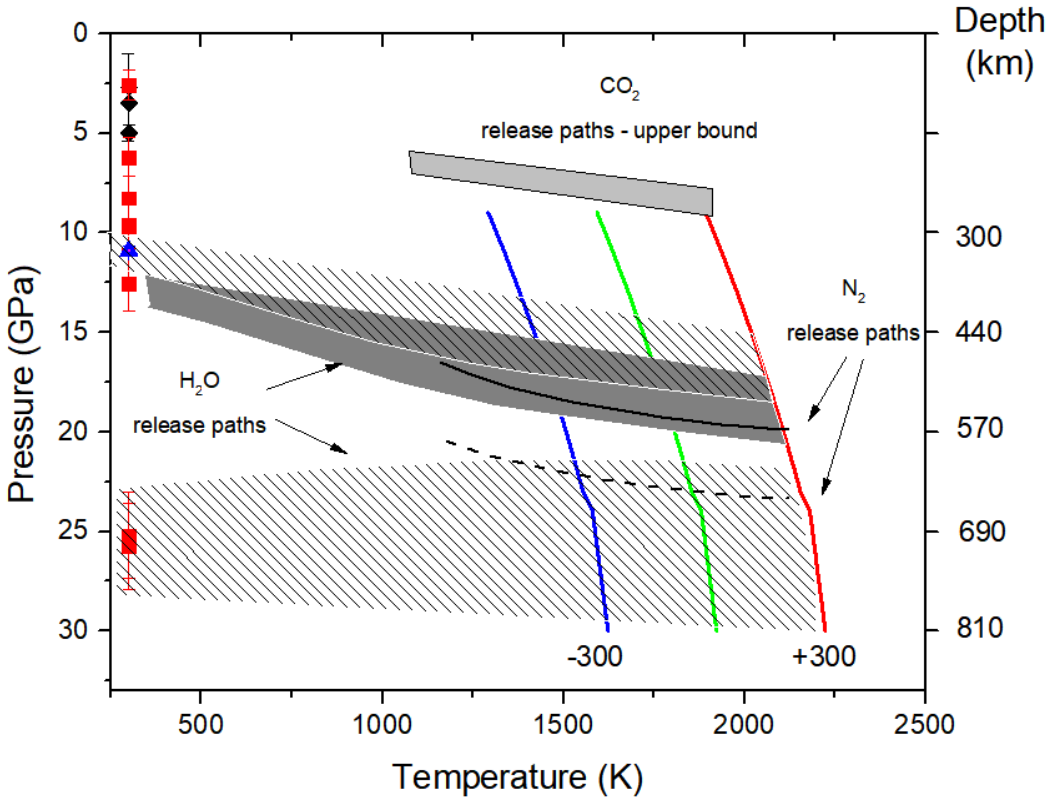

Figure 3: Residual pressures and source regions of dense molecular mineral inclusions in diamonds from the Earth's mantle. Red squares: ice-VII (Tschauner et al. 2018), Black diamonds: CO_2 (Navon and Schrauder 1994, Tschauner 2019), blue triangle: δ-N_2 (Navon et al. 2017). In all these studies the release paths were assessed as isochores with correction for thermal expansion and elasticity of diamond. These paths tie the current pressure of the inclusions (corrected for diamond relaxation, Angel et al. 2014) to the depth of entrapment in diamond. These end points are defined by intersection of the release path with the geotherm. Here we

2514 only give for reference the average mantle geotherm (Brown and Shankland 1981) and two
2515 adiabates 300 K higher and lower. Hashured and dark grey areas: Release paths for ice-VII, grey:
2516 CO_2 (after Schrauder and Navon 1994), black solid and dashed lines: N_2 (after Navon et al. 2017).

2517

2518

2519

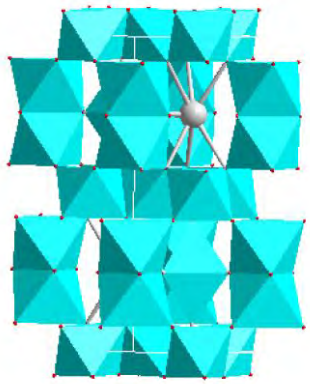

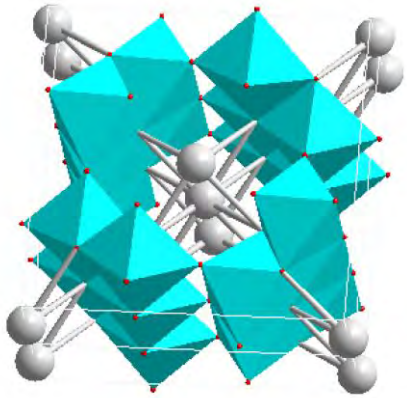

2520

2521 Figure 4: a Structural representation of zagamiite, $Ca_{1.601}$ $Si_{5.131}$ $Al_{3.763}$ $Na_{0.199}$ $O_{22.001}$, the
2522 dioctahedral layers are predominantely occupied by Si, the face-sharing interlayer octahedral
2523 are partially occupied by Al.
2524 b.Representation of the silicate-hollandites lingunite, liebermannite, and stöfflerite. The central
2525 channel is occupied by Na, K, and Ca, the octahedral sites by Si and Al.
2526
2527
2528
2529

This is a preprint, the final version is subject to change, of the American Mineralogist (MSA)
Cite as Authors (Year) Title. American Mineralogist, in press.
DOI: https://doi.org/10.2138/am-2019-6594

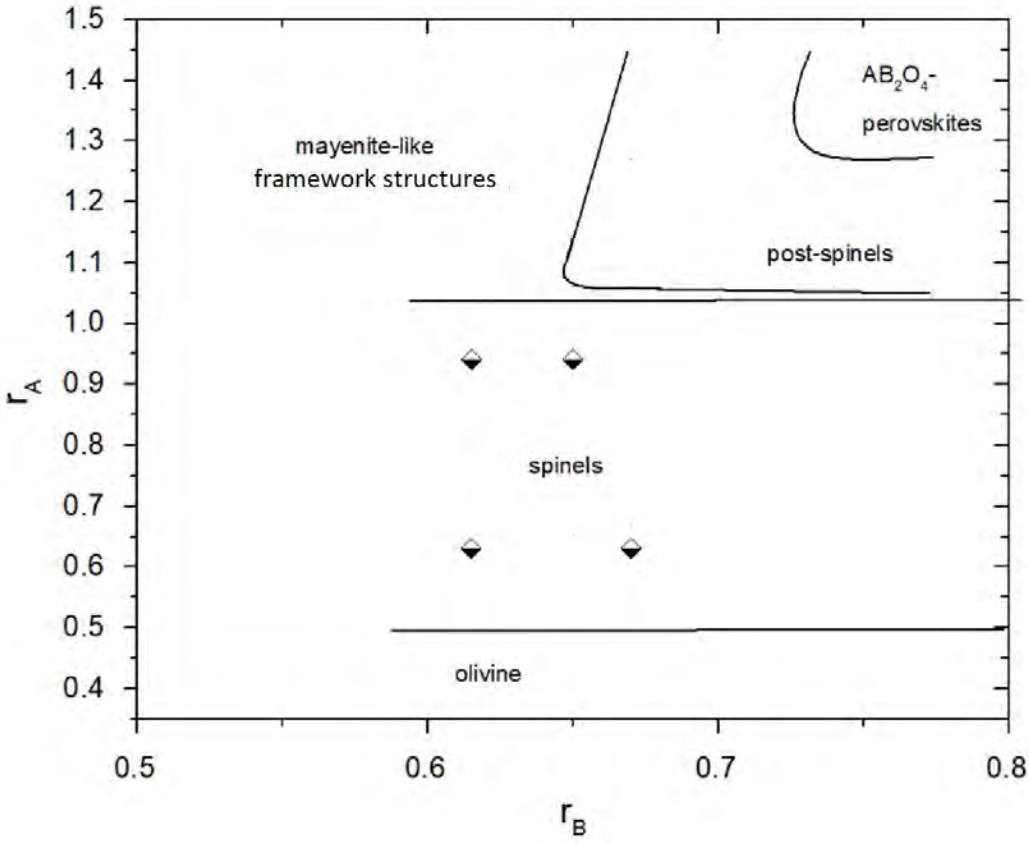

Figure 5. Relations of effective radii and structure fields of AB_2O_4 oxides (adapted from Glasser and Glasser 1963). The spinels magnesioferrite, chromite, magnesiochromite, and ulvospinel are indicated by half-filled diamonds. The corresponding high-pressure minerals maohokite (Chen et al. 2017), xieite (Chen et al. 2003), chenmingite (Ma et al. 2018), and tschaunerite (Ma et al. 2018) are in the postspinel field whch at ambient pressure is occupied by phases with r_A >1.05 Å. It is noteworthy that the transition from spinels to postspinel AB_2O_4 is not direct but through a regime of partial decomposition into sesquioxides and ludwigite-type oxides (Nishio-Hamame et al. 2012, Ishii et al. 2014, 2016, Akaogi et al. 2018)

This is a preprint, the final version is subject to change, of the American Mineralogist (MSA)
Cite as Authors (Year) Title. American Mineralogist, in press.
DOI: https://doi.org/10.2138/am-2019-6594

2541

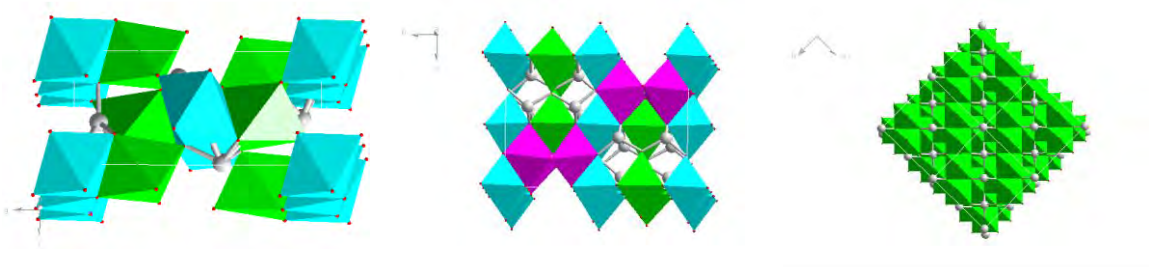

2542 Figure 6. Representations of the structures of olivine (a), wadsleyite (b), and ringwoodite (c).
2543 Only the polyhedra with six-fold coordinates centra cations (M-sites, 'octahedral' sites) are
2544 indicated. Different M-sites are color-coded. Grey spheres = Si.

2545

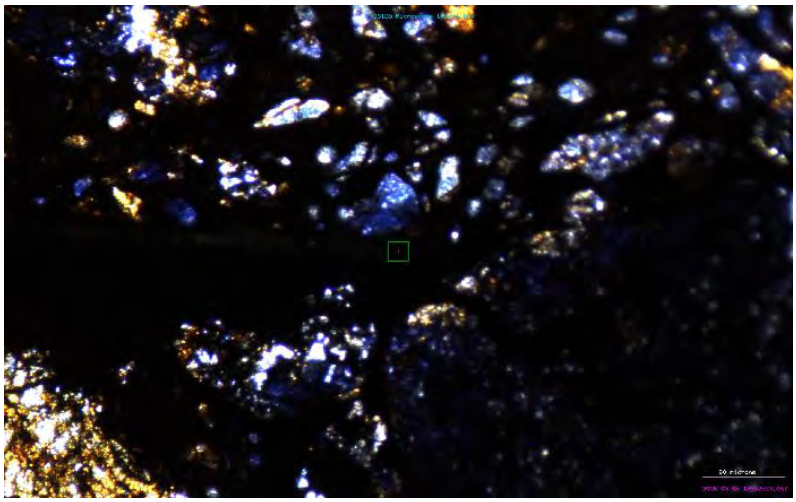

2546

2547 Figure 7. Acfer 040 L6 chondrite with cornflower-bue ringwoodite, center green rectangle has
2548 edge length 40 μm. Microscope image was taken witl parallel polarizers. The apparent grains of
2549 ringwoodite are actually aggregates of μm-to subμm-scale crystallites. This is typical for high-
2550 pressure minerals in shock-metamorphic environments: In shergottites and chondrites grainsize
2551 is usually below μm in diameter, shock-melt veins in bedrock from terrestrial impact sites
2552 contains crystallites up to 5 μm in diameter (see for instance: Walton et al. 2018).

2553

2554

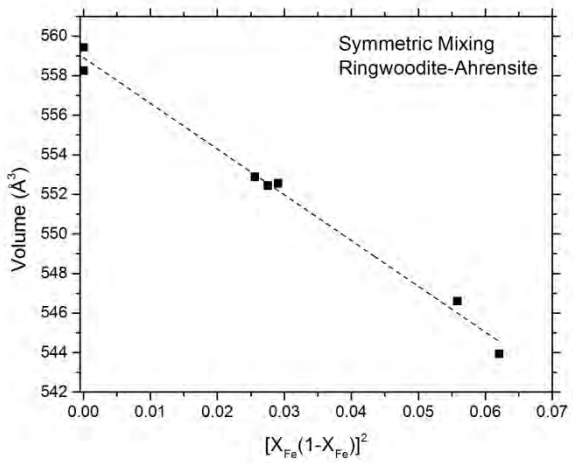

2555

2556 Figure 8: Symmetric mixing relation in the ringwoodite-ahrensite binary system. Synthetic

2557 samples by Ito and Takahashi (1989), Hazen et al. (1992), and Horiuchi (). Type ahrensite is the

2558 data point with 56 mol% ahrensite.

2559

2560

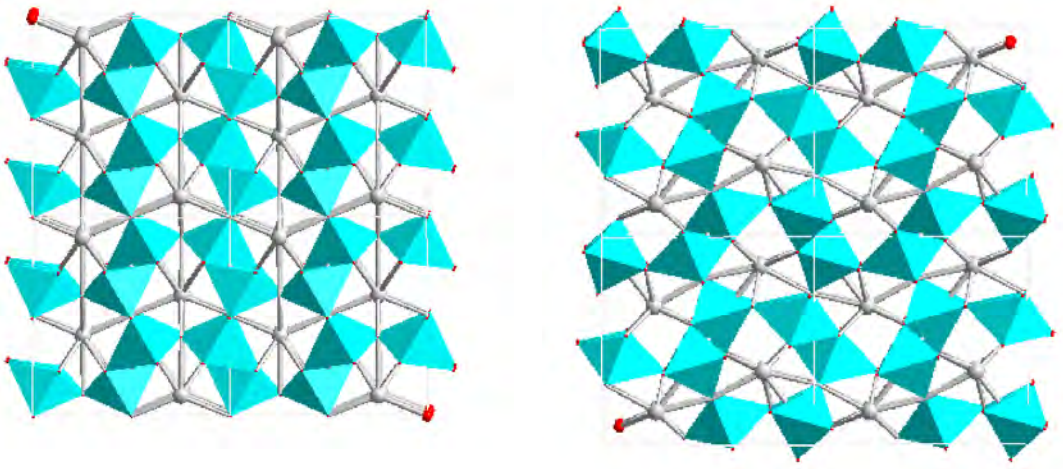

This is a preprint, the final version is subject to change, of the American Mineralogist (MSA)
Cite as Authors (Year) Title. American Mineralogist, in press.
DOI: https://doi.org/10.2138/am-2019-6594

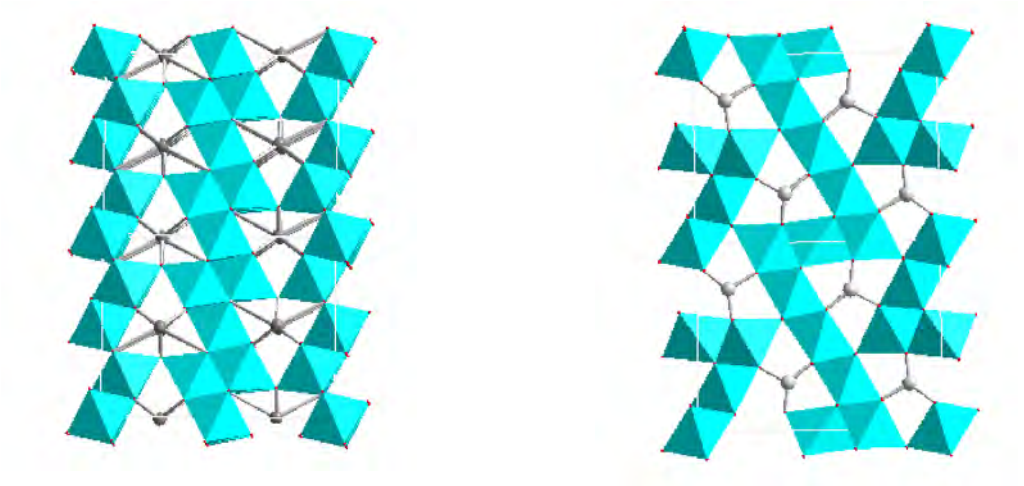

2561

2562 Figure 9: Representations of high-pressure transition metal oxide structures. a. Xieite, the

2563 $FeCr_2O_4$ postspinel phase isotypic to $CaTi_2O_4$ (Chen et al. 2003). b. Chenmingite, the $FeCr_2O_4$

2564 postpinel phase isotypic to harmunite ($CaFe_2O_4$) (Ma et al. 2018). c. Feiite, $Fe_2(FeTi)_2O_5$ (Ma et al.

2565 2018), d. $Fe(Fe,Ti)_3O_5$ ludwigite, a synthetic high pressure phase that occurs in the Fe-Cr- and the

2566 Fe-Ti-oxide systems (Ishii et al. 2015, 2016).

2567

2568

2569

2570

2571

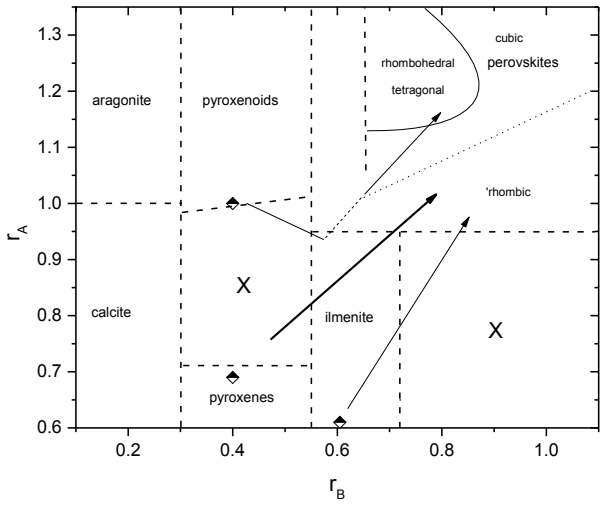

Figure 10. Structure fields and effective ionic radii of ABO_3-compounds after Roth (1957). Diamonds: radii of enstatite, wollastonite, and ilmenite at reference conditions. X = no known crystalline structures. Arrows indicate the 'trend' of structural evolution with pressure: While enstatite crosses the intermediate field of ilmenite-type structures through the transition sequence enstatite -> high-pressure clinoenstatite -> akimotoite -> bridgmanite, ilmenite itself undergoes a transition to a rhombohedral perovskite (wandaodeite) first before adapting the orthorhombic GdFeO3-type perovskite structure (liuite). Wollastonite exhibits a more complex transformation behaviour with partial decomposition at intermediate pressure, formation of an ilmenite-type phase, then formation of a cubic or pseudo-cubic perovskite.

This is a preprint, the final version is subject to change, of the American Mineralogist (MSA)
Cite as Authors (Year) Title. American Mineralogist, in press.
DOI: https://doi.org/10.2138/am-2019-6594

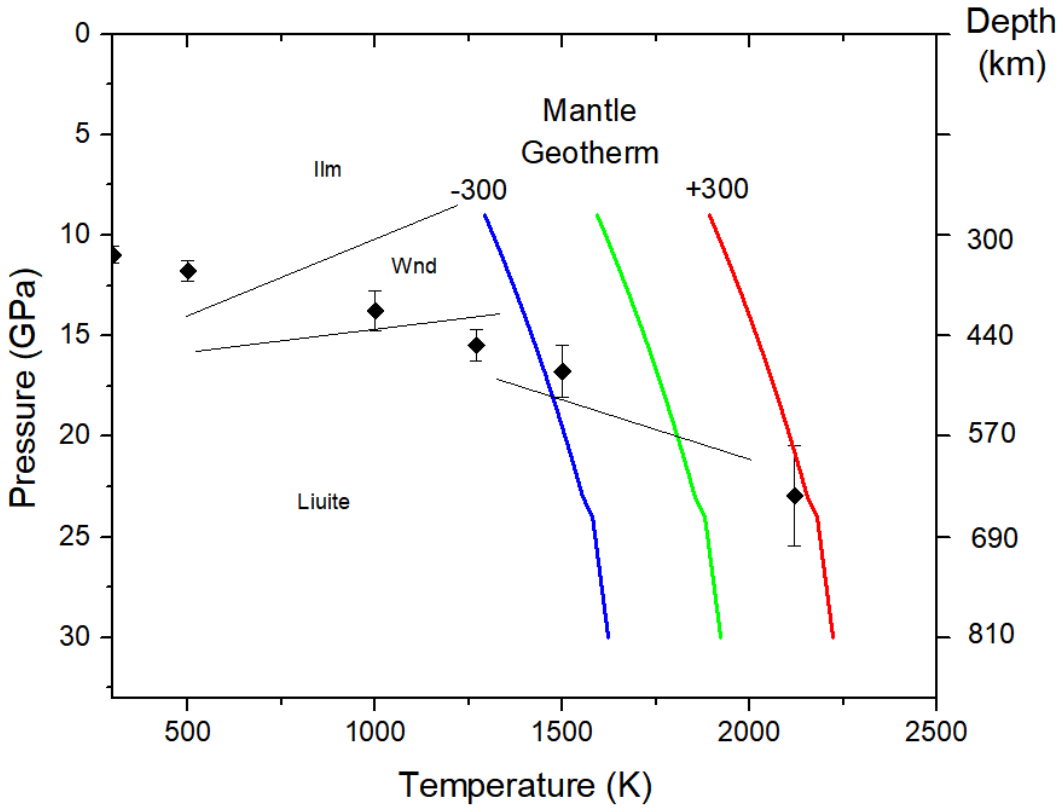

Figure 11: Entrapment path of an ilmenite inclusion (Ilm90Gk10) with 10± 1GPa residual pressure in a sublithospheric diamond, after (Tschauner et al. 2018). The modeled entrapment path intersects for this composition the phase boundary to wandaodeite at 700 ±60K, 12.5 ±0.4 GPa and, possibly, liuite above 1000K 14.6 GPa to > 18 GPa and <1500 K depending on the slope of the transition boundary (Ming et al. 2006, Nishio-Hamame et al. 2012). Thus, the ilmenite inclusion is a retrograde transformation product of (Fe,Mg)TiO_3-perovskite.

This is a preprint, the final version is subject to change, of the American Mineralogist (MSA)
Cite as Authors (Year) Title. American Mineralogist, in press.
DOI: https://doi.org/10.2138/am-2019-6594

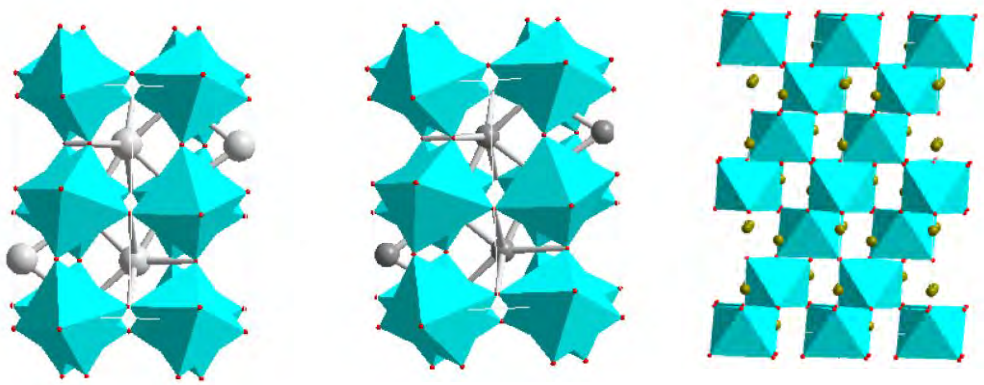

2596

2597 Figure 12: Structural representations of bridgmanite, liuite, and wandaodeite, the

2598 three known perovskite-type high-pressure minerals: a. Bridgmanite $(Mg,Fe)SiO_3$, in

2599 standard setting Pnma of space group 62; b. liuite $(Fe,Mg)(Ti,Si)O_3$, in same setting

2600 and with noticeably larger tilt of the octahedra than in bridgmanite; c.

2601 wangdaodeite $FeTiO_3$, is a rhombohedral perovskite of the $LiNbO_3$-type.

2602

2603

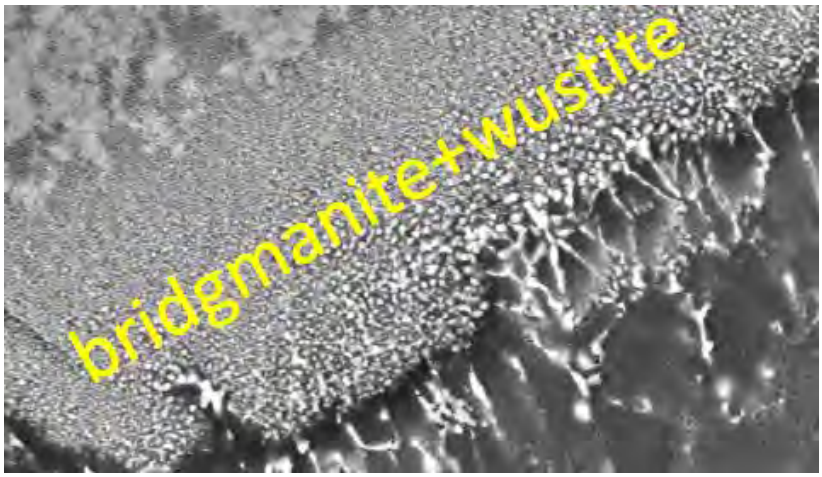

2604

2605 Figure 13. Bridgmanite-wuestite intergrowth at the border of a shock-melt pocket in the Tissint

2606 shergottitic martian meteorite. The intergrowth occupies the diagonal band running from the

2607 lower left to the upper right corner of the image and coarsens toward the melt pocket in the
2608 lower right corner with idiomorphic wuestite. The much finer grained material in the upper left
2609 corner of the image is ahrensite (γ-Fe_2SiO_4).

2610

2611

2612